S. K. SAHAY

Data Analysis of Gravitational Waves

SVENSKA FYSIKARKIVET • 2008

Sanjay Kumar Sahay
Birla Institute of Technology and Science,
Pilani – Goa Campus, India

Data Analysis of Gravitational Waves

Databehandling av gravitationsvågor

2008

Swedish physics archive
Svenska fysikarkivet

Svenska fysikarkivet (that means the Swedish physics archive) is a publisher registered with the Royal National Library of Sweden (Kungliga biblioteket), Stockholm.

Postal address for correspondence:
Svenska fysikarkivet, Näsbydalsvägen 4/11, 183 31 Täby, Sweden

Edited by Dmitri Rabounski

Cover image: the "blue marble" image is the most detailed true-color image of the entire Earth to date. This image came from a single remote-sensing device-NASA's Moderate Resolution Imaging Spectroradiometer, or MODIS. Flying over 700 km above the Earth onboard the Terra satellite. Sensor: Terra/MODIS. Visualization Date: February 08, 2002. Credits — NASA Goddard Space Flight Center Image by Reto Stöckli (land surface, shallow water, clouds). Enhancements by Robert Simmon (ocean color, compositing, 3D globes, animation). Data and technical support: MODIS Land Group; MODIS Science Data Support Team; MODIS Atmosphere Group; MODIS Ocean Group Additional data: USGS EROS Data Center (topography); USGS Terrestrial Remote Sensing Flagstaff Field Center (Antarctica); Defense Meteorological Satellite Program (city lights). This image is a part of NASA's Visible Earth catalog of NASA images and animations of our home planet. Courtesy of NASA. This image is free of licensing fees. See http://visibleearth.nasa.gov for NASA's Terms of Use.

This book was typeset using teTEX typesetting system and Kile, a TEX/LATEX editor for the KDE desktop. Powered by Ubuntu Linux.

Signed to print on August, 2008

ISBN: 978-91-85917-05-1
Printed in India

Contents

Foreword of the Editor

Initial attention of experimental physicists and astronomers was focused on gravitational waves in 1968–1970 when Joseph Weber, the professor at Maryland University (USA), performed his first observations with solid-body gravitational wave detectors, constructed at his laboratory. He registered a few weak signals, in common with all his independent detectors, which were as distant located from each other as up to 1000 km (the distance between Maryland and Illinois where the detectors were located). He supposed that the registered signals were due to a gravitational wave splash originated in some processes at the centre of the Galaxy, and registered by his detectors.

The observations were continued in the next decades by many groups of researchers working at laboratories and research institutes throughout the world, who operated a new generation of gravitational wave detectors which were much more sensitive than those of Weber. In addition to gravitational antennae of the solid-body kind, constructed by Weber, many antennae based on free masses (laser interferometric detectors) were constructed. However even the new generation of gravitational wave detectors have not led scientists to the expected results yet.

Nonetheless no doubt that gravitational radiation will have been discovered in the future, because this is one of the main effects predicted in the framework of the General Theory of Relativity. The main arguments in support of this thesis are: (i) gravitational fields bear an energy described by the energy-momentum pseudotensor; (ii) a linearized form of Einstein's equations permits a solution describing weak plane gravitational waves, which are transverse; (iii) an energy flux, radiated by gravitational waves, can be calculated through the energy-momentum pseudotensor of a gravitational field.

The search for gravitational waves has continued. Higher precision and more sensitive modifications of the gravitational wave detectors are used in this search. Because theoretical considerations showed that gravitational waves should be accompanied by other radiations, the researchers conducted a search for gravitational wave splashes connected to radio outbreaks and neutron outbreaks, which are many in the sky. Gravitational wave antennae in general are no high selective instruments. Even modern detectors of the GRAIL type, based on a solid-body polyhedron, have no such a selectivity as radio-telescopes have, for instance. Being resting bulky instruments, gravitational wave detectors

actually scan the sky due to the rotation of the Earth. A gravitational wave detector is a highly sensitive instrument working at the limits of the modern measurement precision. It answers almost everything so that it has noisy output. Therefore another problem rose in the search for gravitational waves, aside for the construction of the detectors and their sensitivity: how to perform the search in the sky, full of other signals of non-gravitational wave origins, scanned by a resting detector which has noisy output?

In this connexion it is important to take into account the research conducted by Dr. S. K. Sahay, I am honoured to present here. His research is spent on the data analysis method known as "Matched Filtering", applied by him to the results of the scanning of the sky performed by a single laser inteferometric gravitational wave detectors in search for gravitational waves.

Matched Filtering is a sort of data analysis methods, which is able to find a signal of known shape "hidden" in the noisy data pattern. An essense of this method, being applied to search for gravitational waves, is the search for correlations between the noisy output of an interferometer's data and a set of theoretical waveform templates calculated according our views on the sources of gravitational radiation.

As a result it was found that, even with use of the current generation of gravitational wave detectors and computers, Matched Filtering provides a substantial advantage in the search for the sources of gravitational radiation in the cosmos that may lead to discovery of gravitational waves in the close future.

I am therefore very pleased to present this research, produced by Dr. S. K. Sahay, to attention of readers.

August, 2008 *Dmitri Rabounski*

To my late father

SHRI KRISHNA SAHAY

Preface

The research in the field of gravitational wave physics started after its formulation by Einstein (1916) as propagating gravitational disturbance described by the linearized field limit of his General Theory of Relativity (GR) but has received serious impetus toward its detection after the announcement of its detection by Weber in 1969 using aluminium bar detectors. This field has now emerged and established itself with General Relativity, astrophysics and numerical analysis as its equally important facets. Of course, the technological advancements being employed in the construction of detectors with day by day improving sensitivity have played the crucial role. To date, although the results of Weber could not be confirmed and we do not have as yet any direct detection of gravitational wave (GW), yet it is not a matter of concern. Because on one hand the sensitivity required for the announcement of definite detection of GW bathing the Earth is yet to be achieved by the detectors whereas on the other hand we have an indirect evidence of the existence of GW observed in 1974 as the slowing down of the binary pulsar PSR $1913+16$ arising because of back reaction of GW emission.

GW scientists all over the globe are putting more persuasive arguments regarding the feasibility of GW detection in "near future" and the advantages to be achieved once the "Gravitational Wave Astronomy" as they call it, is established. A huge amount of money is involved in these projects to the extent that many of the detectors are built in collaboration e.g. American Laser Interferometric Gravitational Wave Observatory (LIGO), Italian-French Gravitational Wave Observatory (VIRGO), British-German Observatory (GE0600). As a consequence the literature is full of update reviews on gravitational wave astronomy notably by Thorne (1987), Blair (1991), Schutz (1999), Grishchuk et al. (2000), where the related issues viz., the fall outs, pre-requisites and prospects are discussed and scrutinized with rigour and minute detail.

The book is mainly based on my PhD thesis and subsequent work and is made up of two parts. The first part (Chapter 1 through Chapter 4) explains gravitational waves, detectors, sources and data analysis concepts. The matters covered in these Chapters are restricted to the extent they are supposed to provide continuity and coherence to the second part (Chapter 5 through Chapter 9). The source codes

of the numerical computations may be provided on the request to the author.

A pulsar will emit a GW signal over extended period of time only when it has a long-living asymmetry. Several mechanisms have been given for such an asymmetry to arise. Some pulsars emit GW almost monochromatically and are remarkably good clocks as its periods have been measured upto 13 significant digits. However, the GW signals from pulsars are very weak ($\leqslant 10^{-25}$) and will be buried in the broadband noise of the detector. In order to detect the signal from the dominant noise one has to analyze the long time observation data of months/years. The output of a detector is highly involved function of many initial parameters. It is usually not possible to obtain the Fourier transform (FT) analytically. Hence, FT has to be obtained via numerical methods. But it appears to be computationally demanding even for the standard computers expected to be available in near future. Therefore, one will have to work with efficient data analysis techniques, efficient not only in picking weak signal from the noisy data but also in terms of computing-cost. Chapter 4 is on the problem and technique for the data analysis. The noises and sensitivity of the detector has been briefly described. The *Matched Filtering*, a technique of the optimal method for detecting unknown signal and which describes drop in signal-to-noise ratio in terms of *Fitting Factor* (*FF*), is discussed. The computational cost and detection criteria are also explained.

In Chapter 5 the noise free complete response of Laser Interferometer detector for a *continuous gravitational wave* (CGW) for its arbitrary location and that of the source has been obtained, taking into account the rotational motion of the Earth about its spin axis as well as its orbital motion around the Sun. Also, analytical FT of frequency modulated output for one day observation time has been developed. In Chapter 6 this analysis has been generalized for (i) one year observation time and for (ii) any arbitrary duration of observation data set. The emission of GW from pulsars as such may contain two or more frequencies. Hence, finally generalize the transform for N-component signal. The method to account for spin down of CGW is also explained.

The strategy for the detection of GW signal is to make use of FT to dig out the signal from the noisy output of the detectors. To achieve this, one constructs the templates which are best educated guesses of the expected signal waveform. In Chapter 7 the results on FT obtained in Chapter 6 are applied and computed on the number of such templates required for an all sky search. Chapter 8 discusses the possibilities of symmetries which may be observed in the sky by π radian with the

source frequency. Finally in Chapter 9 the Earth azimuth effect in the bank of search templates or an all sky search has been discussed.

I would like to thank Prof. D. C. Srivastava, D.D.U. Gorakhpur University, Gorakhpur for constant encouragement throughout the work. I am indebted to Prof. A. K. Kembhavi, Dean of Visitor Academic Programmes for his kindness and help. Hence, benefited by the discussions, comments and suggestions of IUCCA Scientists. I thankfully acknowledge the facilities made available to me during the course of stay as a Visiting Associate and Research Scholar at IUCAA, Pune, where a part of the work has been carried out.

I am very much thankful to my mother and sisters for their love and continuous support.

Goa, India, August 2008 *S. K. Sahay*

Chapter 1

GRAVITATIONAL WAVES

§1.1 Introduction

Gravitational waves (GW) like any other type of waves are propagating perturbations of some flat background space-time. These are identified as small ripples rolling across space-time in the same manner as water waves are on an otherwise flat ocean. These waves originate from the most energetic events in our Universe such as rotating neutron stars, colliding binaries, supernovae explosions and gravitational collapse in black holes. They manifest themselves as strains in space-time that periodically stretch and compress matter. The GW emanating from a binary may be represented as in Fig. (1.1).

Newtonian gravitation does not have the provision for GW. In several Lorentz covariant gravitational theories, e.g. scalar, vector, tensor theories, GW arise as the spreading out gravitational influence. The basis of most current thinking of GW is Einstein's theory of General Relativity (GR). In fact, GW phenomenon was first studied by Einstein in 1916 by applying linear field approximation to GR. However, he was misled to the result that an accelerated spherical mass would emit GW. He corrected his mistake in 1918 and showed that the first order term of GW was quadrupolar.

The strength of GW is so small that there is no hope of its detection in the manner Hertz demonstrated the existence of electromagnetic waves. The reason may be attributed to the extremely small value of the universal constant of gravitation ($G \simeq 6.7 \times 10^{-11}\,\mathrm{N\,m^2\,kg^{-2}}$). The dimensionless amplitude of typical GW reaching the Earth is only of the order of 10^{-17}. This put in other words means that such a GW will put a rod of one meter length into an oscillation with an amplitude of one millionth of the radius of a hydrogen atom. Any chance to observe the effects of GW would require acceleration of astrophysical size masses at relativistic speeds. Several GW-detectors are running, or have been proposed for the future, that hope to detect these very small vibrations. The best known of these are *Laser Interferometer Ground Observatory* (LIGO), and *Laser Interferometer Space Antenna* (LISA). As the names

suggest, the former is a terrestrial observatory and the latter a space-based one. Needless to say, what enormous engineering achievements these detectors require to detect the oscillations mentioned above.

The interaction of GW with matter is also very small and this leads to some profound benefits for astrophysics. The wave will not scatter, so they emanate undisturbed from the regions of their origin viz., densest regions of the Universe, inner cores of imploding stars, the earliest instants of the primeval Universe, and the formation of black holes. Hence, they will provide an information on the dynamics in these regions about which there are no other means.

A piece of indirect evidence affirming the existence of GW came in 1974 when Joseph Taylor and Russell Hulse studied the pulsar PSR $1913+16$ which is a binary partner of a compact neutron star and is orbiting around the other in a slowly decreasing eight hour period. The orbital frequency acceleration was observed to be in perfect agreement with what expected from the energy loss arising due to their calculated GW emission (Damour and Taylor, 1992). For their accomplishment, Hulse and Taylor were awarded the 1993 Nobel Prize.

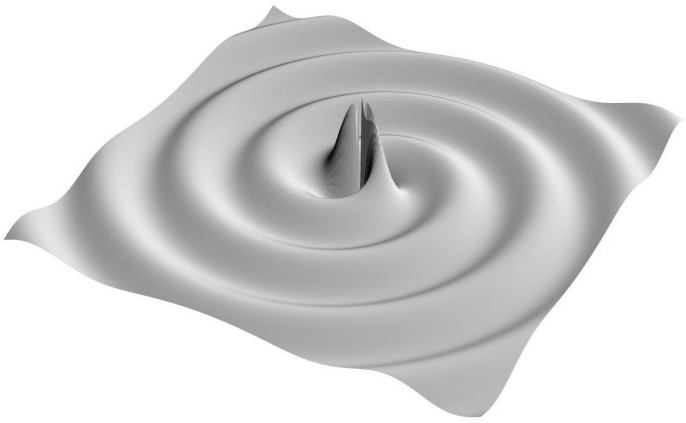

Figure 1.1: Gravitational wave produced by a binary star.

Unfortunately PSR $1913+16$ is presently emitting GW too feeble for their direct detection on the Earth and such a condition will continue until the end of its pas-de-deux inspiraling some 350 million years hence. Interestingly, the density of observed binaries in our galaxy is such that a few late stage inspiraling events are expected per century to occur. Hence, the study of the orbits of the binary neutron star system and their coalescence have played important role in the setting design criteria

for some of the instruments to come into operation in the next few years. To the date we have only the indirect evidence of GW. Yet this has not been of much concern for theoretical physicists, because the strength of the postulated GW signals are below the detection threshold currently available.

The quest to detect GW started in its earnest as early as in 1965 with the pioneering work of J. Weber on resonating bars. These are basically high quality *bells* designed to be rung by transient GW. With this beginning a small GW detection community has arisen and thrived continuing to improve on the original idea. The main effort is directed towards noise reduction by introducing ever lower cryogenic temperature and ever more sensitive displacement sensor to improve detector sensitivity. Many more bars, progressively sophisticated ones, have been built. The *Explorer* which is quietly functioning at CERN since 1989, is one such detectors worth mention.

There is an excellent prospect of detection of GW in the near future. There will emerge what has been called "Gravitational Wave Astronomy". This will provide another window for observing the Universe. The expectation is that it will uncover new phenomena as well as add new insights into phenomena already observed in electromagnetic part of the spectrum. GW emanation is due to the accelerated motions of mass in the interior of objects. As remarked earlier, these regions are otherwise obscure in electromagnetic, and possibly, even in neutrino astronomy. GW arise due to the coherent effects of masses moving together rather than individual motions of smaller constituents such as atoms or charged particles which generate electromagnetic radiation.

§1.2 Einstein's tensor

Gravitational waves like electromagnetic waves may be defined as time varying gravitational fields in the absence of its sources. The gravitation theory, widely believed, is the one proposed by Einstein and famous as GR. In its mathematical essence it is expressed via the equation known by his name viz.*

$$\mathrm{G}_{\alpha\beta} = \mathrm{R}_{\alpha\beta} - \frac{1}{2}\, g_{\alpha\beta}\mathrm{R} = 8\pi\,\mathrm{T}_{\alpha\beta}\,. \tag{1.1}$$

The conceptual meaning of this equation is that the localized density distribution characterized by the energy-momentum tensor, $T_{\alpha\beta}$, curves the space-time around the source. The curvature and other geometrical properties of the space-time are characterized by Ricci's curvature

*For notations, conventions and definitions the reader may refer to Schutz (1989).

tensor $R_{\alpha\beta}$ and the underlying metric tensor $g_{\alpha\beta}$. The curved space-time forces a free mass particle or light to follow the geodesics. These geodesics measure the effect of gravitation. GR in the limit of a weak field yields the Newton's theory of gravitation. In this approximation the gravitational field is considered to be represented by a metric with a linear modification of the background Lorentz space-time metric, $\eta_{\alpha\beta}$. It is important to remark that many of the basic concepts of GW theory can be understood in this approximation and were introduced and developed by Einstein himself.

§1.3 Linear field approximation

The metric of the space-time may be expressed as

$$g_{\alpha\beta} = \eta_{\alpha\beta} + h_{\alpha\beta}\,, \qquad |h_{\alpha\beta}| \ll 1\,. \tag{1.2}$$

It is straight forward to compute Einstein's tensor, $\mathrm{G}_{\alpha\beta}$, and one obtains

$$\mathrm{G}_{\alpha\beta} = -\frac{1}{2}\left[\bar{h}_{\alpha\beta,\ \mu}^{\ \ ,\mu} + \eta_{\alpha\beta}\bar{h}_{\mu\nu}^{\ \ ,\mu\nu} - \bar{h}_{\alpha\mu,\ \beta}^{\ \ ,\mu} - \bar{h}_{\beta\mu,\ \alpha}^{\ \ ,\mu} + O\left(h_{\alpha\beta}^2\right)\right], \tag{1.3}$$

where

$$\bar{h}^{\alpha\beta} = h^{\alpha\beta} - \frac{1}{2}\,\eta^{\alpha\beta}h\,, \qquad h = h^{\alpha}_{\ \alpha} = -\,\bar{h}^{\alpha}_{\ \alpha}\,. \tag{1.4}$$

We lift and lower the tensor indices using the Lorentz metric. Note that the expression for $\mathrm{G}_{\alpha\beta}$ would simplify considerably, if we were requiring

$$\bar{h}^{\mu\nu}_{\ \ ,\,\nu} = 0\,. \tag{1.5}$$

In fact there is a gauge freedom available as an infinitesimal coordinate transformation defined as

$$x^{\alpha} \to x'^{\,\alpha} = x^{\alpha} + \xi^{\alpha}\left(x^{\beta}\right), \quad |\xi^{\alpha}| \ll 1\,, \tag{1.6}$$

where ξ^{α} is taken arbitrary. This gauge transformation preserves (1.2). It can be shown that, in order to achieve the condition (1.5), ξ^{α} has to be chosen as to satisfy

$$\Box\,\xi^{\mu} = \xi^{\mu\nu}_{\ \ ,\,\nu} = \bar{h}^{(old)\mu\nu}_{\ \ \ \ ,\,\nu}\,, \tag{1.7}$$

where the symbol $\Box$ is used for the four-dimensional Laplacian:

$$\Box\, f = f^{\,,\,\mu}_{\ \ ,\,\mu} = \eta^{\mu\nu} f_{,\,\mu\nu} = \left(-\frac{\partial^2}{\partial t^2} + \bigtriangledown^2\right) f\,. \tag{1.8}$$

The gauge condition defined via (1.5) is called the Lorentz gauge. We adopt this gauge. In literature harmonic gauge and de Donder gauge

are other names for this gauge. Einstein's tensor, to the first order in $h_{\alpha\beta}$, becomes

$$\mathrm{G}^{\alpha\beta} = -\frac{1}{2}\,\Box\,\bar{h}^{\alpha\beta}\,. \tag{1.9}$$

Thus the weak-field Einstein equations take the form

$$\Box\,\bar{h}^{\mu\nu} = -16\pi\,\mathrm{T}^{\mu\nu}. \tag{1.10}$$

In the Newtonian limit, where the gravitational fields are too weak to produce velocities near the speed of light,

$$\left|\mathrm{T}^{00}\right| \gg \left|\mathrm{T}^{0j}\right| \gg \left|\mathrm{T}^{ij}\right|\,, \quad \mathrm{T}^{00} \simeq \varrho\,, \quad \Box^2 \simeq \bigtriangledown^2. \tag{1.11}$$

Equation (1.10) now results into

$$\bigtriangledown^2\bar{h}^{00} = -16\pi\varrho\,. \tag{1.12}$$

This equation may be compared to the Newtonian equation for gravitational potential φ, i.e.

$$\bigtriangledown^2\varphi = -\,4\pi\varrho\,. \tag{1.13}$$

One obtains, after some calculations

$$h^{00} = 2\varphi\,, \quad h^{xx} = h^{yy} = h^{zz} = -\,2\varphi\,, \tag{1.14}$$

and accordingly the space-time metric for a Newtonian gravitational field is represented via

$$ds^2 = -(1+2\varphi)dt^2 + (1-2\varphi)(dx^2+dy^2+dz^2)\,. \tag{1.15}$$

§1.4 Propagation of gravitational waves

A GW in the region far distant from its source may be described in the weak field approximation. Einstein's equations in the absence of matter and electromagnetic fields ($\mathrm{T}_{\alpha\beta} = 0$) take the form

$$\Box\,\bar{h}^{\mu\nu} = \left(-\frac{\partial^2}{\partial t^2} + \bigtriangledown^2\right)\bar{h}^{\alpha\beta} = 0\,. \tag{1.16}$$

This is the three-dimensional wave equation, and its solution may be taken as

$$\bar{h}^{\alpha\beta} = \mathrm{A}^{\alpha\beta}\exp\left(ik_\gamma x^\gamma\right), \tag{1.17}$$

where $\left\{\mathrm{A}^{\alpha\beta}\right\}$ are constant components of some tensor and $\{k_\alpha\}$ are the constant components of a form satisfying the equation

$$\eta^{\mu\nu}k_\mu k_\nu = k^\nu k_\nu = 0\,. \tag{1.18}$$

This means that (1.17) represents a solution of (1.16) provided k_γ is null form and the associated four vector k^α is null. The value of $\bar{h}^{\alpha\beta}$ is constant on a hyper-surface on which $k_\alpha x^\alpha$ is constant i.e.

$$k_\alpha x^\alpha = k_0 t + \mathbf{k}\cdot\mathbf{x} = const\,, \qquad \mathbf{k} = \{k^i\}\,. \tag{1.19}$$

It is conventional to refer k^0 as w, which is called the frequency of the wave

$$k^\alpha = \{w, \mathbf{k}\}\ . \tag{1.20}$$

The gauge condition (1.5) now requires

$$\mathrm{A}^{\alpha\beta}k_\beta = 0\,, \tag{1.21}$$

which means that $\mathrm{A}^{\alpha\beta}$ must be orthogonal to k_β.

The solution (1.17) represents a plane wave propagating with the velocity of light. In physical applications one has to consider the real part of the solution.

Having the solution $\bar{h}^{\alpha\beta}$ obtained, one still has the freedom of choosing specific ξ^α with the requirement that it represents some solution of the Eq. (1.7) which, in view of (1.16), becomes

$$\left(-\frac{\partial^2}{\partial t^2} + \bigtriangledown^2\right)\xi^\alpha = 0\,. \tag{1.22}$$

Take a solution of it as

$$\xi_\alpha = \mathrm{B}_\alpha \exp(ik_\mu x^\mu)\,, \tag{1.23}$$

where B_α is constant. It can be shown that the freedom available in choosing the values of B_α may be employed such that the new $\mathrm{A}_{\alpha\beta}$ satisfy the conditions

$$\mathrm{A}^\alpha{}_\alpha \ = \ 0\,, \tag{1.24}$$

$$\mathrm{A}_{\alpha\beta}\mathrm{U}^\beta \ = \ 0\,, \tag{1.25}$$

where U^α is some fixed four-velocity. Eqs. (1.21), (1.24), and (1.25) are called the transverse traceless (TT) gauge conditions. We choose U^α as the time basis vector $\mathrm{U}^\alpha = \delta^\alpha_0$. Let the direction of propagation of the wave be the z-axis of the coordinate frame. Now using (1.18) and (1.20) we have k^μ: (w, 0, 0, w). Now Eq. (1.25) in view of (1.21) implies: (i) $\mathrm{A}_{\alpha 0} = 0$, and (ii) $\mathrm{A}_{\alpha z} = 0$ for all α. This is the reason to call the gauge "transverse gauge". Further the trace free condition (1.24) requires $\mathrm{A}_{xx} = -\mathrm{A}_{yy}$. Now the non-vanishing component of $\mathrm{A}_{\alpha\beta}$ may be

expressed as

$$\mathrm{A}^{TT}_{\mu\nu} = \begin{pmatrix} 0 & 0 & 0 & 0 \\ 0 & \mathrm{A}_+ & \mathrm{A}_\times & 0 \\ 0 & \mathrm{A}_\times & -\mathrm{A}_+ & 0 \\ 0 & 0 & 0 & 0 \end{pmatrix}; \quad \mathrm{A}_{xx} = \mathrm{A}_+ \,,\ \mathrm{A}_{xy} = \mathrm{A}_\times \,. \quad (1.26)$$

Thus there are only two independent components of $\mathrm{A}_{\alpha\beta}$, A_+, and $\mathrm{A}_\times$. Note that the traceless condition (1.24) results into

$$\bar{h}^{TT}_{\alpha\beta} = h^{TT}_{\alpha\beta} \,. \quad (1.27)$$

We have considered the plane wave solution of Eq (1.16). We know that any solution of Eqs. (1.21) and (1.16) may be expressed, because of the theorems on Fourier analysis, as a superposition of plane waves. Hence if considering the waves propagating along z-axis, we can put all such planes waves into the form (1.27). Thus any wave has only two independent components h^{TT}_{xx} and h^{TT}_{xy} represented, respectively, as h_+ and $h_\times$ corresponding to A_+ and $\mathrm{A}_\times$.

§1.5 The effect of waves on free particles and its polarization

The independent components h_+ and $h_\times$ represent the polarization states of the wave. To understand their nature in little detail it is instructive to discuss the effect of a GW as it hits a free particle. Let us choose a background Lorentz frame where the particle is initially at rest. We may employ the initial four-velocity of the particle ($\mathrm{U}^\alpha = \delta^\alpha_0$) to define the TT gauge of the wave. A free particle obeys the geodesic equation

$$\frac{d\mathrm{U}^\alpha}{d\tau} + \Gamma^\alpha_{\ \mu\nu}\mathrm{U}^\mu\mathrm{U}^\nu = 0 \,. \quad (1.28)$$

This geodesic equation may be used to obtain the initial acceleration of the particle

$$\left(\frac{d\mathrm{U}^\alpha}{d\tau}\right)_{t=0} = -\,\Gamma^\alpha_{\ 00} = -\,\frac{1}{2}\,\eta^{\alpha\beta}\left(h_{\beta 0,\,0} + h_{0\beta,\,0} - h_{00,\,\beta}\right). \quad (1.29)$$

In view of Eqs. (1.17, 1.26, 1.27), the initial acceleration of the particle vanishes. This means that the particle will be at rest a instant later and, consequently, will be there forever. What does it mean? Is there no effect of a GW on a free particle? No, the interpretation presented at its face value is quite misleading. The result only means that the choice of the TT gauge employed resulted into a coordinate frame for the wave which stays attached to the individual particles.

To get a better measure of the effect of the wave, we consider two nearby particles situated at the origin $(0,0,0)$ and on the x-axis, $(\bar{\epsilon},0,0)$ separated by a distance $\bar{\epsilon}$. In view of the above discussion the particles remain at their initial coordinate positions. The proper distance between them is

$$\begin{aligned}
\triangle l &= \int \left| ds^2 \right|^{1/2} = \int \left| g_{\alpha\beta} dx^\alpha dx^\beta \right|^{1/2} \\
&= \int_0^\epsilon |g_{xx}|^{1/2} \, dx \approx |g_{xx}(x=0)|^{1/2} \, \bar{\epsilon} \\
\triangle l &= \left\{ 1 + \frac{1}{2} \, h_{xx}^{TT}(x=0) \right\} \bar{\epsilon} \, . \qquad (1.30)
\end{aligned}$$

Thus the proper distance between two particles (as opposed to their coordinate distance) does change with time. The effects of the wave may also be described in terms of the geodesic deviation of the separation vector, η^α, connecting these two particles. It obeys the equation

$$\frac{d^2}{d\tau^2} \, \eta^\alpha = \mathrm{R}^\alpha{}_{\mu\nu\beta} \, \mathrm{U}^\mu \mathrm{U}^\nu \eta^\beta . \qquad (1.31)$$

It can be shown that for the particles initially having the separation vector, $\eta^\alpha \to (0,\bar{\epsilon},0,0)$, one would get

$$\frac{\partial^2}{\partial t^2} \, \eta^x = \frac{1}{2} \, \bar{\epsilon} \, \frac{\partial^2}{\partial t^2} \, h_{xx}^{TT} , \quad \frac{\partial^2}{\partial t^2} \, \eta^y = \frac{1}{2} \, \bar{\epsilon} \, \frac{\partial^2}{\partial t^2} \, h_{xy}^{TT} . \qquad (1.32)$$

Similarly, for initial separation vector, $\eta^\alpha \to (0,0,\bar{\epsilon},0)$ we would get

$$\left.\begin{aligned}
\frac{\partial^2}{\partial t^2} \, \eta^y = \frac{1}{2} \, \bar{\epsilon} \, \frac{\partial^2}{\partial t^2} \, h_{yy}^{TT} &= -\frac{1}{2} \, \bar{\epsilon} \, \frac{\partial^2}{\partial t^2} \, h_{xx}^{TT} \\
\frac{\partial^2}{\partial t^2} \, \eta^x = \frac{1}{2} \, \bar{\epsilon} \, \frac{\partial^2}{\partial t^2} \, h_{xy}^{TT} &
\end{aligned}\right\} . \qquad (1.33)$$

Note that, in view of the results of the previous §1.4 of this book, we may write (1.17) as

$$h_{\alpha\beta} = \mathrm{A}_{\alpha\beta} \exp(wt - kz) \, . \qquad (1.34)$$

Thus the separation vector η^α of the particles oscillates.

Consider a ring of particles initially resting in the (x,y) plane as shown in Fig. (1.2-a). Suppose a wave having $h_{xx}^{TT} \neq 0$, $h_{xy}^{TT} = 0$ hits the system of the particles. The particles will be moved (in terms of the proper distance relative to the one in the centre) in the way shown in Fig. (1.2-b). Similarly, for a wave with $h_{xx}^{TT} = 0 = h_{yy}^{TT}$, $h_{xy}^{TT} \neq 0$ the picture would distort as in Fig. (1.2-c). Since h_{xx}^{TT} and h_{xy}^{TT} are indepen-

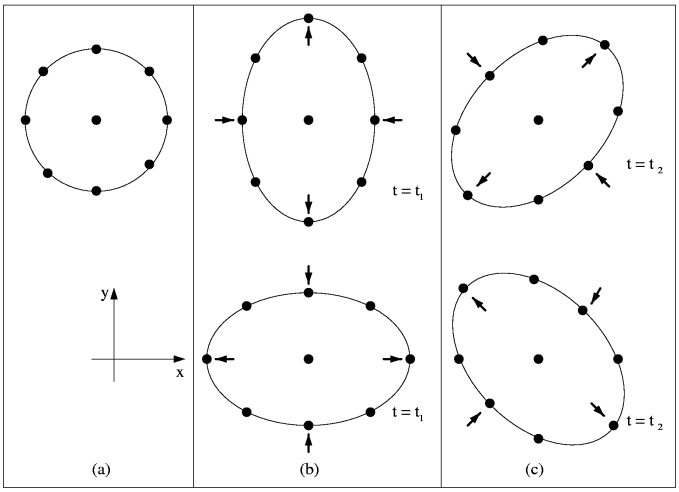

Figure 1.2: (a) A circle of free particles before a wave travelling in the z direction reaches them. The (b) and (c) distortions of the circle are due to a wave with the "+" and "×" polarization. These two pictures represent the same wave at the phases separated by 180°. The particles are positioned according to their proper distances from one another.

dent, Fig. (1.2-b) and (1.2-c) provide the pictorial representation of the polarization states of the wave. Note that these two polarization states are simply rotated by 45° relative to each other. This is in contrast to electromagnetic waves where such two polarization states are at 90° to each other.

§1.6 Generation of gravitational waves

To understand the generation of GW it is sufficient to discuss the weak field limit Equation (1.10), rewritten as

$$\left(-\frac{\partial^2}{\partial t^2} + \bigtriangledown^2\right) \bar{h}_{\mu\nu} = -16\,\pi\,\mathrm{T}_{\mu\nu}\,. \tag{1.35}$$

We assume, for sake of simplicity, the time dependence of $\mathrm{T}_{\mu\nu}$ as a harmonic oscillation of an angular frequency ω, i.e.

$$\mathrm{T}_{\mu\nu} = \mathrm{S}_{\mu\nu}(x^j)\, e^{-i\omega t}\,, \tag{1.36}$$

and look for a solution for $\bar{h}_{\mu\nu}$ in the form

$$\bar{h}_{\mu\nu} = \mathrm{B}_{\mu\nu}(x^j)\, e^{-i\omega t}\,. \tag{1.37}$$

This, in view of Eqs. (1.35) and (1.36), would require $B_{\mu\nu}$ to satisfy

$$\left(\bigtriangledown^2 + \omega^2\right) \mathrm{B}_{\mu\nu} = -\,16\,\pi\,\mathrm{S}_{\mu\nu}\,. \tag{1.38}$$

Outside the source, i.e. where $\mathrm{S}_{\mu\nu} = 0$, we want a solution which would represent outgoing radiation far away. Hence we may take the solution as

$$\mathrm{B}_{\mu\nu} = \left(\frac{\mathbb{A}_{\mu\nu}}{r}\right) e^{i\omega r}\,. \tag{1.39}$$

Obviously, $\mathbb{A}_{\mu\nu}$ is to be related to $\mathrm{S}_{\mu\nu}$. Under the assumption that the region of the space where $\mathrm{S}_{\mu\nu} \neq 0$ is small compared to $\frac{2\pi}{\omega}$, it can be deduced that

$$\mathbb{A}_{\mu\nu} = 4\,\mathrm{J}_{\mu\nu}\,; \quad \mathrm{J}_{\mu\nu} = \int \mathrm{S}_{\mu\nu}\, d^3x\,. \tag{1.40}$$

This assumption is referred to as the slow motion approximation since it implies that the typical velocity inside the source, which is ω times the size of that region, should be much less than 1. All, except the most powerful sources, satisfy this assumption. Thus we get

$$\bar{h}_{\mu\nu} = \left(\frac{4}{r}\right) \mathrm{J}_{\mu\nu}\, e^{i\omega(r-t)}\,. \tag{1.41}$$

This means that the generated GW has the frequency ω. This relation may be expressed in terms of the useful quantities with the help of the following results:

(i) The energy-momentum satisfies the conservation equation

$$\mathrm{T}^{\mu\nu}{}_{,\,\nu} = 0\,, \tag{1.42}$$

(ii) and obeys the identity

$$\frac{d^2}{dt^2} \int \mathrm{T}^{00}\, x^l x^m d^3x = 2 \int \mathrm{T}^{lm} d^3x\,; \tag{1.43}$$

(iii) The quadrupole moment tensor $\mathbf{I}^{lm}$ is defined as

$$\mathbf{I}^{lm} = \int \mathrm{T}^{00}\, x^l x^m d^3x \tag{1.44}$$

and which, in view of (1.36), may be expressed as

$$\mathbf{I}^{lm} = \mathrm{D}^{lm}\, e^{-i\omega t}\,, \tag{1.45}$$

where D^{lm} represents the time independent factor of $\mathbf{I}^{lm}$ (Misner et al., 1973).

The first result gives

$$\mathrm{J}^{\mu o} = 0 \;\Rightarrow\; \bar{h}_{\mu 0}\,, \tag{1.46}$$

whereas the others let us write (1.41) as

$$\bar{h}_{jk} = \left(\frac{-2}{r}\right)\omega^2\,\mathrm{D}_{jk}\,e^{i\omega(r-t)}\,. \tag{1.47}$$

We have still freedom of adopting TT gauge and may use it to achieve further simplification. Let us choose the z-axis along the direction of propagation of the wave. We will then have

$$\bar{h}^{TT}_{zi} = 0\,, \tag{1.48}$$

$$\bar{h}^{TT}_{xx} = -\,\bar{h}^{TT}_{yy} \;=\; -\,\omega^2\,(\mathbb{I}_{xx} - \mathbb{I}_{yy})\left(\frac{e^{i\omega r}}{r}\right), \tag{1.49}$$

$$\bar{h}^{TT}_{xy} = -\left(\frac{2}{r}\right)\omega^2\,\mathbb{I}_{xy}\,e^{i\omega r}\,, \tag{1.50}$$

where $\mathbb{I}_{jk}$ represents the trace free part of the quadrupole moment tensor, i.e.

$$\mathbb{I}_{jk} = \mathbf{I}_{jk} - \frac{1}{3}\,\delta_{jk}\,\mathbf{I}^{i}{}_{i}\,. \tag{1.51}$$

As an application of our results we determine the amplitude of the GW generated by a laboratory source.

§1.6.1 Laboratory generator (bar)

Consider a system of two equal mass points capable to be oscillating about their mean position. Let the system oscillates longitudinally with an angular frequency w about its mean position, i.e.

$$\left.\begin{aligned} x_1 &= -\,\frac{1}{2}\,l_0 - \mathrm{A}\cos\mathrm{w}t \\ x_2 &= \frac{1}{2}\,l_0 + \mathrm{A}\cos\mathrm{w}t \end{aligned}\right\}, \tag{1.52}$$

where l_0 is the normal separation between the mass points, and A represents the amplitude of oscillation. Now it is straight forward to compute $\mathbf{I}_{jk}$. The only non-zero component is

$$\begin{aligned} \mathbf{I}_{xx} &= \mathrm{m}\left[(x_1)^2 + (x_2)^2\right] \\ &= const + \mathrm{mA}^2\cos 2\mathrm{w}t + 2\mathrm{m}l_0\mathrm{A}\cos\mathrm{w}t\,. \end{aligned} \tag{1.53}$$

For purpose of wave generation the constant term is irrelevant. We may obtain the non-vanishing components of $\mathbb{I}_{jk}$ as

$$\left.\begin{aligned} \mathbb{I}_{xx} &= \frac{4}{3}\,\mathrm{m}\,l_0\,\mathrm{A}\,e^{-i\mathrm{w}t} + \frac{2}{3}\,\mathrm{m}\,l_0\,\mathrm{A}^2\,e^{-2i\mathrm{w}t} \\ \mathbb{I}_{yy} = \mathbb{I}_{zz} &= -\frac{2}{3}\,\mathrm{m}\,l_0\,\mathrm{A}\,e^{-i\mathrm{w}t} - \frac{1}{3}\,\mathrm{m}\,l_0\,\mathrm{A}^2\,e^{-2i\mathrm{w}t} \end{aligned}\right\}. \tag{1.54}$$

Finally one obtains, after taking the real part,

$$\left.\begin{aligned} \bar{h}^{TT}_{xx} &= -\,\bar{h}^{TT}_{xy} = -\left[\,2\mathrm{m}\mathrm{w}^2\,l_0\,\mathrm{A}\,\cos(\mathrm{w}(r-t)) \right. \\ &\qquad\qquad \left. + 4\,\mathrm{m}\,\mathrm{w}^2\,\mathrm{A}^2\,\cos(2\,\mathrm{w}\,(r-t))\right]/r \\ \bar{h}^{TT}_{xy} &= 0 \end{aligned}\right\}. \tag{1.55}$$

For a laboratory generator, we take

$$\mathrm{m} = 10^3\ \mathrm{kg}\,, \quad l_0 = 1\ \mathrm{m}\,, \quad \mathrm{A} = 10^{-4}\ \mathrm{m}\,, \quad \mathrm{w} = 10^{-4}\,\mathrm{s}^{-1}. \tag{1.56}$$

The chosen data represent a typical bar detector. Substituting the values after converting them into geometrized units ($\mathrm{G} = 1 = c$) the amplitude of the generated wave is about $10^{-34}/r$

$$|\,h\,| \simeq 10^{-34}/r\,; \qquad \textit{laboratory source.} \tag{1.57}$$

This manifests that laboratory generators are unlikely to produce a useful GW for its demonstration. For sake of comparison, we estimate the strength of the waves produced by powerful astrophysical sources.

§ 1.6.2 Astrophysical sources

For a strong GW we should have $h_{\mu\nu} = O(1)$. This would occur near a source where the Newtonian potential would be of the order 1. For a source of a mass M, this should be at a distance of order M. As we have seen the amplitude of a GW falls off as r^{-1} far distant from the source. This means that the largest amplitude expected to be incident on the Earth would be $\sim$ M/R, where R is the distance between the source and the Earth. For the formation of a 10 $\mathrm{M}_\odot$ black hole in a supernova explosion in a nearby galaxy 10^{23} away, this is about 10^{-17}. Thus

$$|\,h\,|_{max} \simeq 10^{-17}\,; \qquad \textit{astrophysical sources.} \tag{1.58}$$

Thus is in fact an upper limit and less violent events will lead to very much smaller amplitudes.

Chapter 2

GRAVITATIONAL WAVE DETECTORS

§ 2.1 Introduction

The strain produced due to the hitting of a GW in two mass points separated by $\bar{\epsilon}$ is of the order of h. In view of Eq. (1.58) we note that even a strong GW signal would produce a space strain of the order of 10^{-17} that is an unbelievably small effect which would jerk masses spaced at one kilometer by a mere 10^{-20} — one thousand of the diameter of a proton!

Joseph Weber (1960) who pioneered the direct detection of GW constructed an instrument consisting of a massive cylinder of aluminium so-called "bar" detector. Such a detector exploit the sharp resonance of the cylinder to get its sensitivity which is normally confined to a narrow bandwidth (one or a few Hz) around the resonant frequency.

Despite their great potential sensitivity the primary drawback of resonant bars is that they are by definition resonant. They are sensitive mainly to the signal with a frequency corresponding to the bar mechanical ringing frequency of the order of 1 kHz. A bar would respond to the hammer blow of the asymmetrical supernova explosion by simply ringing at its own bell tones and would be excited by a twin neutron star inspiraling only in that brief instant when these two stars crib up through the bell tone frequency.

Bar detectors continue to be developed, and they have until very recently had a sensitivity to broadband bursts. However, the best hope for the first detection of GW lies with large-scale interferometers. Within ten years from now, we may see the launch of a space-based interferometer, LISA, to search for signals at frequencies lower than those that are not accessible from the ground. To measure the strain produced by GW to a bar or an interferometric detector, one must fight against the different sources of noises.

An interesting additional twist is given by the fact that gravitational waves may be accompanied by gamma ray bursts. The GW detectors will then work in coincidence not only with themselves and GW bar antennae, but also with conventional high-energy physics detectors like the underground neutrino experiments and the orbital gamma rays burst monitors.

§2.2 Bar detectors

A bar detector, in its simplest form, may be idealized as a system of two mass points coupled to a spring. Let the system lies on the x-axis of our TT coordinate frame with the masses at the coordinate positions x_1 and x_2. The force free oscillation of the system, in the flat space time, may be expressed via

$$\left.\begin{aligned} \mathrm{m}\, x_{1,\,00} &= -\kappa(x_1 - x_2 + l_0) - \nu(x_1 - x_2)_{,\,0} \\ \mathrm{m}\, x_{2,\,00} &= -\kappa(x_2 - x_1 + l_0) - \nu(x_2 - x_1)_{,\,0} \end{aligned}\right\}, \tag{2.1}$$

where l_0, κ, and ν represent respectively the outstretched length of the spring, spring constant, and damping constant. We can combine these equations to obtain the usual damped harmonic oscillator equation

$$\xi_{,\,00} + 2\gamma\xi_{,\,0} + w_0^2\,\xi = 0 \tag{2.2}$$

by introducing

$$\xi = x_2 - x_1 - l_0\,, \quad w_0^2 = \frac{2\kappa}{\mathrm{m}}\,, \quad \gamma = \frac{\nu}{m}\,. \tag{2.3}$$

We recall that the TT coordinate frame is not convenient for discussion of the dynamics of such a system because in this frame a free particle *always* (before the arrival and after the passage of the wave) remains at rest. However this fact is useful in assigning a local inertial frame $\{x^{\alpha'}\}$ at some TT coordinate. Suppose that the only motions in the system are those produced by the wave then masses velocities will be very small so we may apply Newton's equations of motion for the masses

$$\mathrm{m}\, x^{j'}_{,\,0'0'} = \mathrm{F}^{j'}, \tag{2.4}$$

where $\{\mathrm{F}^{j'}\}$ are the components of any non-gravitational forces on the mass. Further as the coordinates $\{x^{j'}\}$ differ negligibly to the order of $h_{\mu\nu}$ from that of its value $\{x^j\}$ in TT coordinate frame, we may write this equation with a negligible error

$$\mathrm{m}\, x^{j}_{,\,00} = \mathrm{F}^{j}. \tag{2.5}$$

The only non-gravitational force on each mass is due to the spring. The spring exerts a force proportional to its instantaneous proper extensions. If the proper length of the spring is l and the direction of propagation of the wave, for simplicity, is assumed to be along the z-axis then

$$l\,(t) = \int_{x_1(t)}^{x_2(t)} \left[1 + h^{TT}_{xx}(t)\right]^{1/2} dx \approx \left[1 + \frac{1}{2}\, h^{TT}_{xx}(t)\right](x_2 - x_1)\,; \tag{2.6}$$

refer to (1.30). Hence, the equation of motion of the system after the hitting of the wave is given via

$$\left.\begin{aligned} \mathrm{m}\, x_{1,\,00} &= -\kappa (l_0 - l) - \nu (l_0 - l)_{\,,\,0} \\ \mathrm{m}\, x_{2,\,00} &= -\kappa (l - l_0) - \nu (l - l_0)_{\,,\,0} \end{aligned}\right\}. \tag{2.7}$$

Let us define

$$\xi = l - l_0 = \left[1 + \frac{1}{2}\, h_{xx}^{TT}\right](x_2 - x_1) - l_0\,, \tag{2.8}$$

leading to

$$x_2 - x_1 \simeq (\xi + l_0)\left(1 - \frac{1}{2}\, h_{xx}^{TT}\right) = \xi + l_0 - \frac{1}{2}\, h_{xx}^{TT} l_0 + O\left(|h_{\mu\nu}|^2\right). \tag{2.9}$$

Using this equation, we may obtain from Eq. (2.7)

$$\xi_{,\,00} + 2\gamma \xi_{,\,0} + w_0^2 \xi = \frac{1}{2}\, l_0\, h_{xx,00}^{TT} \tag{2.10}$$

correct to the first order in h_{xx}^{TT}.

This is the fundamental equation governing the response of the detector to a GW. It has the simple form of a forced, damped harmonic oscillator.

Let a GW of frequency ω described via

$$h_{xx}^{TT} = \mathrm{A} \cos \omega t \tag{2.11}$$

be hitting the detector. Then the steady solution for ξ may be taken as

$$\left.\begin{aligned} \xi &= \mathrm{R} \cos(\omega t + \varphi) \\ \mathrm{R} &= \frac{1}{2} \frac{l_0 \omega^2 \mathrm{A}}{\left[(w_0 - \omega)^2 + 4\omega^2 \nu^2\right]^{1/2}} \\ \tan \varphi &= \frac{2\nu\omega}{w_0^2 - \omega^2} \end{aligned}\right\}. \tag{2.12}$$

The average energy of the detector's oscillation over one period, $\frac{2\pi}{\omega}$:

$$\langle \mathrm{E} \rangle = \frac{1}{8}\, \mathrm{m} \mathrm{R}^2 (w_0^2 + \omega^2). \tag{2.13}$$

If we wish to detect a specific source whose frequency ω is known, we should adjust w_0 equal to ω for maximum response (resonance).

The resonance amplitude and energy of the detector will be

$$\mathrm{R}_{resonant} = \frac{1}{4}\, l_0\, \mathrm{A}\, \frac{\omega}{\gamma}\,, \tag{2.14}$$

$$\mathrm{E}_{resonant} = \frac{1}{64}\, \mathrm{m}\, l_0^2 \omega^2 \mathrm{A}^2 \left(\frac{\omega}{\gamma}\right)^2. \tag{2.15}$$

The ratio ω/γ is related to what is called the quality factor Q.

$$\mathrm{Q} = \frac{\omega}{2\gamma}\,, \tag{2.16}$$

$$\mathrm{E}_{resonant} = \frac{1}{16}\, \mathrm{m}\, l_0^2 \omega^2 \mathrm{A}^2 \mathrm{Q}^2. \tag{2.17}$$

The bar detectors are massive cylindrical bars; its elasticity provides the function of the spring. When waves hit the bar broadside, they excite its longitudinal modes of vibration. The first detectors built by Weber were aluminium bars of the mass 1.4×10^3 kg, length $l_0 = 1.5$ m, resonant frequency $w_0 = 10^4$ s^{-1} and Q about 10^5. This means that a strong resonant GW of A $= 10^{-20}$ will excite the bar to an energy of the order of 10^{-20} J. The resonant amplitude given by (2.14) is only about 10^{-15} m, roughly the diameter of an atomic nucleus.

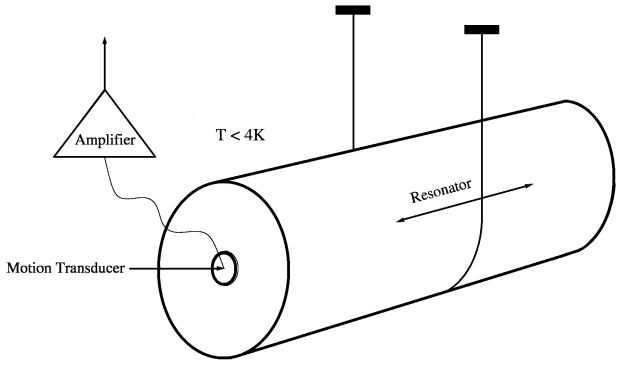

Figure 2.1: A schematic resonant bar detector.

Clearly, the detections of such small levels of excitations will be hampered by random noise in the oscillator. For example, thermal noise in any oscillator induces random vibration with a mean energy of kT, where k is the Boltzmann constant having value 1.38×10^{-23} J/K. At room temperature (T $\sim$ 300K) the thermal noise amounts to the energy $\sim 4\times10^{-21}$ J. Other sources of noise such as vibrations from passing

Detector	Location	Taking data since
NAUTILUS	Frascati, Rome	1993
EXPLORER	Cern (Rome group)	1990
ALLEGRO	Louisiana, USA	1991
AURIGA	Padua, Italy	1997
NIOBE	Perth, Australia	1993

Table 2.1: Location of the resonant bar detectors.

vehicles and every day seismic disturbances could be considerably larger than this, so the apparatus has to be carefully isolated.

A typical "bar" detector consists of an aluminium cylinder with a length $l_0 \sim 3$ m, a resonant frequency of order $w_0 \sim 500$ Hz to 1.5 kHz, and a mass ~ 1000 kg whose mechanical oscillations are driven by GW; see Fig. (2.1). A transducer converts mechanical vibrations of the bar into an electrical signal, which is then amplified by an amplifier and recorded.

Currently there are a number of bar detectors in operation; see Table (2.1). Some of these operate at room temperature and some others at cryogenic temperature. Some detectors (NAUTILUS and EXPLORER) may be cooled down to ultra cryogenic temperature. They can detect signal amplitudes $h \sim 10^{-20}$ in a band width of 10–20 Hz around a central frequency of 1 kHz. Asymmetric supernovae in our Galaxy are the best candidates for these detectors. For example, a supernova collapse in our galaxy at a distance of 10 kpc emits GW of the amplitude $h \sim 10^{-17}$. At present this sensitivity has been achieved by some of the bar detector. They may also see continuous radiation emitted by a neutron star if the frequency happens to lie in their sensitivity band.

§ 2.3 Ground-based laser interferometric detectors

The effect of GW is to produce a transverse shear strain and this fact makes the Michelson interferometer an obvious candidate for such a detector. The Michelson interferometers must have kilometric arms, constituted by "high fineness" Fabry Perot cavities to trap the light for long period and to increase the sensitivity. Laser standing power measured in KW will be stored within the cavities. Beam losses at the level of 10^{-6} per passages are required. The mirrors must be 20

Detector	Location	Length (m)	Corner Location	Arm 1	Arm 2
Glasgow	Glasgow, GBR	10	55.87°N – 4.28°W	77.00°	167.00°
CIT	Pasadena, CA, USA	40	34.17°N – 118.13°W	180.00°	270.00°
MPQ	Garching, GER	30	48.24°N – 11.68°W	329.00°	239.00°
ISAS-100	Tokyo, JPN	100	35.57°N – 139.47°W	42.00°	135.00°
TAMA-20	Tokyo, JPN	20	35.68°N – 139.54°W	45.00°	315.00°
Glasgow	Glasgow, GBR	10	55.87°N – 4.28°W	62.00°	152.00°
TAMA-300	Tokyo, JPN	300	35.68°N – 139.54°W	90.00°	180.00°
GEO-600	Hannover, GER	600	52.25°N – 9.81°W	25.94°	291.61°
VIRGO	Pisa, ITA	3000	43.63°N – 10.5°W	71.50°	341.50°
LIGO	Hanford, WA, USA	4000	46.45°N – 119.41°W	36.80°	126.80°
LIGO	Livingston, LA, USA	4000	30.56°N – 90.77°W	108.00°	198.00°

Table 2.2: The site and orientation of the ground-based interferometric gravitational wave detectors.

or 30 cm in diameter just to hold diffraction losses, and coating with parts per million reflection losses have been developed. Vacuum tubes whose diameter is in the order of a meter are necessary just to contain the diffraction limited laser beams and vacuum exceeding 10 torr is required to prevent the introduction of spurious signal by refraction index fluctuations. The list of the ground-based laser interferometric detector sites and orientations is given in Table (2.2).

The first generation of laser interferometric detectors is in operation. The Japanese TAMA-300 having sensitivity 10^{-20} is collecting data since 1999. The British-German 600 m interferometer (GEO) in Hannover, Germany, the French-Italian 3 km detector (VIRGO) near Pisa, Italy and the American two 4 km antennas (LIGO), one in Livingston and the other in Hanford in the USA had achieved the sensitivity 10^{-21} are also analyzing data for the signature of GW signal. The larger of these detectors, LIGO and VIRGO, are likely to be upgraded in sensitivity by an order of magnitude with a better low-frequency performance. These ground based interferometers will eventually be sensitive to sources in the frequency range from 10 Hz to several kHz.

When a GW, having a frequency high compared to the ~ 1 Hz pendulum frequency, passes through a detector of the arm length l_0 then one arm of the detector gets stretched in one direction whereas the other arm gets compressed. If the total change in the arm-length is δl, the response $R(t)$ of the detector which is defined as $\frac{\delta l}{l_0}$ may be given via

$$R(t) = \frac{\delta l}{l_0} = F_+ \, h_+(t) + F_\times h_\times(t)\,, \tag{2.18}$$

where h_+, $h_\times$ are two polarizations of the signal and F_+, $F_\times$ are the beam pattern functions arising due to the transformation equations relating to the wave frame and the detector frame; refer to Eq. (1.31). Let the detector frame (x, y, z) and the wave frame (X, Y, Z) are related via a transformation matrix $\mathbf{A}$, i.e.

$$\xi^i = \mathbf{A}^i_R \xi^R\,, \quad \xi^k = \mathbf{A}^k_j \xi^j, \tag{2.19}$$

where the capital Roman letters refer to the wave frame quantities, and the lower case of the Romans — for the detector frame quantities. It can be shown that the response of the detector may be expressed as

$$\frac{\delta l}{l_0} = -\sin 2\Omega \big[(\mathbf{A}^x_X \mathbf{A}^y_Y - \mathbf{A}^x_Y \mathbf{A}^y_Y)\, h_+ + (\mathbf{A}^x_X \mathbf{A}^y_Y + \mathbf{A}^x_Y \mathbf{A}^y_X)\, h_\times \big]\,, \tag{2.20}$$

where 2Ω is the angle between the arms of the detector, normally kept equal to 90° (Schutz and Tinto, 1987).

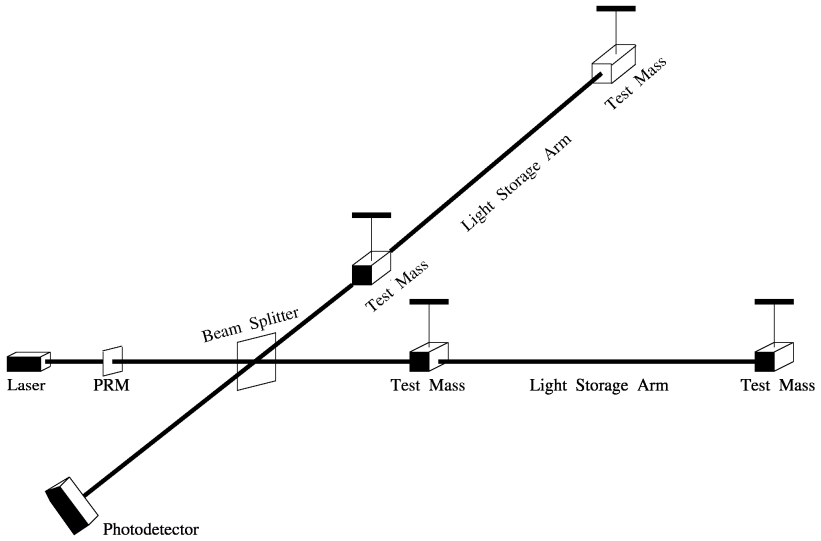

Figure 2.2: A schematic of an Earth-based laser interferometric gravitational wave detector.

A laser interferometric detector consists of four test masses/mirrors that hang from vibration isolated supports as shown in Fig. (2.2). The mirrors facing each other on each arm form a Fabry-Perot cavity. A beam splitter splits a carefully prepared laser beam in two ones, and directs the resulting beams down these two arms. Each beams penetrates through the mass, and through the dielectric coating (the mirror). The length of the arm's of the Fabry-Perot cavity is adjusted to be nearly an integral number of half wave-length of light. The cavity's end mirror has much higher reflectivity than its corner mirror, so the trapped light leaks back out through the corner mirror, and then hits the beam splitter where it recombines with light from the other arm. Most of the recombined light goes back toward the laser (where it can be returned to the interferometer by a "power recycled mirror" labelled PRM, but a tiny portion goes toward the photo-diode).

When a GW hits the detector and moves the masses, thereby changing the lengths of the arms of these two cavities, it shifts each cavity's resonant frequency slightly relative to the laser frequency, and the phase of the light that exists from the cavity toward the beam splitter. Correspondingly, the relative phase of these two beams returning to the splitter is altered by an amount $\triangle\Phi \propto \delta l$, and this relative phase shift

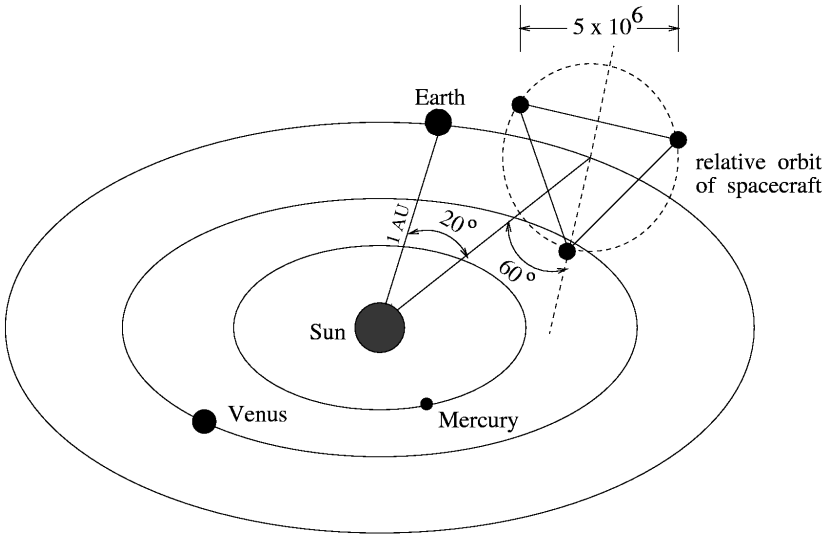

Figure 2.3: A schematic diagram of the laser interferometric space antenna.

causes a change in the intensity of the recombined light at photo-diode, $\triangle I_{pd} \propto \triangle\Phi \propto \delta l \propto R(t)$. Thus, the change of photo-diode output current is directly proportional to the GW strain.

Scientists are now studying the technologies that may be needed for a further improvement of the sensitivity of the detectors. This may involve cooling mirrors, using ultra-massive mirrors of special materials, using purely non-transmissive optics, and even circumventing the quantum limit in interferometers, as has been studied for the bars. The goal of next-generation detectors would be limited just by gravity-gradient noise and quantum effects.

§2.4 Laser interferometric space antenna

Gravity-gradient noise on the Earth is much larger than the amplitude of any expected waves from astronomical sources at frequencies below about 1 Hz, but this noise falls off a $1/r^3$ as one moves away from the Earth. A detector in space would not notice the Earth's noisy environment. The Laser interferometric space antenna (LISA) project, efforts underway by both European Space Agency (ESA) and NASA with a view toward a collaborative mission around 2017–2018, would open up the frequency window between 0.1 mHz and 0.1 Hz.

A concept of the project is shown in Fig. (2.3). Three spacecraft are placed in a solar orbit at 1 A.U., about 20 degrees behind the Earth in it orbit. The spacecrafts are located at the corners of an equilateral triangle with 5×10^6 km long sides. Two arms of the triangle comprise a Michelson interferometer with vertices at the corners. The third arm permits another interferometric observable to be measured, which can determine a second polarization. The interferometers use one micron light as the terrestrial detectors but need only a single pass in the arms to gain the desired sensitivity. The end points of the interferometers are referenced to proof masses which are free-floating within and shielded by the spacecraft. The spacecrafts are incorporated in a feedback loop with precision thrust control to follow the proof masses.

The main environmental disturbances to LISA are the forces from the Sun: fluctuations in the solar radiation pressure and the pressure due to the solar wind. To minimize these, LISA incorporates a drag-free technology. Interferometry is referenced to an internal proof mass that falls freely, not attached to the spacecraft. The job of the spacecraft is to shield this mass from external disturbances. It does this by sensing the position of the mass and firing its own jets to keep itself (the spacecraft) stationary relative to the proof mass. To do this, it needs thrusters of very small thrust that have accurate control. The availability of such thrusters, of the accelerometers needed to sense disturbances to the spacecraft, and of the lasers capable of continuously emitting 1 W infrared light for years, have enabled the LISA mission.

LISA is supposed to see many exciting sources for example the coalescence of giant black holes in the centre of galaxies. LISA will see such events with extraordinary sensitivity, recording typical signal-to-noise-ratios of 1000 or more for events at redshift 1.

Chapter 3

SOURCES OF GRAVITATIONAL WAVES

§3.1 Introduction

Astronomical observations have led to the belief that luminous matter constitutes a small fraction of the total matter content of the Universe. More than 90% of the mass in the Universe is electro-magnetically silent. The presence of dark matter is inferred from the gravitational influence it causes on luminous matter. It is possible that some fraction of this dark matter is a strong emitter of GW. There are many reviews on GW sources (Thorne, 1987; Blair, 1991; Schutz, 1989, 1993, 1999; Sathyaprakash, 1999). The discussion on the GW sources in this Chapter is introductory and for details one may refer to these reviews. The anticipated GW sources can be classified into (i) transients, (ii) continuous, and (iii) stochastic.

§3.2 Supernovae explosions

The type II Supernovae explosions, which are believed to occur as a result of the core collapse of an evolved massive ($> 9M_\odot$) star and which are associated with violent mass ejection with velocities of order 0.03 with formation of a compact remnant — a neutron star or a black hole — may emit significant amount of GW depending upon how asymmetric the collapse is. The emission occurs essentially during the rotational core collapse, bounce and oscillations, rotation-induced bars and convective instabilities set up in the core of the new born neutron star.

Rapid rotation flattens of the collapsing core induces a strong quadrupole moment; thus generating GW. Study of a wide range of rotational core collapse models suggests that the largest signals are produced by models which are (i) initially slow rotating and have a stiff equation of state, or (ii) initially rapid rotating and have a soft equation of state. In the first case bounce occurs at densities above the nuclear matter density, with a fast deceleration of the collapsing core resulting in the emission of GW signals. In the second case, the quadrupole moment is strong due to the rapid rotation which facilitates the emission of GW. However, in either case the signals are not strong enough to be interesting sources for the first generation detectors.

When the core's rotation is *speedy enough* , it may cause the core to flatten before it reaches the nuclear density leading to an instability transforming the flattened core into a bar-like configuration spinning about its transverse axis. Some of these instabilities could also fragment the core into two or more pieces which then rotate about each other. Both are efficient ways of the losing energy in the form of GW.

Instabilities in the core of the newly born neutron star, which last for about a second after the collapse, are likely to produce GW due to anisotropic mass distribution and motion.

§ 3.3 Inspiraling compact binaries

The binary systems whose either member is a compact star e.g. a neutron star (NS) and a black hole (BH) are the most promising transient sources of GW during the phase of their coalescence. The well known binary pulsar PSR $1913+16$ is such a system but it will coalesce in a time scale of 10^9 years from now — not a right candidate. However, there are binaries in our galaxy with coalescence time scale much shorter than this one. Further, statistical analysis of binary pulsars estimates three NS-NS coalescence per year out to a distance of 200 Mpc (Phinney, 1991; Narayanan et al. 1991). The initial LIGO/VIRGO interferometers have a fair chances to see the inspiral events. Compact inspiraling binaries emit quasi-periodic GW with a frequency that sweeps upward toward a maximum frequency. The maximum frequency may be of the order of 1 KHz for neutron stars. In the lower frequency regime the wave form is easily computed from the quadrupole formalism. At higher frequencies post-Newtonian corrections would be required (Thorne, 1987; Królak, 1989). In view of the strong potentialities of such sources the various aspects related to the emission of GW has been dealt extensively in full details, and one may refer to Sathyprakash (1999).

§ 3.4 Continuous gravitational wave

Continuous gravitational wave (CGW) sources are of our prime interest because such sources can be observed again and again and hence single interferometer is sufficient to confirm its detection. However, one can't expect a continuous source to be strong. For emission of GW from pulsars, there should be some asymmetry in it. There are several mechanisms which may lead to deformations of the star, or to precession of its rotation axis. The characteristic amplitude of GW from pulsars scales as

$$h \sim \frac{\mathrm{I} f_0^2 \varepsilon}{r}\,, \tag{3.1}$$

where I is the moment of inertia of the pulsar, f_0 is the GW frequency, ε is a measure of deviation from axissymmetry, and r is the distance between the detector and the pulsar.

As remarked earlier, pulsars are born in supernovae explosions. The outer layers of the star crystallizes as the newborn star pulsar cools by neutrino emission. Estimates, based on the expected breaking strain of the crystal lattice, suggest that anisotropic stresses, which build up as the pulsar looses rotational energy, could lead to $\varepsilon \leqslant 10^{-5}$; the exact value depends on the breaking strain of the neutron star crust as well as the neutron star's "geological history", and could be several orders of magnitude smaller. Nonetheless, this upper limit makes pulsars a potentially interesting source for kilometer scale interferometers.

Large magnetic fields trapped inside the super fluid interior of a pulsar may also induce deformation of the star. This mechanism has been explored recently, indicating that the effect is extremely small for standard neutron star models ($\varepsilon \leqslant 10^{-9}$).

Another plausible mechanism for CGW is the Chandrasekhar-Friedman-Schutz (CFS) instability, which is driven by GW back reaction. It is possible that newly-formed neutron stars may undergo this instability spontaneously as they cool soon after formation. The frequency of the emitted wave is determined by the frequency of the unstable normal mode, which may be less than the spin frequency.

Accretion is another way to excite neutron stars. There is also the Zimmermann-Szedinits mechanism where the principal axes of the moment of inertia are driven away from the rotational axes by accretion from a companion star. Accretion can in principle produce a relatively strong wave since the amplitude is related to the accretion rate rather than to structural effects in the star.

§ 3.5 Stochastic waves

Catastrophic processes in the early history of Universe, as well as the astrophysical sources distributed all over the cosmos, generate stochastic background of GW. A given stochastic background will be characteristic of the sources that are responsible for it and it may be possible to discriminate different backgrounds provided their spectral characteristics are sufficiently different.

Primordial background: It is believed that similar to cosmic microwave background (CMBR) a GW background was also produced at the same time as a result of quantum fluctuations in the early Universe (Grischuk, 1997). Primordial background radiation would freely travel

to us from almost the very moment of the creation because GW couples very weakly with matter. Hence, its detection would help us in the getting a picture of the first moments after the big bang. The COBE data have set limits on the strength of the GW background. The strength are far too weak to be detected by any running ground-based detectors. However, advanced LIGO detectors may observe the background generated by the collisions of a cosmic string network (for details one may refer to Allen, 1997).

Phase transitions in the early Universe, inspired by fundamental particle physics theories, and cosmological strings and domain walls are also sources of a stochastic background. These processes are expected to generate a background which has a different spectrum and strength than the primordial one. Future ground-based detectors will achieve good enough sensitivity to measure this background GW and such measurements will prove to be a good test bed for these cosmological models.

Supernovae background: Even though an individual supernova may not be detectable out to a great distance, the background produced by all supernovae within the Hubble radius might indeed be detected (Blair and Ju, 1996). The coincidence between an advanced interferometer and a resonant bar within 50 km of the interferometer will enable the detection of this background. These studies may shed light on the history of star formation rate, a subject of vigorous debate amongst astrophysicists.

Galactic binary background: Binaries with orbital periods $P \sim 10^{-4} - 10^{-2}$ s will be observable in space-based detectors. A large number of them are present in our galaxy but they will not be identifiable separately because they are at a large distances and consequently have a feeble amplitude. However they would contribute to background GW. In addition to binaries of compact stars, there are also other binaries consisting of white dwarfs, cataclysmic variables, etc., which will also contribute to the background radiation produced by compact binaries. The net effect is that these sources will appear as a background noise in space interferometers. By studying the nature of this background one can learn a lot about binary population in our Galaxy.

Galactic pulsar background: CGW from pulsars could also produce a background of GW radiation which will limit the sensitivity of the ground-based laser interferometers (Giazotto, Gourgoulhon, and Bonazzola, 1997). There are about 10^9 neutron stars in our Galaxy of which

about 2×10^5 will contribute to the background radiation. This background radiation will be prominent and observable in the LIGO/VIRGO detectors, in the frequency range of 5–10 Hz, at an rms amplitude of $h_{rms} \sim 2\times10^{-26}$, where the rms is computed over 10^5 sources. At frequency of 10 Hz, the wavelength of GW will be around 30,000 km. Hence, it would be possible to cross-correlate data from two distant detectors, such as two LIGOs, or LIGO and VIRGO, and discriminate the background against other sources of noise.

Chapter 4

DATA ANALYSIS CONCEPT

§4.1 Introduction

The GW data analysis strategy is different in many ways from conventional astronomical data analysis. This is due to the following:

- GW antennae are essentially omni-directional with their response better than 50% of the average over 75% of the sky. Hence our data analysis systems will have to carry out all-sky searches for the sources;
- Interferometers are typically broad-band covering 3 to 4 orders of magnitude in the frequency. While this is obviously to our advantage, as it helps to track sources whose frequency may change rapidly, it calls for searches to be carried over a wide-band of frequencies;
- In contrast to electromagnetic (EM) radiation, most astrophysical GWs are tracked in the phase, and the signal-to-noise ratio (SNR) is built up by coherent superposition of many wave cycles emitted by a source. Consequently, the SNR is proportional to the amplitude and only falls off, with the distance to the source, r, as $1/r$. Therefore, the number of sources of a limiting SNR increases as r^3 for a homogeneous distribution of the sources in a flat Universe, as opposed to EM sources that increase only as $r^{3/2}$;
- GW antennae acquire data continuously for many years at the rate of several mega-bytes per second. It is expected that about a hundredth of this data will have to pass through our search analysis systems. Unless on-line processing can be done we cannot hope to make our searches. This places huge demands on the speed of our data analysis hardware. A careful study of our search algorithms with a view to making them as optimal (maximum SNR) and efficient (least search times) as one possibly can is required.

§4.2 Gravitational wave antenna sensitivity

The performance of a GW detector is characterized by the one sided *power spectral density* (PSD) of its noise background. The analytical fits

to noise power spectral densities $S_n(f)$ of ground based interferometers are given in Table (4.2), where S_0 and f_{n_0} represent respectively the value of the minimum noise and the corresponding frequency. At the lower-frequency cutoff f_l and the high-frequency cutoff f_u, $S_n(f)$ can be treated as infinite. One can construct the noise PSD as follows.

A GW detector output represents a dimensionless data train, say $x(t)$. In the absence of any GW signal the detector output is just an instance of noise $n(t)$, that is, $x(t) = n(t)$. The noise auto-correlation function c is defined as

$$\mathrm{c}\,(t_1, t_2) \equiv \langle n(t_1)\, n(t_2)\rangle, \tag{4.1}$$

where $\langle\ \rangle$ represents the average over an ensemble of the noise realizations. In general, c depends on both t_1 and t_2. However, if the detector output is a stationary noise process, i.e. its performance is, statistically speaking, independent from time, c depends only on $\tau \equiv t_2 - t_1$. We shall, furthermore, assume that $\mathrm{c}\,(\tau) = \mathrm{c}\,(-\tau)$. For data from real detectors the above average can be replaced by a time average under the assumption of ergodicity:

$$\mathrm{c}\,(\tau) = \frac{1}{T}\int_{-T/2}^{T/2} n(t)\, n(t-\tau)\, dt\,. \tag{4.2}$$

The assumption of stationarity is not strictly valid in the case of real GW detectors; however, if their performance does not vary greatly over time scales much larger than typical observation time scales, stationarity could be used as a working rule. While this may be good enough in the case of binary inspiral and coalescence searches, it is a matter of concern for the observation of continuous and stochastic GW. Under such an assumption the one-sided noise PSD, defined only at positive frequencies, is the Fourier Transform (FT) of the noise auto-correlation function:

$$\begin{aligned} S_n(f) &\equiv \frac{1}{2}\int_{-\infty}^{\infty} \mathrm{c}\,(\tau)\, e^{-2\pi i f\tau}\, d\tau, \quad f \geqslant 0\,, \\ &\equiv 0\,, \qquad f < 0\,, \end{aligned} \tag{4.3}$$

where a factor of $\frac{1}{2}$ is included by convention because it has been assumed that $\mathrm{c}\,(\tau)$ is an even function. This equation implies that $S_n(f)$ is real. It is straightforward to show that

$$\langle \tilde{n}(f)\, \tilde{n}^*(f')\rangle = S_n(f)\, \delta\,(f - f')\,, \tag{4.4}$$

where $\tilde{n}(f)$ represents the Fourier transform of $n(t)$ and * denotes complex conjugation. This identity implies that $S_n(f)$ is positive definite.

Detector	Fit to noise power spectral density	S_0 $(\mathrm{Hz})^{-1}$	f_{n_0} (Hz)	f_l (Hz)	f_u (Hz)
LIGO I	$\frac{S_0}{3}\left[\left(\frac{f_{n_0}}{f}\right)^4+2\left(\frac{f}{f_{n_0}}\right)^2\right]$	8.0×10^{-46}	175	40	1300
LIGO II	$\frac{S_0}{11}\left\{2\left(\frac{f_{n_0}}{f}\right)^{9/2}+\frac{9}{2}\left[1+\left(\frac{f}{f_{n_0}}\right)^2\right]\right\}$	7.9×10^{-48}	110	25	900
LIGO III	$\frac{S_0}{5}\left\{\left(\frac{f_{n_0}}{f}\right)^4+2\left[1+\left(\frac{f}{fn_0}\right)^2\right]\right\}$	2.3×10^{-48}	75	12	625
VIRGO	$\frac{S_0}{4}\left[290\left(\frac{f_s}{f}\right)^5+2\left(\frac{f_{n_0}}{f}\right)+1+\left(\frac{f}{f_{n_0}}\right)^2\right]$	1.1×10^{-45}	475	16	2750
GEO600	$\frac{S_0}{5}\left[4\left(\frac{f_{n_0}}{f}\right)^{3/2}-2+3\left(\frac{f}{f_{n_0}}\right)^2\right]$	6.6×10^{-45}	210	40	1450
TAMA	$\frac{S_0}{32}\left\{\left(\frac{f_{n_0}}{f}\right)^5+13\left(\frac{f_{n_0}}{f}\right)+9\left[1+\left(\frac{f}{f_{n_0}}\right)^2\right]\right\}$	2.4×10^{-44}	400	75	3400

Table 4.1: Analytical fits to noise power spectral densities $S_n(f)$ of the ground-based interferometers.

The autocorrelation function $\mathrm{c}(\tau)$ at $\tau = 0$ can be expressed as an integral over $S_n(f)$. Indeed, it is easy to see that

$$\langle n^2(t)\rangle = 2\int_0^\infty S_n(f)\,df\,. \tag{4.5}$$

The above equation justifies the name *power spectral density* given to $S_n(f)$. It is obvious that $S_n(f)$ has a dimension of time but it is conventional to use, instead, a dimension of Hz^{-1} since it is a quantity defined in the frequency domain. The square-root of $S_n(f)$ is the noise amplitude, $\sqrt{S_n(f)}$, and has a dimension of *per root Hz*. It is often useful to define the dimensionless quantity $h_n^2(f) \equiv fS_n(f)$ called the *effective noise*. In GW interferometer literature one also comes across the *displacement noise* or *strain noise* defined as $h_{l_0}(f) \equiv l_0 h_n(f)$, and the corresponding noise spectrum $S_{l_0}(f) \equiv l_0^2 S_n(f)$, where l_0 is the arm length of the interferometer. The displacement noise gives the smallest strain $\delta l/l_0$ in the arms of an interferometer which can be measured at a given frequency.

§ 4.2.1 Sensitivity vs source amplitudes

One compares the GW amplitudes of astronomical sources with the instrumental sensitivity and assesses what sort of sources will be observable in the following way. First, as comparisons are almost always made in the frequency-domain, it is important to note that the Fourier component $\tilde{h}(f)$ of a deterministic signal $h(t)$ has a dimension of Hz^{-1} and the quantity $f\,|\tilde{h}(f)|$ is dimensionless. It is the last quantity that should be compared with $h_n(f)$ to deduce the strength of a source relative to the detector noise. Second, it is quite common also to compare the amplitude spectrum per logarithmic bin of a source, $\sqrt{f}\,|\tilde{h}(f)|$, with the amplitude spectrum of the noise, $\sqrt{S_n(f)}$, both of which have dimensions of per root Hz. For monochromatic sources, one compares the effective noise in a long integration period with the expected "instantaneous" amplitudes in the following way: a monotonic wave of a frequency f_0 observed for a time T_0 is simply a narrow line in a frequency bin of width $\Delta f \equiv 1/T_0$ around f_0. The noise in this bin is $S_n(f)\Delta f = S_n(f)/T_0$. Thus the SNR after a period of observation T_0 is

$$\frac{S}{N} = \frac{h_0}{\sqrt{S_n(f_0)/T_0}}\,. \tag{4.6}$$

One, therefore, computes this dimensionless noise spectrum for a given duration of observation, $S_n(f)/T_0$, to assess the detectability of a continuous GW. Surely, if the observation time is T_0 then the total

energy (that is, the integrated power spectrum) of both signal and noise must increase in proportion to T_0^2. Then how does the SNR for a continuous wave improve with the duration of observation? The point is that while the signal energy is all concentrated in one bin, the noise is distributed over the entire frequency band. As T_0 increases, the frequency resolution improves as $1/T_0$ and the number of the frequency bins increases in proportion to T_0. Consequently, the noise intensity *per frequency bin* increases only as T_0. Now, the signal intensity is concentrated in just one bin since the signal is assumed to be monochromatic. Therefore, the power SNR increases as T_0, or, the amplitude SNR increases as $\sqrt{T_0}$.

§4.3 Noises in the Earth-based interferometric detectors

As mentioned in the earlier section the performance of GW detector is characterized by the one-sided PSD. The sensitivity of ground-based detectors is limited at frequencies less than a Hertz by the time-varying local gravitational field caused by a variety of different noise sources, e.g. low frequency seismic vibrations, density variation in the atmosphere due to winds, etc. Thus, for data analysis purposes, the noise PSD is assumed to be essentially infinite below a certain lower cutoff f_s. The effective noise $h_n(f)$ expected in these detectors is equal to $\sqrt{fS_n(f)}$. Type of noises that one have to fight to detect the signals are:

Ground vibration: External mechanical vibrations are a problem for bar detectors, too, but are more serious for interferometers, not least because interferometers bounce light back and forth between the mirrors, and so each reflection introduces further vibrational noise. Suspension/isolation systems are based on pendula. A pendulum is a good mechanical filter for frequencies above its natural frequency. By hanging the mirrors on pendula of perhaps 0.5 m length, one achieves filtering below a few Hz. Since the spectrum of ground noise falls at higher frequencies, this provides suitable isolation. But these systems can be very sophisticated; the GEO600 detector has a three-stage pendulum and other vibration isolation components. Among all the ground based laser interferometer detectors, VIRGO has the best isolation system.

Thermal noise: Vibrations of the mirrors and of the suspending pendulum can mask gravitational waves. As with vibrational noise, this is increased by the bouncing of the light between the mirrors. Unlike bars, interferometers process measurements only at the frequencies which are far from the resonant frequency, where the amplitude of vibration is smaller. Thus, the pendulum suspensions have thermal noises at a few

Hz, but measurements were performed at above 20 or 30 Hz in the first detectors. Internal vibrations of the mirrors have natural frequencies of several kilohertz. By ensuring that both kinds of oscillations have very high Q, one can confine most of the vibration energy to a small bandwidth around the resonant frequency, so that at the measurement frequencies the vibration amplitudes are small. This allows interferometers to operate at room temperature. But mechanical Qs of 10^7 or higher are required, and this is technically demanding.

Shot noise: The photons that are used to do interferometry are quantized, so they arrive at random and make random fluctuations in the light intensity that can look like a gravitational wave signal. The more photons one uses, the smoother will be the interference signal. As a random process, the error improves with the square-root of the number N of photons. Using infrared light with a wavelength $\lambda \sim 1\,\mu$m, one can expect to measure to an accuracy of

$$\triangle \mathrm{L}_{shot} \sim \frac{\lambda}{2\pi\sqrt{\mathrm{N}}}\,.$$

To perform measurement at a frequency f, one has to make at least $2f$ measurements per second i.e. one can accumulate photons for a time $\frac{1}{2}f$. With light power P and GW amplitude h one gets $\mathrm{N} = \frac{\mathrm{P}}{(hc/\lambda)(2f)}$ photons. In order that $\triangle \mathrm{L}_{shot}$ be below 10^{-16} m, one needs strong light power far beyond the output of any continuous laser.

Light-recycling techniques overcome this problem by using light efficiently. An interferometer actually has two places where light leaves. One is where the interference is measured. The other goes back towards the input laser. Normally one arranges that no light goes to the interference sensor, so that only when a gravitational wave passes makes a signal registered there. This means that all the light normally returns to the mirror, apart from small losses at the mirrors. Since mirrors are of good quality, only one part in 10^3 or less of the light is lost during a 1 ms storage time. By placing a power-recycling mirror in front of the laser, one can reflect this wasted light back in, allowing power to build up in the arms until the laser merely resupplies the mirror losses. This can dramatically reduce the power requirement for the laser.

Quantum effects: Shot noise is a quantum noise, but in addition there are effects like bar detectors face: zero-point vibrations of mirror surfaces and so on. These are small compared to present operating limits of detectors, but they may become important in 5 years or so. Practical schemes to reduce this noise have already been demonstrated

in principle, but they need to be improved considerably. They can be reduced by making the mirror masses large, since the amplitude of vibration scales inversely as the square-root of the mass.

Gravity gradient noise: One noise which cannot be screened out is that arises due to changes in the local Newtonian gravitational field on the time scale of the measurements. A gravitational wave detector will respond to tidal forces from local sources just as well as to gravitational waves. Environmental noise comes not only from man-made sources, but even more importantly from natural ones: seismic waves are accompanied by changes in the gravitational field, and changes in air pressure are accompanied by changes in air density. The spectrum falls steeply with increasing frequency. Hence, the running interferometers does not have problem, but it may limit the performance of detectors a decade from now. And it is the primary reason that detecting gravitational waves in the low-frequency band around 1 mHz must be done in space.

§4.4 Matched Filtering and optimal signal-to-noise ratio

Matched Filtering is a data analysis technique that efficiently searches for a signal of known shape buried in the noisy data (Helstrom, 1968). The technique consists in correlating the noisy output of each interferometer data with a set of theoretical waveform templates. If the maximum of the correlation exceeds a preset threshold, a detection is announced. However, even if a signal is present in the data, the accompanying noise can mask its presence by preventing such crossing of the threshold in some cases. Thus a signal can be detected with only a certain probability called the detection probability. Also there will be a non-zero probability called the false alarm probability, of a false detection due to noise alone. A formalism to choose the optimal set of templates using a criterion was first given by Sathyaprakash and Dhurandhar (1991), and Dhurandhar and Sathyaprakash (1994) known as the S-D formalism.

These search templates will be discrete subset of a continuous, multi parameter family, each of which approximate a possible signal. Given a signal $h(t)$ buried in a noise $n(t)$, the task is to find an "optimal" template $q(t)$ that would produce, on the average, the best possible SNR. The enhancement in the signal-to-noise ratio not only increases the number of detectable events but, more importantly, it also allows a more accurate determination of signal parameters — the error in the estimation of parameter being inversely proportional to the signal-to-noise ratio.

If the functional form of the template is identical to that of the sig-

nal, the mean signal-to-noise ratio in the presence of a signal is highest of the possible for any linear data processing technique, which is why matched filtering is also known as optimal filtering (Helstrom, 1968). A *matched filter*, in the frequency domain, is a best-guess template of the expected signal waveform divided by the interferometer's spectral noise density.

In order to take full advantage of matched filtering it is essential that the phase of the waveform shall be known to a very high degree of accuracy to accumulate the SNR (Cutler et al., 1993). This is referred to as coherent integration of the signal, where the SNR grows $\sqrt{T_0}$. This is in contrast to incoherent methods, such as *stacking* and *tracking* (Brady et al., 1998, 2000), where one disregards the phase information and the SNR does not accumulate as quickly. *Tracking* involves tracking of lines in the time-frequency plane built from the FT of short (around 40 minutes long) stretches of data. The other *stacking* involves dividing the data into shorter (around a day long) stretches, searching each stretch for signals, and enhancing the detectability by incoherently summing the FT of data stretches.

There are several questions that must be answered in order to determine the feasibility of a matched filtering search strategy and, if feasible, to implement it. Which parameters significantly affect the wave form? How should the spacing of the template parameters (lattice points) be chosen? Is there a parametrization that is in some sense preferred by the template waveforms? How many templates are needed to cover a given region of interest in the parameter space and how much computing power and memory will it cost to process the data through them? In the case of a modulated pulsar signal we must also ask what approximation to the true wave form is good enough?

Ambiguity function, well known in the statistical theory of signal detection (Helstrom, 1968), is a very powerful tool in signal analysis. It helps to access the number of templates required to span the parameter space of the signal. However, Apostolatos (1995) defined a term called *Fitting Factor* (FF) which quantitatively describes the closeness of the true signals to the template manifold in terms of the reduction in SNR due to cross correlation of a signal outside the manifold with all the templates lying inside the manifold.

§4.4.1 Fitting factor

One of the standard measurements for deciding what class of wave form is good enough is the *Fitting Factor* and has already been used by

various authors* as a measure of adequateness of a template family, but previous discussions have not shown explicitly how this intuitively well-formed function is connected with detectability.

Previously FF has sometimes been called the "correlation", a number that is often used in so many different ways. The name comes from the fact that, by maximizing the quantity FF, the parameters of the templates can be adjusted to best fit of the true waveform.

Consider a detector receiving almost monochromatic GW signals from a pulsar. The signal will be Doppler modulated due to the motion of the Earth and stars, represented by the function $S(t)$. The output $X(t)$ of the detector will be

$$X(t) = S(t) + n(t)\,. \tag{4.7}$$

If the search template is the exact waveform $h(t)$, we achieve the highest possible signal-to-noise ratio given as

$$\left(\frac{S}{N}\right)_{max} = \langle S(f)|S(f)\rangle^2. \tag{4.8}$$

where the inner product of two waveforms $\langle h_1|h_2\rangle$ is defined as

$$\begin{aligned}\langle h_1|h_2\rangle &= 2\int_0^\infty \frac{\tilde{h}_1^*(f)\tilde{h}_2(f) + \tilde{h}_1(f)\tilde{h}_2^*(f)}{S_n(f)}\,df \\ &= 4\int_0^\infty \frac{\tilde{h}_1^*(f)\tilde{h}_2(f)}{S_n(f)}\,df\,.\end{aligned} \tag{4.9}$$

The SNR ratio will be reduced below $(S/N)_{max}$ whenever the template is not the exact waveform but some other approximate one. In the case where the search is performed with some family of templates $S_T(f;\vec{\xi})$ for a signal vector $\vec{\xi}$ (the signal is considered as a vector in the parametric space), then the SNR is given by

$$\left(\frac{S}{N}\right) = \overset{max}{\vec{\xi}}\ \frac{\langle X(f)|S_T(f;\vec{\xi})\rangle}{rms\langle n|S_T(f;\vec{\xi})\rangle}\,. \tag{4.10}$$

For an ensemble of realizations of the detector noise, the expectation values $\langle n|S_T(f;\vec{\xi})\rangle$ and $\langle n|S_T(f;\vec{\xi})\rangle\langle n|S_T(f;\vec{\xi})\rangle$ are zero, and $\langle S_T(f;\vec{\xi})|S_T(f;\vec{\xi})\rangle$, respectively. Thus the ensemble-averaged signal-to-noise ratio turns out to be

*Sathyaprakash and Dhurandhar (1991), Dhurandhar and Sathyaprakash (1994).

$$\left(\frac{S}{N}\right) = \overset{max}{\vec{\xi}} \frac{\langle S(f)|S_T(f;\vec{\xi})\rangle}{\sqrt{\langle S_T(f;\vec{\xi})|S_T(f;\vec{\xi})\rangle}}$$
$$= \left[\overset{max}{\vec{\xi}} \frac{\langle S(f)|S_T(f;\vec{\xi})\rangle}{\sqrt{\langle S_T(f;\vec{\xi})|S_T(f;\vec{\xi})\rangle\langle S(f)|S(f)\rangle}}\right]\left(\frac{S}{N}\right)_{max}. \quad (4.11)$$

The name *Fitting Factor* is given to the reduction in signal-to-noise ratio that results because of using the chosen template family, rather than the true signal h, in the search:

$$FF(\vec{\xi}) = \overset{max}{\vec{\xi}} \frac{\langle S(f)|S_T(f;\vec{\xi})\rangle}{\sqrt{\langle S_T(f;\vec{\xi})|S_T(f;\vec{\xi})\rangle}}$$
$$= \overset{max}{\vec{\xi}} \frac{\langle S(f)|S_T(f;\vec{\xi})\rangle}{\sqrt{\langle S_T(f;\vec{\xi})|S_T(f;\vec{\xi})\rangle\langle S(f)|S(f)\rangle}}. \quad (4.12)$$

Therefore, if the family of search template used at the detection stage does not contain the true signal waveform, the reduction in the signal-to-noise ratio will be given by

$$\left(\frac{S}{N}\right) = FF(\vec{\xi}) \times \left(\frac{S}{N}\right)_{max} \quad (4.13)$$

The spacing of the grid of filters is decided by the fractional loss due to the imperfect match that can be tolerated. Given the parameters space that one needs to scan, it is then easy to estimate the total number of filters required to carry out the search for the signal. The signal strength scales is inverse with distance, the fraction of event rate retained is approximately FF^3. Therefore it has become conventional to regard $FF = 0.9$ as the lowest acceptable FF value for some template family to be considered adequate. A reduction in SNR by 10% means a 27% loss in the event rate. On the other hand a 10% reduction in SNR is equivalent to a roughly 10% shortening of the detectors arms.

§4.5 Computational costs

Matched Filtering places stringent demands on the knowledge of the signal's phase evolution which depends on two things: (i) our modelling of the signal, and (ii) the parameters characterizing the signal. If our signal model is inaccurate or if the signal's parameters are unknown, there could be a loss in the SNR extracted. For instance, in the case of

inspiral signals, a mismatch of one cycle in 10^4 cycles leads to a drop in the SNR by more than a factor of two, losing a factor of eight in the number of potentially detectable events. Recall that the SNR is inversely proportional to the distance to a source; thus an SNR loss by a factor "a" will reduce the span of a detector by the same factor, resulting a decrease in the volume of observation, and hence the number of events, by a factor a^3. Moreover, since the parameters of a signal will not be known in advance, it is necessary to filter the data with a family of templates located at various points in the parameter space e.g., placed on a lattice such that any signal will lie close enough to at least one of the templates to have a good cross-correlation with that template. The number of such templates is typically very large. This places a great demand on the computational resources needed to make an on-line search.

The search problem for continuous waves from spinning neutron stars is the most computer-intensive job in gravitational wave data analysis. Today, there is little hope that all-sky searches lasting for a year or more can be made. It is easy to see why this is such an intensive job: first, the data has to be collected continuously for months together and at a good sensitivity; second, though a neutron star emits a periodic signal in its rest frame, save for the neutron star spin-down which indeed induces some modulation in the waveform, because of the Earth's acceleration relative to the source, the detector does not see a periodic wave. The wave is both frequency and amplitude modulated. One can, fortunately, de-modulate these effects since the Earth's motion is known quite accurately, and hence recover the original periodic signal. But de-modulation requires a knowledge about the source's direction and its frequency, which are unknown in a blind search. The angular resolution one obtains in a year's integration is $\Delta\theta = \lambda/D$, where λ is the wave length of radiation and D is the baseline of the detector in a year's integration, namely 1 A.U. Thus, for $f = 1$ kHz we have $\Delta\theta = 10^{-6}$ rad or about two arcsec. Now, assuming that the source may be in any one of the 4 arcsec^2 patches on the sky we get the number of patches in the sky for which we will have to try out a de-modulation correction to be $4\pi/(\Delta\theta)^2 = 4\pi\times10^{12}$. It is a quite impossible task to apply Doppler de-modulation to the detector output for each of these $\sim 10^{13}$ paths and compute as many Fourier transforms.

One, therefore, asks a question: given a compute power what is the best possible search one can do? Is there any advantage in going from a one-step search to a two or multi-step hierarchical search? What about directional searches? These are some of the problems for which we have

some answer; but a great deal of work is needed and is currently under progress, to improve and optimize search algorithms.

The differential geometric studies shows that with a TFLOPS-class computer, the number of days of data can be analyzed on-line and we can carry out a blind search. Unfortunately, the longest data we can integrate on-line for neutron stars with spin frequencies $f \leqslant 100$ Hz and spin-down rates less than 1000 years is about 18 days. This yields a SNR lower by a factor of 5 as compared to a year's worth of observing. On-line searches for neutron stars with $f \leqslant 500$ Hz (the largest observed frequencies of millisecond pulsars) and spin-down rates of 40 years (shortest observed spin-down rates) can only be made for a data set lasting for a duration of 20 hours or less. If source's position is known in advance, but not its frequency, then one can carry out an on-line search, again with a TFLOPS-class computer, for the frequency of the source in a data set that is worth 3 months long. This is good news since there are many known pulsars and X-ray binary systems that are potential sources of radiation. In addition, the obvious targeted search locations are the centre of the Galaxy and globular clusters.

There have been efforts to study the effectualness of a two-step hierarchical method for a blind search. Here the basic idea is to construct Fourier transforms of data sets of duration smaller than the period in which Doppler modulations will be important and to stack spectral densities obtained in this way and to add them all up. This is an incoherent way of building the signal since one adds spectral densities that have no phase information. Therefore, one gains in SNR less than what an optimal matched filtering method is able to achieve. However, this does not matter since (i) the targeted SNR's are quite high ~ 10, and (ii) candidate events can always be followed-up using coherent integration methods. These methods afford an on-line all-sky blind search for continuous gravitational waves for a period of 4 months or less using a 20 GFLOPS computer.

§ 4.6 Detection criteria

A signal needs to be above the noise experienced in the instrument and environment. However, this alone is insufficient to establish it as a gravitational wave in the terrestrial detectors. The most satisfying circumstance is that a gravitational wave observation be made in a set of widely distributed detectors (the Gravitational Wave Network, or GWN in short) and the resorted wave forms allow the solutions for the polarization of the wave and the position of the source. Armed

with this information an electromagnetic (or neutrino) search could be attempted in the error circle of the gravitational wave detection: a time honoured approach bringing gravitational wave of observation into the main stream of Astrophysics. The strategy would apply to all classes of sources: impulsive chirps, quasiperiodic and periodic.

The confident detection of impulsive sources is most difficult, while the periodic and quasiperiodic detection will have confidence limits based on quasi-stationary system noise (the signals last long enough to take a meaningful sample of the noise spectrum), the impulsive signals especially if rare, will be particularly dependent of the non-Gaussian component of the noise; the noise most difficult to reduce and control in a signal detectors. The technique of multiple coincidence of several detectors is one of the best means to gain confidence. The coincidence must occur within a time window to permit a consistent solution for a location in the sky. If the general character of the source can be guessed in advance (for example, a binary coalescence chirp, or a black-hole normal mode oscillation), the signal is filtered prior to the coincidence measurement to improve the sensitivity. The more detectors involved, the greater the confidence assigned to the detection.

There is still a possibility of coincidence due to environmental or anthropogenic causes. The various sites throughout the world are far enough apart that most environmental perturbations should not correlate between them. The acoustic noise, the seismic noise, and the power line (especially if the network includes detectors in a different power grids and significantly different time zones) will be uncorrelated. There are correlations in the magnetic field fluctuations (thunderstorms) and in radio frequency emissions. As part of the detection strategy a large number of environmental parameters will be measured along with the gravitational wave signals at each site. One of the requirements for the authenticity of impulsive sources will be the lack of correlation with environmental perturbations and other ancillary internal signals developed to monitor the performance of the instruments.

Chapter 5

DATA ANALYSIS — PART I

§5.1 Introduction

The first generation of long-baseline laser interferometers and ultra cryogenic bar detectors is in operation. The network of detectors will not only confirm the existence of GWs but will also yield an information about their important parameters viz; amplitude, frequency and phase. In addition, a careful monitoring of the signal will also provide an information about the structure and dynamics of their source. The data analysis depends largely upon the study of the expected characteristic of the potential sources and the waveforms. The most part of the experimental searches is focused on the detection of burst and *chirp* signals. However, the interest in the data analysis for CGW signals is growing up. A prime example of the sources of GW signals of this type is a spinning neutron star. Many research groups around the globe are working extensively on the data analysis for spinning neutron stars; see Jaranwoski et al. (1998, 1999, 2000), Brady et al. (1998, 2000).

Our Galaxy is expected to have, on logistic grounds, at least 10^8 spinning neutron stars, with a birth rate of one per every 30 years. However, a very insignificant fraction of them is observed — the number of known pulsars has gone up to ~ 1600. There are compelling arguments that nearby millisecond pulsars can provide a detectable source of CGW. Hence, there is a strong case for scanning all the sky for the presence of neutron stars with the philosophy that they are emitting GWs but otherwise unknown optically. This study will help us to understand the pulsar population in our Galaxy.

The detection of GW signals in the output has its own problems, not the least of which is the sheer volume of data analysis. Bar detectors have essentially the same problems as interferometers in the reference to CGW sources. The possibility that these detectors are capable to search for signals of different kinds makes them very versatile, but also complicates the data analysis. Each detector produces a single data stream that may contain many kinds of signals. Detectors don't point, but rather sweep their broad quadrupolar beam pattern across the sky as the Earth moves. So possible sources could be anywhere on the sky

and accordingly the data analysis algorithms need to accommodate the signals from any arbitrary location of its source.

In this Chapter and the next Chapter we analyze the FT of the output data of a ground-based laser interferometer. The output data has prominently dominant broad band noise and the signal is to be extracted out of it. For this, one has to enhance SNR. This is achieved by analyzing a long observation time data as SNR is directly proportional to the square root of the observation time $\sqrt{T_0}$. However, in a data for long duration, the monochromatic signal gets Doppler modulated due to: (i) the orbital motions of the Earth around the Sun, and (ii) the spin of the Earth. The Frequency Modulation (FM) will spread the signal in a very large number of bins depending on the source location and the frequency. In addition to it there is the Amplitude Modulation (AM). As we will see in the sequel the amplitude of the detector output consists of simple harmonic terms with frequencies w_{rot} and $2w_{rot}$, where w_{rot} stands for the angular rotational frequency of the Earth. Accordingly, the AM results in splitting of FT into frequencies $\pm w_{rot}$ and $\pm 2w_{rot}$.

§5.2 The noise free response of detector: beam pattern and amplitude modulation

Let a plane GW falls on a laser interferometer, and produces changes in the arms of the detector. In order to express these changes quantitatively we would require to specify the wave and the detector. Let XYZ and xyz represent respective frames characterizing the wave and the detector. We assume the direction of propagation of the wave to be the Z-axis, and the vertical at the place of detector to be the z-axis. Proceeding from §2.3 of Chapter 2, the difference of the changes δl in the arm lengths of the detector is given via

$$R(t) = \frac{\delta l}{l_0} = -\sin 2\Omega \left[(\mathbf{A}_X^x \mathbf{A}_X^y - \mathbf{A}_Y^x \mathbf{A}_Y^y)\, h_+ + (\mathbf{A}_X^x \mathbf{A}_Y^y + \mathbf{A}_Y^x \mathbf{A}_X^y)\, h_\times \right], \tag{5.1}$$

where l_0 is the normal length of the arms of the detector, and 2Ω expresses the angle between them (Schutz and Tinto, 1987). The matrix $\left(\mathbf{A}_K^j\right)$ represents the transformation expressing the rotations to bring the wave frame (X, Y, Z) to the detector frame (x, y, z). The direction of the source may be expressed in any of the coordinates employed in spherical astronomy. However, we find it convenient to define it in the Solar System Barycentre (SSB) frame (X', Y', Z'). This SSB frame is nothing but astronomer's ecliptic coordinate frame. Let θ and ϕ denote

the celestial co-latitude and the celestial longitude of the source. These coordinates are related to the right ascension $\bar{\alpha}$ and the declination $\bar{\delta}$ of the source via

$$\left.\begin{aligned} \cos\theta &= \sin\bar{\delta}\cos\epsilon - \cos\bar{\delta}\sin\epsilon\sin\bar{\alpha} \\ \sin\theta\cos\phi &= \cos\bar{\delta}\cos\bar{\alpha} \\ \sin\theta\sin\phi &= \sin\bar{\delta}\sin\epsilon + \cos\bar{\delta}\cos\epsilon\sin\bar{\alpha} \end{aligned}\right\}, \tag{5.2}$$

where ϵ represents the obliquity of the ecliptic. We choose the x-axis as the bisector of the angle between the arms of the detector. At this stage the orientation of the detector in the horizontal plane is arbitrary. It is assigned with the help of the angle γ which the x-axis makes with the local meridian.

The location of the detector on the Earth is characterized by the angle α, the co-latitude and the β, the local sidereal time expressed in radians. The transformation matrix $\left(\mathbf{A}_K^j\right)$ may be expressed as

$$\mathbf{A} = \mathbf{DCB}, \tag{5.3}$$

where we introduced the following denotations:

B : a rotation required to bring XYZ to $X'Y'Z'$;

C : a rotation required to bring $X'Y'Z'$ to $x'y'z'$;

D : a rotation required to bring $x'y'z'$ to xyz.

Here $x'y'z'$ represents the frame associated with the Earth. The Euler angles defining the corresponding rotation matrices (Goldstein, 1980) are given via

$$\left.\begin{aligned} \mathbf{B} &: (\theta,\ \phi,\ \psi) \\ \mathbf{C} &: (0,\ \epsilon,\ 0) \\ \mathbf{D} &: (\alpha,\ \beta+\tfrac{\pi}{2},\ \gamma-\tfrac{\pi}{2}) \end{aligned}\right\}, \tag{5.4}$$

where ψ is a measure of the polarization of the wave. Let us express Eq. (5.1) as

$$R(t) = \frac{\delta l}{l_0} = -\sin 2\Omega\left[F_+ h_+ + F_\times h_\times\right]. \tag{5.5}$$

The functions F_+ and $F_\times$ involve the angles θ, ϕ, ψ, ϵ, α, β, γ and express the effect of the interaction between the wave and the detector. These are called antenna or beam patterns. After a straight forward calculation one obtains Eqs. (5.6) and (5.7); see Jotania and Dhurandhar (1994) for detail. The next two pages of this book provide these equations written in complete form.

$$
\begin{aligned}
F_+(t) = \frac{1}{2}\big[&\big\{(\cos\psi\cos\phi - \cos\theta\sin\phi\sin\psi)^2 - (\cos\psi\sin\phi + \cos\theta\cos\phi\sin\psi)^2\big\} \\
&\times \{2(\cos\alpha\cos\beta\cos\gamma - \sin\beta\sin\gamma)(-\cos\alpha\cos\beta\sin\gamma - \sin\beta\cos\gamma)\} \\
&+ \big\{(-\sin\psi\cos\phi - \cos\theta\sin\phi\cos\psi)^2 - (\cos\theta\cos\phi\cos\psi - \sin\psi\sin\phi)^2\big\} \\
&\times \big[\cos^2\epsilon\,\{2(\cos\alpha\sin\beta\cos\gamma + \cos\beta\sin\gamma)(\cos\beta\cos\gamma - \cos\alpha\sin\beta\sin\gamma)\} \\
&- \sin^2\epsilon\sin^2\alpha\sin 2\gamma + \sin 2\epsilon\,\{(\cos\alpha\sin\beta\cos\gamma + \cos\beta\sin\gamma)\sin\alpha\sin\gamma \\
&- \ (\cos\beta\cos\gamma - \cos\alpha\sin\beta\sin\gamma)\sin\alpha\cos\gamma\}] \\
&- (\sin^2\theta\cos 2\phi) \\
&\times \big[\sin^2\epsilon\,\{2(\cos\alpha\sin\beta\cos\gamma + \cos\beta\sin\gamma)(\cos\beta\cos\gamma - \cos\alpha\sin\beta\sin\gamma)\} \\
&- \cos^2\epsilon\sin^2\alpha\sin 2\gamma - \sin 2\epsilon\,\{(\cos\alpha\sin\beta\cos\gamma + \cos\beta\sin\gamma)\sin\alpha\sin\gamma \\
&- \ (\cos\beta\cos\gamma - \cos\alpha\sin\beta\sin\gamma)\sin\alpha\cos\gamma\}]] \\
&+ \{(\cos\psi\cos\phi - \cos\theta\sin\phi\sin\psi)(-\sin\psi\cos\phi - \cos\theta\sin\phi\cos\psi) \\
&- \ (\cos\psi\sin\phi + \cos\theta\cos\phi\sin\psi)(\cos\theta\cos\phi\cos\psi - \sin\psi\sin\phi)\} \\
&\times [\cos\epsilon\,\{(\cos\beta\cos\gamma - \cos\alpha\sin\beta\sin\gamma)(\cos\alpha\cos\beta\cos\gamma - \sin\beta\sin\gamma) \\
&- \ (\cos\alpha\sin\beta\cos\gamma + \cos\beta\sin\gamma)(\cos\alpha\cos\beta\sin\gamma + \sin\beta\cos\gamma)\} \\
&+ \sin\epsilon\,\{(\cos\alpha\cos\beta\cos\gamma - \sin\beta\sin\gamma)(\sin\alpha\sin\gamma) \\
&+ \ (\cos\alpha\cos\beta\sin\gamma + \sin\beta\cos\gamma)(\sin\alpha\cos\gamma)\}] \\
&+ \{(\cos\psi\cos\phi - \cos\theta\sin\phi\sin\psi)(\sin\theta\sin\phi) \\
&+ \ (\cos\psi\sin\phi + \cos\theta\cos\phi\sin\psi)(\sin\theta\cos\phi)\} \\
&\times [-\sin\epsilon\,\{(\cos\beta\cos\gamma - \cos\alpha\sin\beta\sin\gamma)(\cos\alpha\cos\beta\cos\gamma - \sin\beta\sin\gamma) \\
&- \ (\cos\alpha\sin\beta\cos\gamma + \cos\beta\sin\gamma)(\cos\alpha\cos\beta\sin\gamma + \sin\beta\cos\gamma)\} \\
&+ \cos\epsilon\,\{(\cos\alpha\cos\beta\cos\gamma - \sin\beta\sin\gamma)(\sin\alpha\sin\gamma) \\
&+ \ (\cos\alpha\cos\beta\sin\gamma + \sin\beta\cos\gamma)(\sin\alpha\cos\gamma\}] \\
&+ \{(-\sin\psi\cos\phi - \cos\theta\sin\phi\cos\psi)(\sin\theta\sin\phi) \\
&+ \ (\cos\theta\cos\phi\cos\psi - \sin\psi\sin\phi)(\sin\theta\cos\phi)\} \\
&\times [-(\cos\epsilon\sin\epsilon)\,\{2(\cos\alpha\sin\beta\cos\gamma + \cos\beta\sin\gamma) \\
&\times \ (\cos\beta\cos\gamma - \cos\alpha\sin\beta\sin\gamma) + \sin^2\alpha\sin 2\gamma\big\} \\
&+ \cos 2\epsilon\,\{(\cos\alpha\sin\beta\cos\gamma + \cos\beta\sin\gamma)(\sin\alpha\sin\gamma) \\
&- \ (\cos\beta\cos\gamma - \cos\alpha\sin\beta\sin\gamma)(\sin\alpha\cos\gamma)\}] \qquad (5.6)
\end{aligned}
$$

$$
\begin{aligned}
F_{\times}(t) = {} & 2(\cos\psi\cos\phi - \cos\theta\sin\phi\sin\psi)(\cos\psi\sin\phi + \cos\theta\cos\phi\sin\psi) \\
& \times (\cos\alpha\cos\beta\cos\gamma - \sin\beta\sin\gamma)(-\cos\alpha\cos\beta\sin\gamma - \sin\beta\cos\gamma) \\
& + (-\sin\psi\cos\phi - \cos\theta\sin\phi\cos\psi)(\cos\theta\cos\phi\cos\psi - \sin\psi\sin\phi) \\
& \times \big[\cos^2\epsilon\,\{2(\cos\alpha\sin\beta\cos\gamma + \cos\beta\sin\gamma)(\cos\beta\cos\gamma - \cos\alpha\sin\beta\sin\gamma)\} \\
& - \sin^2\epsilon\sin^2\alpha\sin 2\gamma + \sin 2\epsilon\,\{(\cos\alpha\sin\beta\cos\gamma + \cos\beta\sin\gamma)\sin\alpha\sin\gamma \\
& - (\cos\beta\cos\gamma - \cos\alpha\sin\beta\sin\gamma)\sin\alpha\cos\gamma\}\big] \\
& - \frac{1}{2}(\sin^2\theta\sin 2\phi) \\
& \times \big[\sin^2\epsilon\,\{2(\cos\alpha\sin\beta\cos\gamma + \cos\beta\sin\gamma)(\cos\beta\cos\gamma - \cos\alpha\sin\beta\sin\gamma)\} \\
& - \cos^2\epsilon\sin^2\alpha\sin 2\gamma - \sin 2\epsilon\,\{(\cos\alpha\sin\beta\cos\gamma + \cos\beta\sin\gamma)\sin\alpha\sin\gamma \\
& - (\cos\beta\cos\gamma - \cos\alpha\sin\beta\sin\gamma)\sin\alpha\cos\gamma\}\big] \\
& + \{(\cos\psi\cos\phi - \cos\theta\sin\phi\sin\psi)(-\sin\psi\sin\phi + \cos\theta\cos\phi\cos\psi) \\
& - (\cos\psi\sin\phi + \cos\theta\cos\phi\sin\psi)(\cos\theta\sin\phi\cos\psi + \sin\psi\cos\phi)\} \\
& \times [\cos\epsilon\,\{(\cos\beta\cos\gamma - \cos\alpha\sin\beta\sin\gamma)(\cos\alpha\cos\beta\cos\gamma - \sin\beta\sin\gamma) \\
& - (\cos\alpha\sin\beta\cos\gamma + \cos\beta\sin\gamma)(\cos\alpha\cos\beta\sin\gamma + \sin\beta\cos\gamma)\} \\
& + \sin\epsilon\,\{(\cos\alpha\cos\beta\cos\gamma - \sin\beta\sin\gamma)(\sin\alpha\sin\gamma) \\
& + (\cos\alpha\cos\beta\sin\gamma + \sin\beta\cos\gamma)(\sin\alpha\cos\gamma)\}] \\
& + \{-(\cos\psi\cos\phi - \cos\theta\sin\phi\sin\psi)(\sin\theta\cos\phi) \\
& + (\cos\psi\cos\phi + \cos\theta\cos\phi\sin\psi)(\sin\theta\sin\phi)\} \\
& \times [-\sin\epsilon\,\{(\cos\beta\cos\gamma - \cos\alpha\sin\beta\sin\gamma)(\cos\alpha\cos\beta\cos\gamma - \sin\beta\sin\gamma) \\
& - (\cos\alpha\sin\beta\cos\gamma + \cos\beta\sin\gamma)(\cos\alpha\cos\beta\sin\gamma + \sin\beta\cos\gamma)\} \\
& + \cos\epsilon\,\{(\cos\alpha\cos\beta\cos\gamma - \sin\beta\sin\gamma)(\sin\alpha\sin\gamma) \\
& + (\cos\alpha\cos\beta\sin\gamma + \sin\beta\cos\gamma)(\sin\alpha\cos\gamma\}] \\
& + \{(-\sin\psi\sin\phi + \cos\theta\cos\phi\cos\psi)(\sin\theta\sin\phi) \\
& + (\cos\theta\sin\phi\cos\psi + \sin\psi\cos\phi)(\sin\theta\cos\phi)\} \\
& \times [-(\cos\epsilon\sin\epsilon)\,\{2(\cos\alpha\sin\beta\cos\gamma + \cos\beta\sin\gamma) \\
& \times (\cos\beta\cos\gamma - \cos\alpha\sin\beta\sin\gamma) + \sin^2\alpha\sin 2\gamma\big\} \\
& + \cos 2\epsilon\,\{(\cos\alpha\sin\beta\cos\gamma + \cos\beta\sin\gamma)(\sin\alpha\sin\gamma) \\
& - (\cos\beta\cos\gamma - \cos\alpha\sin\beta\sin\gamma)(\sin\alpha\cos\gamma)\}] \qquad (5.7)
\end{aligned}
$$

It is easy to understand the structure of the above complicated looking expressions for F_+ and $F_\times$ by introducing following abbreviations

$$\left.\begin{aligned} U &= \cos\alpha\cos\beta\cos\gamma - \sin\beta\sin\gamma \\ V &= -\cos\alpha\cos\beta\sin\gamma - \sin\beta\cos\gamma \\ X &= \cos\alpha\sin\beta\cos\gamma + \cos\beta\sin\gamma \\ Y &= -\cos\alpha\sin\beta\sin\gamma + \cos\beta\cos\gamma \end{aligned}\right\}, \tag{5.8}$$

$$\left.\begin{aligned} L &= \cos\psi\cos\phi - \cos\theta\sin\phi\sin\psi \\ M &= \cos\psi\sin\phi + \cos\theta\cos\phi\sin\psi \\ N &= -\sin\psi\cos\phi - \cos\theta\sin\phi\cos\psi \\ P &= -\sin\psi\sin\phi + \cos\theta\cos\phi\cos\psi \\ Q &= \sin\theta\sin\phi\,, \qquad R = \sin\theta\cos\phi \end{aligned}\right\}, \tag{5.9}$$

$$\left.\begin{aligned} A &= 2XY\cos^2\epsilon - \sin^2\epsilon\,\sin^2\alpha\,\sin 2\gamma \\ &\quad + \sin 2\epsilon\,(X\sin\alpha\sin\gamma - Y\sin\alpha\cos\gamma) \\ B &= 2XY\sin^2\epsilon - \cos^2\epsilon\,\sin^2\alpha\,\sin 2\gamma \\ &\quad - \sin 2\epsilon\,(X\sin\alpha\sin\gamma - Y\sin\alpha\cos\gamma) \\ C &= \cos\epsilon\,(YU + XV) \\ &\quad + \sin\epsilon\,(U\sin\alpha\sin\gamma - V\sin\alpha\cos\gamma) \\ D &= -\sin\epsilon\,(YU + XV) \\ &\quad + \cos\epsilon\,(U\sin\alpha\sin\gamma - V\sin\alpha\cos\gamma) \\ E &= -2XY\cos\epsilon\,\sin\epsilon - \cos\epsilon\,\sin\epsilon\,\sin^2\alpha\,\sin 2\gamma \\ &\quad + \cos 2\epsilon\,(X\sin\alpha\sin\gamma - Y\sin\alpha\cos\gamma) \end{aligned}\right\}. \tag{5.10}$$

One obtains:

$$\begin{aligned} F_+(t) &= \frac{1}{2}\big[\,2(L^2 - M^2)UV + (N^2 - P^2)A\, + (Q^2 - R^2)B\,\big] \\ &\quad + (LN - MP)C + (LQ + MR)D + (NQ + PR)E\,, \end{aligned} \tag{5.11}$$

$$\begin{aligned} F_\times(t) &= 2LMUV + NPA - \frac{1}{2}\,B\sin^2\theta\,\sin 2\phi \\ &\quad + (LP + MN)C + (MQ - LR)D + (PQ - NR)E\,. \end{aligned} \tag{5.12}$$

The compactification achieved here is due to the fact that these abbreviations find places in the transformation matrices as

$$\mathbf{B} = \begin{pmatrix} L & N & Q \\ M & P & -R \\ \sin\theta\sin\psi & \sin\theta\cos\psi & \cos\theta \end{pmatrix}, \tag{5.13}$$

$$\mathbf{C} = \begin{pmatrix} 1 & 0 & 0 \\ 0 & \cos\epsilon & \sin\epsilon \\ 0 & -\sin\epsilon & \cos\epsilon \end{pmatrix}, \tag{5.14}$$

$$\mathbf{D} = \begin{pmatrix} U & V & \sin\alpha\cos\beta \\ X & Y & \sin\alpha\sin\beta \\ -\sin\alpha\cos\gamma & \sin\alpha\sin\gamma & \cos\alpha \end{pmatrix}. \tag{5.15}$$

After algebraic manipulation Eqs. (5.11) and (5.12) may be expressed as

$$F_+(t) = F_{1_+}\cos 2\beta + F_{2_+}\sin 2\beta + F_{3_+}\cos\beta + F_{4_+}\sin\beta + F_{5_+}\,, \tag{5.16}$$

$$F_\times(t) = F_{1_\times}\cos 2\beta + F_{2_\times}\sin 2\beta + F_{3_\times}\cos\beta + F_{4_\times}\sin\beta + F_{5_\times}\,, \tag{5.17}$$

where F_{i_+} and $F_{i_\times}$ $(i = 1, 2, 3, 4, 5)$ are time independent expressions given via

$$\left.\begin{aligned} F_{1_+} &= -2G\cos\alpha\,\cos 2\gamma + \frac{H\sin 2\gamma}{2}\,(\cos^2\alpha + 1) \\ F_{2_+} &= H\cos\alpha\,\cos 2\gamma + G\sin 2\gamma\,(\cos^2\alpha + 1) \\ F_{3_+} &= I\sin\alpha\,\cos 2\gamma + J\sin 2\alpha\,\sin 2\gamma \\ F_{4_+} &= 2J\sin\alpha\,\cos 2\gamma - \frac{I}{2}\,\sin 2\alpha\,\sin 2\gamma \\ F_{5_+} &= \frac{3\sin^2\alpha\,\sin 2\gamma}{2}\big[H + L^2 - M^2\big] \end{aligned}\right\}, \tag{5.18}$$

$$\left.\begin{aligned} G &= \frac{1}{2}\big[(LQ + MR)\sin\epsilon - (LN - MP)\cos\epsilon\big] \\ H &= \frac{1}{2}\big[(N^2 - P^2)\cos^2\epsilon - (L^2 - M^2) + (Q^2 - R^2)\sin^2\epsilon \\ &\quad - (NQ + PR)\sin 2\epsilon\big] \\ I &= \frac{1}{2}\big[(Q^2 - R^2)\sin 2\epsilon - (N^2 - P^2)\sin 2\epsilon \\ &\quad - 2\,(NQ + PR)\cos 2\epsilon\big] \\ J &= \frac{1}{2}\big[(LN - MP)\sin\epsilon + (LQ + MR)\cos\epsilon\big] \end{aligned}\right\}. \tag{5.19}$$

Note that $F_{i_\times}$ is related to F_{i_+} via

$$F_{i_\times}\left(\theta,\ \phi,\ \psi,\ \alpha,\ \beta,\ \gamma,\ \epsilon\right) = F_{i_+}\left(\theta,\ \phi - \tfrac{\pi}{4}\,,\ \psi,\ \alpha,\ \beta,\ \gamma,\ \epsilon\right), \quad (5.20)$$

where $i = 1, 2, 3, 4, 5$.

This symmetry represents the quadrupolar nature of the detector and the wave. A detector in different orientations will record different amplitudes in the response. The explicit beam pattern functions may be computed easily for any instant of time. Due to symmetries involved in F_+ and $F_\times$, it is sufficient to discuss either of the beam patterns.

The amplitude modulation of the received signal is a direct consequence of the non-uniformity of the sensitivity pattern. The antenna response is not peaked in any direction but is anisotropic. As remarked earlier they are fairly complicated function of their arguments. Equations (5.16) and (5.17) reveal that the monochromatic signal frequency will split, due to AM, into five lines. This results in the distribution of energy in various frequencies and consequent reduction of the amplitude of the signal. The periodicity of the beam patterns F_+ and $F_\times$ with a period equal to one sidereal day is due to the diurnal motion of the Earth.

§5.3 Doppler shift and frequency modulation

The frequency of a monochromatic signal will be Doppler shifted due to the translatory motion of the detector, acquired from the motions of the Earth. Let us consider a CGW signal of a constant frequency f_0. The frequency f' received at an instant t by the detector is given by

$$f'(t) = f_0\,\gamma_0\left(1 + \frac{\mathbf{v}\cdot\mathbf{n}}{c}\,(t)\right), \quad \gamma_0 = \left(1 - \frac{v^2}{c^2}\right)^{-1/2}, \quad (5.21)$$

where $\mathbf{n}$ is the unit vector from the antenna to the source, $\mathbf{v}$ is the relative velocity of the source and the antenna, and c is the velocity of light. The unit vector $\mathbf{n}$ from the antenna to the source, because of the fact that the distance of the source is very large compared to the average distance of the centre of the SSB frame and the detector, may be taken parallel to the unit vector drawn from the centre of the SSB frame to the source. Hence,

$$\mathbf{n} = \big(\sin\theta\cos\phi\,,\ \sin\theta\sin\phi\,,\ \cos\theta\big). \quad (5.22)$$

As $\mathbf{v}$ keeps on changing continuously in its both amplitude and direction, f' is a continuous function of t. Further, since $v \ll c$ we take into account that $\gamma_0 = 1$.

The radius vector $\mathbf{r}(t)$ in the SSB frame is given, in component notation, by

$$\begin{aligned}\mathbf{r}(t) = \big[\, & R_{se}\cos(w_{orb}\,t) + R_e \sin\alpha\cos\beta\,, \\ & R_{se}\sin(w_{orb}\,t) + R_e\sin\alpha\sin\beta\cos\epsilon - R_e\cos\alpha\sin\epsilon\,, \\ & R_e\sin\alpha\sin\beta\sin\epsilon + R_e\cos\alpha\cos\epsilon\,\big]; \end{aligned} \tag{5.23}$$

$$\beta = \beta_0 + w_{rot}\,t\,, \tag{5.24}$$

where R_e, R_{se}, and w_{orb} represent respectively the Earth's radius, the average distance between the Earth's centre from the centre of SSB frame, and the orbital angular velocity of the Earth. Here, t represents the time in seconds elapsed from the instant Sun is at the Vernal Equinox and β_0 is the local sidereal time at that instant. The Doppler shift is now given via

$$\begin{aligned}\frac{f'-f_0}{f_0} = \frac{\mathbf{v}\cdot\mathbf{n}}{c}\,(t) \;=\; \frac{\dot{\mathbf{r}}_\mathbf{t}\cdot\mathbf{n}}{c} \;=\; & \frac{R_{se}\,w_{orb}}{c}\,\sin\theta\,\sin(\phi - w_{orb}\,t) \\ & + \frac{R_e w_{rot}}{c}\,\sin\alpha\,\big[\,\sin\theta\big(\cos\beta\,\cos\epsilon\,\sin\phi - \cos\phi\,\sin\beta\big) \\ & + \cos\beta\,\sin\epsilon\,\cos\theta\big]. \end{aligned} \tag{5.25}$$

The phase $\Phi(t)$ of the received signal is given by

$$\Phi(t) = 2\pi\int_0^t f'(t')\,dt' = 2\pi f_0\int_0^t \Big[1 + \frac{\mathbf{v}\cdot\mathbf{n}}{c}\,(t')\Big]\,dt'. \tag{5.26}$$

Here, we assume the initial phase of the wave to be zero. After a straight forward calculation we obtain

$$\begin{aligned}\Phi(t) = \; & 2\,\pi\,f_0\Big\{t + \frac{R_{se}}{c}\,\sin\theta\,\cos\phi' \\ & + \frac{R_e}{c}\,\sin\alpha\,\big[\,\sin\theta\,\big(\sin\beta\,\cos\epsilon\,\sin\phi + \cos\phi\,\cos\beta\big) \\ & + \sin\beta\,\sin\epsilon\,\cos\theta\big] - \frac{R_{se}}{c}\,\sin\theta\,\cos\phi \\ & - \frac{R_e}{c}\,\sin\alpha\,\big[\,\sin\theta\,\big(\sin\beta_0\,\cos\epsilon\,\sin\phi + \cos\phi\,\cos\beta_0\big) \\ & + \sin\beta_0\,\sin\epsilon\,\cos\theta\big]\Big\} \\ = \; & 2\pi f_0 t + \mathcal{Z}\cos(w_{orb}\,t - \phi) + \mathcal{P}\sin(w_{rot}\,t) + \mathcal{Q}\cos(w_{rot}\,t) - \mathcal{R} - \mathcal{Q} \\ = \; & 2\pi f_0 t + \mathcal{Z}\cos\left(a\,\xi_{rot} - \phi\right) + \mathcal{N}\cos\left(\xi_{rot} - \delta\right) - \mathcal{R} - \mathcal{Q}\,, \end{aligned} \tag{5.27}$$

where

$$\left.\begin{aligned}
\mathcal{P} &= 2\pi f_0 \frac{R_e}{c} \sin\alpha \big[\cos\beta_0 \, (\sin\theta\cos\epsilon\sin\phi + \cos\theta\sin\epsilon) \\
&\quad - \sin\beta_0 \sin\theta\cos\phi \big] \\
\mathcal{Q} &= 2\pi f_0 \frac{R_e}{c} \sin\alpha \big[\sin\beta_0 \, (\sin\theta\cos\epsilon\sin\phi + \cos\theta\sin\epsilon) \\
&\quad + \cos\beta_0 \sin\theta\cos\phi \big] \\
\mathcal{N} &= \sqrt{\mathcal{P}^2 + \mathcal{Q}^2} \\
\mathcal{Z} &= 2\pi f_0 \frac{R_{se}}{c} \sin\theta \\
\mathcal{R} &= \mathcal{Z}\cos\phi
\end{aligned}\right\}, \tag{5.28}$$

$$\left.\begin{aligned}
\delta &= \tan^{-1}\frac{\mathcal{P}}{\mathcal{Q}} \\
\phi' &= w_{orb}t - \phi \\
\xi_{orb} &= w_{orb}t \;=\; a\,\xi_{rot}; \quad a \;=\; w_{orb}/w_{rot} \;\approx\; 1/365.26 \\
\xi_{rot} &= w_{rot}\,t
\end{aligned}\right\}. \tag{5.29}$$

These two polarization states of the signal can be taken as

$$h_+(t) = h_{0_+} \cos\big[\Phi(t)\big] \,, \tag{5.30}$$

$$h_\times(t) = h_{0_\times} \sin\big[\Phi(t)\big] \,, \tag{5.31}$$

where h_{0_+} and $h_{0_\times}$ are the time independent amplitude of $h_+(t)$, and $h_\times(t)$ respectively.

To understand the nature of the FM, let us consider the FT of $h_+(t)$ and $h_\times(t)$. We may begin by considering the function

$$h(t) = \cos\big[\Phi(t)\big] \tag{5.32}$$

and analyzing the data for one day observation. The FT is given via

$$\big[\tilde{h}(f)\big]_d = \int_0^T \cos\big[\Phi(t)\big]\, e^{-i2\pi ft}\, dt \,, \tag{5.33}$$

where T is one sidereal day, 86164 sec.

This may be split into two terms as

$$\big[\tilde{h}(f)\big]_d = I_{\nu_-} + I_{\nu_+} \,; \tag{5.34}$$

$$I_{\nu_-} = \frac{1}{2w_{rot}} \int_0^{2\pi} e^{i[\xi\nu_- + \mathcal{Z}\cos(a\xi-\phi)+\mathcal{N}\cos(\xi-\delta)-\mathcal{R}-\mathcal{Q}]}\, d\xi\,, \quad (5.35)$$

$$I_{\nu_+} = \frac{1}{2w_{rot}} \int_0^{2\pi} e^{-i[\xi\nu_+ + \mathcal{Z}\cos(a\xi-\phi)+\mathcal{N}\cos(\xi-\delta)-\mathcal{R}-\mathcal{Q}]}\, d\xi\,, \quad (5.36)$$

$$\nu_\pm = \frac{f_0 \pm f}{f_{rot}}\,; \qquad \xi = \xi_{rot} = w_{rot}\, t\,. \quad (5.37)$$

Numerical result shows that I_{ν_+} oscillates very fast and contributes very little into $\left[\tilde{h}(f)\right]_d$. Hence, hereafter, we drop I_{ν_+} from Eq. (5.34) and write ν in the place of ν_-. Using the identity

$$e^{\pm i\kappa\cos\vartheta} = J_0(\pm\kappa) + 2\sum_{l=1}^{l=\infty} i^l J_l(\pm\kappa)\cos l\vartheta\,, \quad (5.38)$$

we obtain

$$\left[\tilde{h}(f)\right]_d \simeq \frac{e^{i(-\mathcal{R}-\mathcal{Q})}}{2w_{rot}} \int_0^{2\pi} e^{i\nu\xi}\left[J_0(\mathcal{Z}) + 2\sum_{k=1}^{k=\infty} J_k(\mathcal{Z})\, i^k \cos k\,(a\,\xi-\phi)\right] \times\left[J_0(\mathcal{N}) + 2\sum_{m=1}^{m=\infty} J_m(\mathcal{N})\, i^m \cos m\,(\xi-\delta)\right] d\xi\,, \quad (5.39)$$

where J stands for the Bessel function of the first kind of integral order. After performing the integration we get

$$\left[\tilde{h}(f)\right]_d \simeq \frac{\nu}{2w_{rot}} \sum_{k=-\infty}^{k=\infty}\sum_{m=-\infty}^{m=\infty} e^{i\mathcal{A}}\,\mathcal{B}\left[\mathcal{C} - i\mathcal{D}\right]; \quad (5.40)$$

$$\begin{aligned}
\mathcal{A} &= \frac{(k+m)\,\pi}{2} - \mathcal{R} - \mathcal{Q}\,,\\
\mathcal{B} &= \frac{J_k(\mathcal{Z})\, J_m(\mathcal{N})}{\nu^2 - (ak+m)^2}\,,\\
\mathcal{C} &= \sin 2\nu\pi\,\cos\left(2ak\pi - k\phi - m\delta\right)\\
&\quad - \frac{ak+m}{\nu}\left\{\cos 2\nu\pi\,\sin\left(2ak\pi - k\phi - m\delta\right) + \sin\left(k\phi + m\delta\right)\right\},\\
\mathcal{D} &= \cos 2\nu\pi\,\cos(2ak\pi - k\phi - m\delta)\\
&\quad + \frac{ka+m}{\nu}\,\sin 2\nu\pi\,\sin\left(2ak\pi - k\phi - m\delta\right) - \cos\left(k\phi + m\delta\right)\,.
\end{aligned}$$

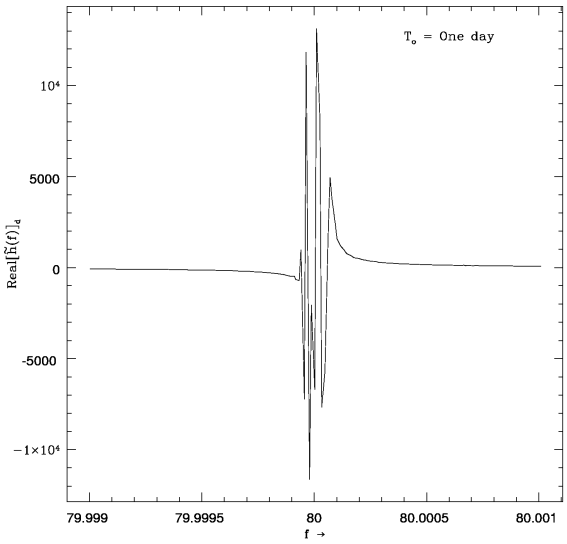

Figure 5.1: FT of a FM signal of a source located at $\left(\frac{\pi}{36}, \pi\right)$ with a resolution of 1.16×10^{-5}.

The FT of these two polarization states of the wave can now be re-written as follows

$$\begin{aligned}\left[\tilde{h}_+(f)\right]_d &= h_{0_+}\left[\tilde{h}(f)\right]_d \\ &\simeq \frac{\nu h_{0_+}}{2w_{rot}} \sum_{k=-\infty}^{k=\infty} \sum_{m=-\infty}^{m=\infty} e^{i\mathcal{A}} \mathcal{B}\left[\mathcal{C} - i\mathcal{D}\right], \end{aligned} \tag{5.41}$$

$$\begin{aligned}\left[\tilde{h}_\times(f)\right]_d &= -\,i\,h_{0_\times}\left[\tilde{h}(f)\right]_d \\ &\simeq \frac{\nu h_{0_\times}}{2w_{rot}} \sum_{k=-\infty}^{k=\infty} \sum_{m=-\infty}^{m=\infty} e^{i\mathcal{A}} \mathcal{B}\left[\mathcal{D} - i\mathcal{C}\right]. \end{aligned} \tag{5.42}$$

The FT of the FM signal contains the double series Bessel functions. The Bessel functions has contributions due to the rotational as well as the orbital motion of the Earth. It is remarked that Jotania et al. (1996) have analyzed FT of FM signal for one day observation time. They have taken a specific detector as well as the source location. They have also neglected the orbital motion. Our analysis generalizes their results. We may now compute $\left[\tilde{h}(f)\right]_d$ and may plot its behaviour. Fig. (5.1)

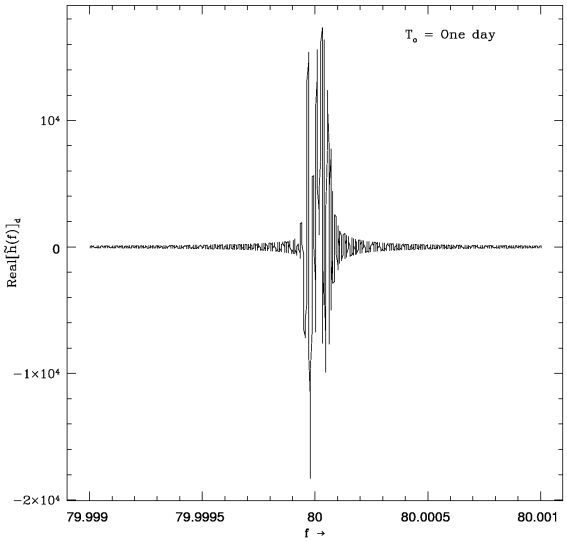

Figure 5.2: FT of a FM signal of a source located at $\left(\frac{\pi}{36}, \pi\right)$ with a resolution of 10^{-6}.

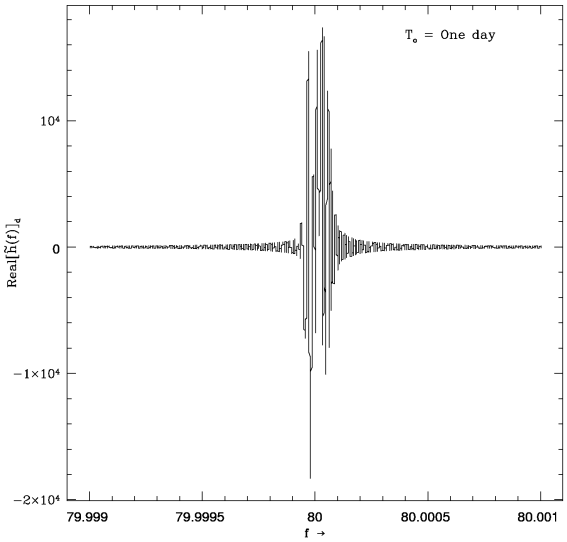

Figure 5.3: FT of a FM signal of a source located at $\left(\frac{\pi}{36}, \pi\right)$ with a resolution of 10^{-7}.

represents such a plot for

$$\left.\begin{array}{lll} f_0 = 80 \text{ Hz}\,, & h_0 = h_\times = 1 & \\ \alpha = \frac{\pi}{3}\,, & \beta_0 = \frac{\pi}{4}\,, & \gamma = \frac{2\pi}{5} \\ \theta = \frac{\pi}{36}\,, & \phi = \pi\,, & \psi = \frac{\pi}{6} \end{array}\right\} \tag{5.43}$$

with the resolution $1/T_0 = 1.16 \times 10^{-5}$ Hz. Figs. (5.2) and (5.3) represent the plot of the FT at resolution 10^{-6} Hz and 10^{-7} Hz. A careful look at these plots reveals that the resolution of Fig. (5.1) does not represent the details of the dominant peaks around f_0, whereas, Fig. (5.3) does not give any new behaviour as compared to Fig. (5.2). Hence, we may say that a resolution of about 10^{-6} Hz is required to understand the correct behaviour of the FT for one day observation time data analysis. In this reference we recall that the data analysis for the Fast Fourier Transform (FFT) limits the resolution to $1/T_0$. However, the detector output may provide us higher resolution. Thus the semi-analytical analysis presented here may provide more information as compared to FFT.

§5.4 Fourier transform of the complete response

The complete response $R(t)$, in view of Eqs. (5.5), (5.16), (5.17), (5.30), and (5.31) may be written as

$$R(t) = R_+(t) + R_\times(t)\,, \tag{5.44}$$

$$\begin{aligned} R_+(t) \;=\; & h_{0_+}\big[F_{1_+}\cos 2\beta + F_{2_+}\sin 2\beta + F_{3_+}\cos\beta \\ & + F_{4_+}\sin\beta + F_{5_+}\big]\cos\big[\Phi(t)\big]\,, \end{aligned} \tag{5.45}$$

$$\begin{aligned} R_\times(t) \;=\; & h_{0_\times}\big[F_{1_\times}\cos 2\beta + F_{2_\times}\sin 2\beta + F_{3_\times}\cos\beta \\ & + F_{4_\times}\sin\beta + F_{5_\times}\big]\sin\big[\Phi(t)\big]\,. \end{aligned} \tag{5.46}$$

Here we have taken for simplicity the angles between the arms of the detector to be $\frac{\pi}{2}$ i.e. $\Omega = \frac{\pi}{4}$. Now the FT of the complete response may be expressed as

$$\tilde{R}(f) = \tilde{R}_+(f) + \tilde{R}_\times(f)\,. \tag{5.47}$$

To evaluate these we substitute β as given by (5.24). One obtains

$$\begin{aligned} R_+(t) \;=\; & h_{0_+}\Bigg[\frac{1}{2}\Big\{e^{-i2\beta_0}(F_{1_+} + iF_{2_+})\,e^{-i2w_{rot}\,t} + \\ & + e^{i2\beta_0}(F_{1_+} - iF_{2_+})\,e^{i2w_{rot}\,t} + e^{-i\beta_0}(F_{3_+} + iF_{4_+})\,e^{-iw_{rot}\,t} \\ & + e^{i\beta_0}(F_{3_+} - iF_{4_+})\,e^{iw_{rot}\,t}\Big\} + F_{5_+}\Bigg]\cos\big[\Phi(t)\big] \end{aligned} \tag{5.48}$$

and similar expression for $R_\times(t)$. Now it is straight forward to obtain the expression for $\tilde{R}_+(f)$ and $\tilde{R}_\times(f)$. We get

$$\begin{aligned}\big[\tilde{R}_+(f)\big]_d \;=\; h_{0_+}\Big[\; & e^{-i2\beta_0}(F_{1_+}+iF_{2_+})\big[\tilde{h}(f+2f_{rot})/2\big]_d \\ & + e^{i2\beta_0}(F_{1_+}-iF_{2_+})\big[\tilde{h}(f-2f_{rot})/2\big]_d \\ & + e^{-i\beta_0}(F_{3_+}+iF_{4_+})\big[\tilde{h}(f+f_{rot})/2\big]_d \\ & + e^{i\beta_0}(F_{3_+}-iF_{4_+})\big[\tilde{h}(f-f_{rot})/2\big]_d \\ & + F_{5_+}\big[\tilde{h}(f)\big]_d\Big]. \end{aligned} \tag{5.49}$$

Similarly we have

$$\begin{aligned}\big[\tilde{R}_\times(f)\big]_d \;=\; h_{0_\times}\Big[\; & e^{-i2\beta_0}(F_{2_\times}-iF_{1_\times})\big[\tilde{h}(f+2f_{rot})/2\big]_d \\ & - e^{i2\beta_0}(F_{2_\times}+iF_{1_\times})\big[\tilde{h}(f-2f_{rot})/2\big]_d \\ & + e^{-i\beta_0}(F_{4_\times}-iF_{3_\times})\big[\tilde{h}(f+f_{rot})/2\big]_d \\ & - e^{i\beta_0}(F_{4_\times}+iF_{3_\times})\big[\tilde{h}(f-f_{rot})/2\big]_d \\ & - iF_{5_\times}\big[\tilde{h}(f)\big]_d\Big]. \end{aligned} \tag{5.50}$$

Collecting our results the FT of the complete response of the detector for one day integration will be

$$\begin{aligned}\big[\tilde{R}(f)\big]_d = {} & e^{-i2\beta_0}\big[\tilde{h}(f+2f_{rot})/2\big]_d\big[h_{0_+}(F_{1_+}+iF_{2_+})+h_{0_\times}(F_{2_\times}-iF_{1_\times})\big] \\ & + e^{i2\beta_0}\big[\tilde{h}(f-2f_{rot})/2\big]_d\big[h_{0_+}(F_{1_+}-iF_{2_+})-h_{0_\times}(F_{2_\times}+iF_{1_\times})\big] \\ & + e^{-i\beta_0}\big[\tilde{h}(f+f_{rot})/2\big]_d\big[h_{0_+}(F_{3_+}+iF_{4_+})+h_{0_\times}(F_{4_\times}-iF_{3_\times})\big] \\ & + e^{i\beta_0}\big[\tilde{h}(f-f_{rot})/2\big]_d\big[h_{0_+}(F_{3_+}-iF_{4_+})-h_{0_\times}(F_{4_\times}+iF_{3_\times})\big] \\ & + \big[\tilde{h}(f)\big]_d\big[h_{0_+}F_{5_+}-ih_{0_\times}F_{5_\times}\big]. \end{aligned} \tag{5.51}$$

This shows that due to AM every Doppler modulated FM signal will split in four additional lines at $f \pm 2f_{rot}$ and $f \pm f_{rot}$, where f_{rot} is the rotational frequency of the Earth ($f_{rot} \approx 1.16\times10^{-5}$ Hz). In terms of the dimensionless scaled frequency ν the power of the signal will be at $\nu \pm 2a$, $\nu \pm a$, and ν.

We have plotted in Fig. (5.4) the power spectrum of the noise free complete response of the signal for its various parameters given by (5.43).

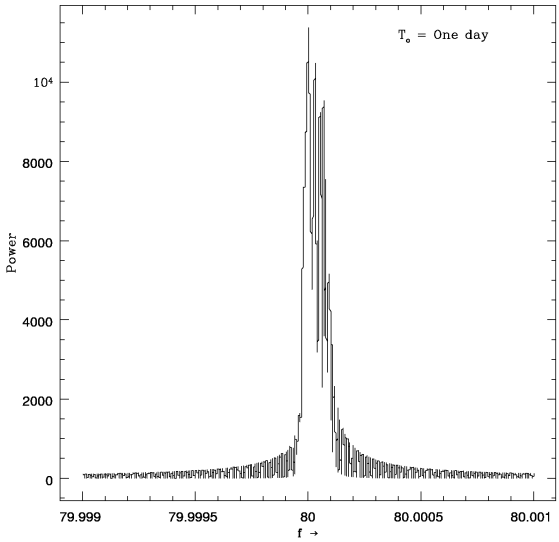

Figure 5.4: Power spectrum of the complete response of a Doppler modulated signal of a source located at $(\frac{\pi}{36}, \pi)$ with a resolution of 10^{-7}.

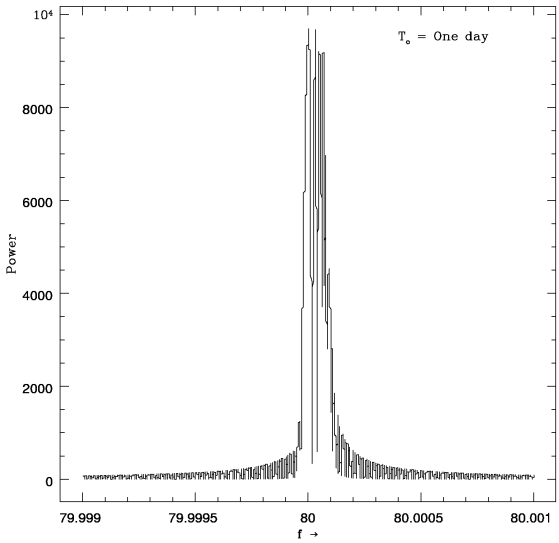

Figure 5.5: Power spectrum of a Doppler modulated signal at frequencies $f + 2f_{rot}$ of a source located at $(\frac{\pi}{36}, \pi)$ with a resolution of 10^{-7}.

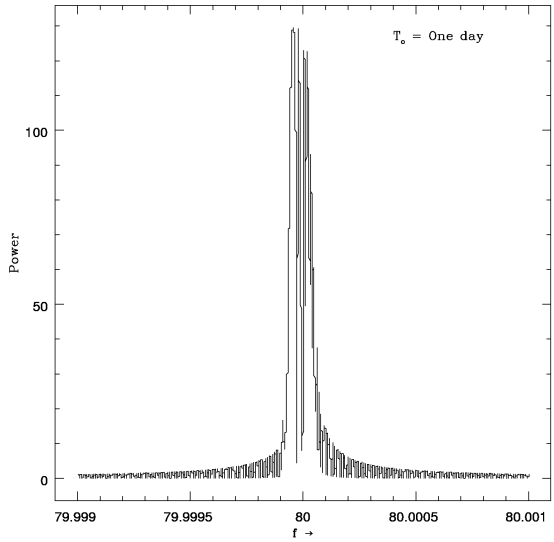

Figure 5.6: Power spectrum of a Doppler modulated signal at frequencies $f - 2f_{rot}$ of a source located at $(\frac{\pi}{36}, \pi)$ with a resolution of 10^{-7}.

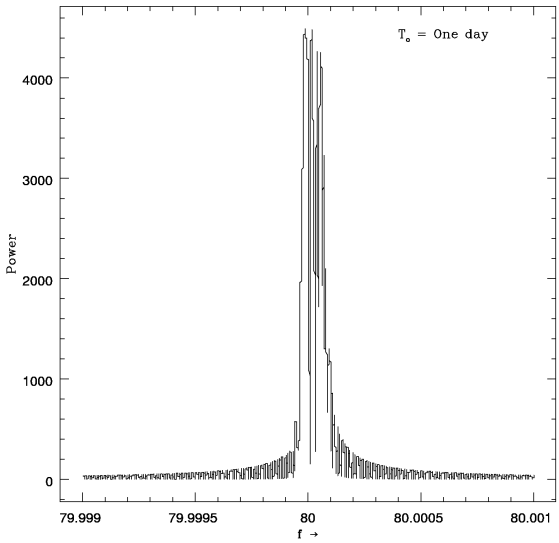

Figure 5.7: Power spectrum of a Doppler modulated signal at frequencies $f + f_{rot}$ of a source located at $(\frac{\pi}{36}, \pi)$ with a resolution of 10^{-7}.

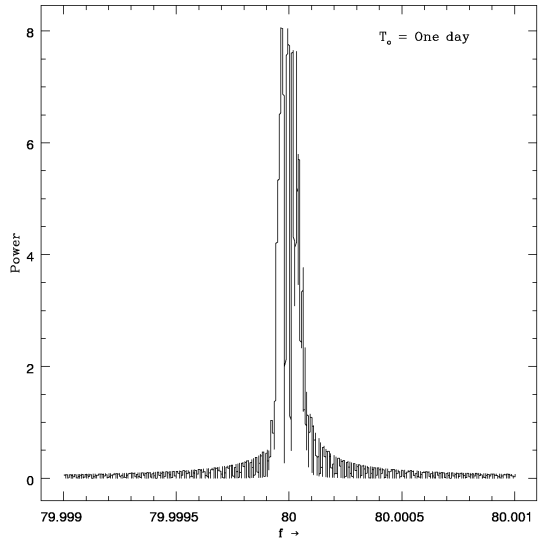

Figure 5.8: Power spectrum of a Doppler modulated signal at frequencies $f - f_{rot}$ of a source located at $(\frac{\pi}{36}, \pi)$ with a resolution of 10^{-7}.

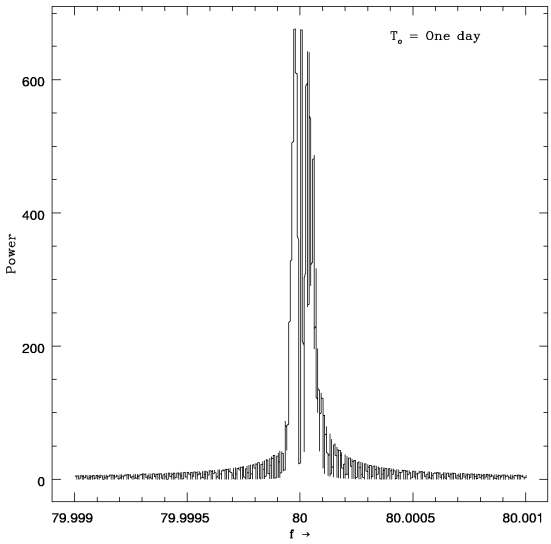

Figure 5.9: Power spectrum of a Doppler modulated signal at frequencies f of a source located at $(\frac{\pi}{36}, \pi)$ with a resolution of 10^{-7}.

The contribution in the power spectrum of modulation at frequencies $f+2f_{rot}$, $f-2f_{rot}$, $f+f_{rot}$, $f-f_{rot}$, and f are represented in Figs. (5.5), (5.6), (5.7), (5.8), and (5.9). It is observed that the most of the power will be at $f+2f_{rot}$, and least power will be in $f-f_{rot}$.

§ 5.5 Discussion

We have considered the effect of the Earth's motion on the response of the detector through FT analysis. It can easily be inferred from Eqs. (5.51) and (5.41, 5.42) that the splitting of the frequencies (i) arises explicitly in AM due to the rotational motion, and (ii) arises in FM due to the rotational as well as the orbital motion of the Eearth. In view of the fact that the data output at the detector is available in discrete form, the analytical FT is not very convenient and one normally employs the popular FFT. However, FFT has a resolution limited to $1/T_0$. Further, it is important to understand for how much time one can ignore the frequency shift arising due to Doppler effect. In fact, Schutz (1991) has demonstrated that these effects due to the rotational motion are important after the time given by

$$T_{max} = \left(\frac{2c}{\omega_{rot}^2 f_0 R_e}\right)^{1/2} \simeq 70 \left(\frac{f_0}{1\text{kHz}}\right)^{-1/2} \text{min}. \qquad (5.52)$$

This means that for GW signal at the frequency 80 Hz one has to take into account these effects after data time $\simeq$4 hours. The analytical FT studied in this Chapter leads to following inferences:

(i) FFT for one day observation data will not provide such a sufficient resolution as to represent the correct picture of the frequency splitting;

(ii) The adequate resolution required for one day observation is $\simeq 10^{-6}$ Hz;

(iii) The frequency splitting due to FM for the frequency $f_0 = 80$ Hz and source at $(\theta, \phi) = (\frac{\pi}{36}, \pi)$ is $\simeq 2\times10^{-4}$ Hz, while due to AM it is $\simeq 4.64\times10^{-5}$ Hz;

(iv) The drop in amplitude due to FM alone is about 56%;

(v) The drop in amplitude due to AM alone is about 18%;

(vi) The drop in amplitude for the complete response is about 74%;

(vii) The maximum power due to AM is associated with $f_0 + 2f_{rot}$.

It is remarked that the drop of the amplitude in complete response is severe due to both AM and FM as the relevant frequency range lie in the same region; see conclusion (iii) that above.

Finally, we would like to mention that we have presented the FT analysis assuming the phase of the GW to be zero at the instant $t = 0$. However, one may relax this condition and may obtain the results easily by taking into consideration the effects of change of the time origin.

Chapter 6

DATA ANALYSIS — PART II

§6.1 Introduction

In Chapter 5 we analyzed the Fourier analysis of one day observation data set of the response of a laser interferometer. We have seen that the amplitude and frequency modulations result into a large number of side bands about the signal frequency f_0. Consequently the maximum power lies in the frequency $f + 2f_{rot}$ with the amplitude reduction by 74% to what one would have expected due to the increased data interval. Hence, for GW detection it is desirable to obtain FT for larger data observation time intervals. To begin with we present in the next §6.2 an analysis for data set of one year observation time. The analysis turns out to be simple in view of the observation that there exists correspondences and identifications to the analysis of Chapter 5 to make them identical. In this Chapter we generalize the results for an arbitrary observation time. To facilitate analogous modifications we have introduced corresponding quantities with tilde viz., $\tilde{\mathcal{C}}$, and $\tilde{\mathcal{D}}$ in the place of $\mathcal{C}$ and $\mathcal{D}$. As an application of the results we have obtained the FT for the spin down and N-component signal.

§6.2 Fourier transform for one year integration

§6.2.1 Frequency modulation

Let us rewrite the expression for phase of the GW signal referring to Eqs. (5.27), (5.28), and (5.29), as follows

$$\Phi(t) = 2\pi f_0 t + \mathcal{Z}\cos\big(w_{orb}t - \phi\big) + \mathcal{N}\cos\big(w_{rot}\,t - \delta\big) - \mathcal{R} - \mathcal{Q}\,. \quad (6.1)$$

The FT for one year observation time T_{obs} is given as

$$\big[\tilde{h}(f)\big]_y = \int_0^{\bar{a}T} \cos\big[\Phi(t)\big]\, e^{-i2\pi ft}\, dt\,, \quad (6.2)$$

$$\bar{a} = a^{-1} = w_{rot}/w_{orb}\,, \quad T = \textit{one sidereal day}, \quad (6.3)$$

$$T_{obs} = \bar{a}\,T \simeq 3.14\times 10^7 \text{ sec}\,. \quad (6.4)$$

This may be split as usual into two terms as

$$\left[\tilde{h}(f)\right]_y = I_{\bar{\nu}_-} + I_{\bar{\nu}_+}\,; \tag{6.5}$$

$$I_{\bar{\nu}_-} = \frac{1}{2\,w_{orb}} \int_0^{2\pi} e^{i\left[\bar{\xi}\bar{\nu}_- + \mathcal{Z}\cos(\bar{\xi}-\phi) + \mathcal{N}\cos(\bar{a}\bar{\xi}-\delta) - \mathcal{R} - \mathcal{Q}\right]} d\bar{\xi}\,, \tag{6.6}$$

$$I_{\bar{\nu}_+} = \frac{1}{2\,w_{orb}} \int_0^{2\pi} e^{-i\left[\bar{\xi}\bar{\nu}_+ + \mathcal{Z}\cos(\bar{\xi}-\phi) + \mathcal{N}\cos(\bar{a}\bar{\xi}-\delta) - \mathcal{R} - \mathcal{Q}\right]} d\bar{\xi}\,, \tag{6.7}$$

$$\bar{\nu}_\pm = \frac{f_0 \pm f}{f_{orb}}\,; \quad \bar{\xi} = \xi_{orb} = w_{orb}\,t\,. \tag{6.8}$$

Hereafter, we neglect the contribution of $I_{\bar{\nu}_+}$ into $\left[\tilde{h}(f)\right]_y$ as it oscillates rapidly and contributes very little, and we write $\bar{\nu}$ in the place of $\bar{\nu}_-$. A careful comparison of Eq. (6.6) with (5.35) reveals that the integrands of the equations are identical with the following identifications and correspondences

$$\left.\begin{array}{ccc} \delta & \leftrightarrow & \phi \\ \mathcal{Z} & \leftrightarrow & \mathcal{N} \\ a & \leftrightarrow & \bar{a} \end{array}\right\}. \tag{6.9}$$

Hence, we may employ the results obtained here by introducing obvious corresponding quantities, i.e. $\bar{\mathcal{B}}$, $\bar{\mathcal{C}}$, $\bar{\mathcal{D}}$ in the place of $\mathcal{B}$, $\mathcal{C}$, $\mathcal{D}$, leaving $\mathcal{A}$ unchanged. Thus

$$\left[\tilde{h}(f)\right]_y \simeq \frac{\bar{\nu}}{2\,w_{orb}} \sum_{k=-\infty}^{k=\infty} \sum_{m=-\infty}^{m=\infty} e^{i\mathcal{A}}\,\bar{\mathcal{B}}\left[\bar{\mathcal{C}} - i\,\bar{\mathcal{D}}\right]; \tag{6.10}$$

$$\begin{aligned}
\mathcal{A} &= \frac{(k+m)\pi}{2} - \mathcal{R} - \mathcal{Q}\,, \\
\bar{\mathcal{B}} &= \frac{J_k(\mathcal{N})\,J_m(\mathcal{Z})}{\bar{\nu}^2 - (\bar{a}k+m)^2}\,, \\
\bar{\mathcal{C}} &= \sin 2\bar{\nu}\pi\,\cos\left(2\bar{a}k\pi - k\delta - m\phi\right) \\
&\quad - \frac{\bar{a}k+m}{\bar{\nu}}\left\{\cos 2\bar{\nu}\pi\,\sin\left(2\bar{a}k\pi - k\delta - m\phi\right) + \sin\left(k\delta + m\phi\right)\right\}, \\
\bar{\mathcal{D}} &= \cos 2\bar{\nu}\pi\,\cos\left(2\bar{a}k\pi - k\delta - m\phi\right) \\
&\quad + \frac{k\bar{a}+m}{\bar{\nu}}\,\sin 2\bar{\nu}\pi\,\sin\left(2\bar{a}k\pi - k\delta - m\phi\right) - \cos\left(k\delta + m\phi\right)\,.
\end{aligned}$$

Now the FT of these two polarization states can be written as

$$\left[\tilde{h}_+(f)\right]_y = h_{0_+}\left[\tilde{h}(f)\right]_y \simeq \frac{\bar{\nu}h_{0_+}}{2w_{orb}} \sum_{k=-\infty}^{k=\infty} \sum_{m=-\infty}^{m=\infty} e^{i\mathcal{A}}\,\bar{\mathcal{B}}\left[\bar{\mathcal{C}} - i\,\bar{\mathcal{D}}\right], \tag{6.11}$$

$$\left[\tilde{h}_{\times}(f)\right]_y = -ih_{0_\times}\left[\tilde{h}(f)\right]_y \simeq \frac{\bar{\nu}h_{0_\times}}{2w_{orb}}\sum_{k=-\infty}^{k=\infty}\sum_{m=-\infty}^{m=\infty} e^{i\mathcal{A}}\bar{\mathcal{B}}\left[\bar{\mathcal{D}}-i\bar{\mathcal{C}}\right]. \quad (6.12)$$

The FT obtained contains the double series of Bessel functions of the order k and m ranging from $-\infty$ to ∞. It is well known that Bessel functions decrease rapidly as the order exceeds the argument. Hence the possible range of k and m, over which the summation of the series is to be considered, depends on the arguments of Bessel functions i.e. $\mathcal{Z}$ and $\mathcal{N}$. Referring to Eq. (5.28) it is found that

$$\left.\begin{aligned} \mathcal{Z}_{max} &= 3133215\left(\frac{f}{1\text{ KHz}}\right) \\ \mathcal{N}_{max} &= 134\left(\frac{f}{1\text{ KHz}}\right) \end{aligned}\right\}. \quad (6.13)$$

The FT of a FM signal for

$$\left.\begin{aligned} &f_0 = 50\text{ Hz}, \quad h_0 = h_\times = 1 \\ &\alpha = \tfrac{\pi}{4}, \qquad \beta_0 = 0, \qquad \gamma = \pi \\ &\theta = \tfrac{\pi}{18}, \qquad \phi = 0, \qquad \psi = \tfrac{\pi}{4} \end{aligned}\right\} \quad (6.14)$$

is shown in Fig. (6.1). A resolution of $1/T_0 \approx 3.17\times10^{-8}$ Hz is attributed to the spectrum. We have convinced ourselves by plotting the FT at higher resolutions that the resolution of $1/T_0$ is sufficient to represent relevant peaks. We notice that the drop in amplitude is about 98%. This may be attributed to the presence of a very large number of side bands.

§6.2.2 Complete response

The complete response of the detector may be obtained employing Eqs. (6.11, 6.12, 5.45, 5.46) and one gets

$$\begin{aligned} \left[\tilde{R}_+(f)\right]_y = h_{0_+}\Big[& e^{-i2\beta_0}(F_{1_+}+iF_{2_+})\left[\tilde{h}(f+2f_{rot})/2\right]_y \\ & + e^{i2\beta_0}(F_{1_+}-iF_{2_+})\left[\tilde{h}(f-2f_{rot})/2\right]_y \\ & + e^{-i\beta_0}(F_{3_+}+iF_{4_+})\left[\tilde{h}(f+f_{rot})/2\right]_y \\ & + e^{i\beta_0}(F_{3_+}-iF_{4_+})\left[\tilde{h}(f-f_{rot})/2\right]_y \\ & + F_{5_+}\left[\tilde{h}(f)\right]_y\Big], \end{aligned} \quad (6.15)$$

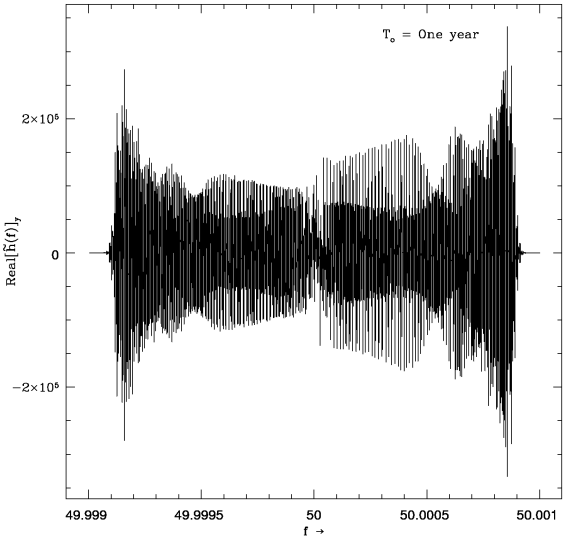

Figure 6.1: FT of a FM signal of a source located at $(\frac{\pi}{18}, 0)$ with a resolution of 3.17×10^{-8}.

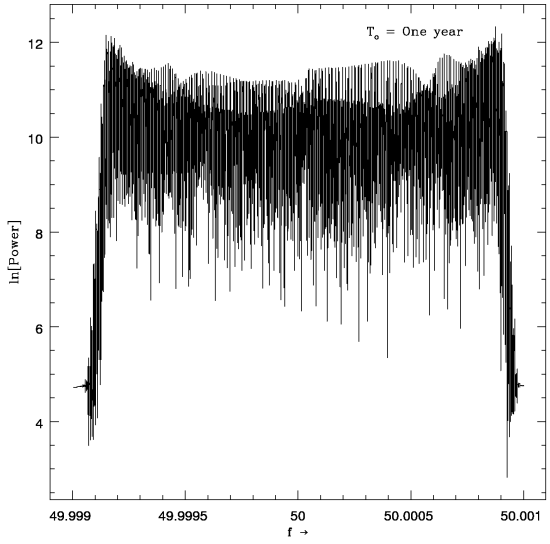

Figure 6.2: Power spectrum of the complete response of a modulated signal of a source located at $(\frac{\pi}{18}, 0)$ with a resolution of 3.17×10^{-8}.

$$\begin{aligned}\big[\tilde{R}_{\times}(f)\big]_y \;=\; h_{0_\times}\Big[\; & e^{-i2\beta_0}(F_{2_\times} - iF_{1_\times})\big[\tilde{h}(f+2f_{rot})/2\big]_y \\ & - e^{i2\beta_0}(F_{2_\times} + iF_{1_\times})\big[\tilde{h}(f-2f_{rot})/2\big]_y \\ & + e^{-i\beta_0}(F_{4_\times} - iF_{3_\times})\big[\tilde{h}(f+f_{rot})/2\big]_y \\ & - e^{i\beta_0}(F_{4_\times} + iF_{3_\times})\big[\tilde{h}(f-f_{rot})/2\big]_y \\ & - iF_{5_\times}\big[\tilde{h}(f)\big]_y\Big]. \end{aligned} \tag{6.16}$$

After rearranging these expressions we obtain

$$\begin{aligned}\big[\tilde{R}(f)\big]_y = {} & e^{-i2\beta_0}\big[\tilde{h}(f+2f_{rot})/2\big]_y\big[h_{0_+}(F_{1_+}+iF_{2_+})+h_{0_\times}(F_{2_\times}-iF_{1_\times})\big] \\ & + e^{i2\beta_0}\big[\tilde{h}(f-2f_{rot})/2\big]_y\big[h_{0_+}(F_{1_+}-iF_{2_+})-h_{0_\times}(F_{2_\times}+iF_{1_\times})\big] \\ & + e^{-i\beta_0}\big[\tilde{h}(f+f_{rot})/2\big]_y\big[h_{0_+}(F_{3_+}+iF_{4_+})+h_{0_\times}(F_{4_\times}-iF_{3_\times})\big] \\ & + e^{i\beta_0}\big[\tilde{h}(f-f_{rot})/2\big]_y\big[h_{0_+}(F_{3_+}-iF_{4_+})-h_{0_\times}(F_{4_\times}+iF_{3_\times})\big] \\ & + \big[\tilde{h}(f)\big]_y\big[h_{0_+}F_{5_+}-ih_{0_\times}F_{5_\times}\big]\,. \end{aligned} \tag{6.17}$$

Figure (6.2) shows the power spectrum of the complete response of the Doppler modulated signal. We have kept here all parameters the same as in FM.

§6.3 Fourier transform for an arbitrary observation time

It is important to obtain the FT for an arbitrary observation time. The results obtained will be employed to outline how the spin down of a pulsar due to the gravitational radiation back reaction or due to some other mechanism can be taken into account.

The FT for data of observation time T_0 is given via

$$\tilde{h}(f) = \int_0^{T_0} \cos\big[\Phi(t)\big]\, e^{-i2\pi ft}\, dt\,. \tag{6.18}$$

As usual, this splits into two terms as

$$\tilde{h}(f) \;= I_{\nu_-} + I_{\nu_+}\,; \tag{6.19}$$

$$I_{\nu_-} \;= \frac{1}{2\,w_{rot}} \int_0^{\xi_0} e^{i[\xi\nu_- + \mathcal{Z}\cos(a\xi-\phi)+\mathcal{N}\cos(\xi-\delta)-\mathcal{R}-\mathcal{Q}]}\, d\xi\,, \tag{6.20}$$

$$I_{\nu_+} \;= \frac{1}{2\,w_{rot}} \int_0^{\xi_0} e^{-i[\xi\nu_+ + \mathcal{Z}\cos(a\xi-\phi)+\mathcal{N}\cos(\xi-\delta)-\mathcal{R}-\mathcal{Q}]}\, d\xi\,, \tag{6.21}$$

$$\nu_{\pm} = \frac{f_0 \pm f}{f_{rot}}\,; \quad \xi_0 = w_{rot}\,T_0\,; \quad \xi = \xi_{rot} = w_{rot}\,t\,. \tag{6.22}$$

As I_{ν_+} contributes very little into $\tilde{h}(f)$, we drop I_{ν_+} and write ν in the place of ν_-. Using the identity (5.38) we get

$$\tilde{h}(f) \simeq \frac{e^{i(-\mathcal{R}-\mathcal{Q})}}{2w_{rot}} \int_0^{\xi_0} e^{i\nu\xi} \Big[J_0(\mathcal{Z}) + 2\sum_{k=1}^{k=\infty} J_k(\mathcal{Z})\, i^k \cos k\,(a\xi - \phi) \Big] \times \Big[J_0(\mathcal{N}) + 2\sum_{m=1}^{m=\infty} J_m(\mathcal{N})\, i^m \cos m\,(\xi - \delta) \Big]\, d\xi\,. \tag{6.23}$$

After performing the integration, we have

$$\tilde{h}(f) \simeq \frac{\nu}{2\,w_{rot}} \sum_{k=-\infty}^{k=\infty} \sum_{m=-\infty}^{m=\infty} e^{i\mathcal{A}}\, \mathcal{B}\,[\tilde{\mathcal{C}} - i\tilde{\mathcal{D}}]\,; \tag{6.24}$$

$$\mathcal{A} = \frac{(k+m)\,\pi}{2} - \mathcal{R} - \mathcal{Q}\,, \qquad \mathcal{B} = \frac{J_k(\mathcal{Z})\,J_m(\mathcal{N})}{\nu^2 - (ak+m)^2}\,,$$

$$\begin{aligned} \tilde{\mathcal{C}} &= \sin\nu\xi_0 \cos\left(a\,k\xi_0 + m\xi_0 - k\phi - m\delta\right) \\ &- \frac{ak+m}{\nu} \left\{ \cos\nu\xi_0 \sin\left(a\,k\xi_0 + m\xi_0 - k\phi - m\delta\right) + \sin\left(k\phi + m\delta\right) \right\}, \\ \tilde{\mathcal{D}} &= \cos\nu\xi_0 \cos\left(a\,k\xi_0 + m\xi_0 - k\phi - m\delta\right) \\ &+ \frac{ka+m}{\nu} \sin\nu\xi_0 \sin\left(a\,k\xi_0 + m\xi_0 - k\phi - m\delta\right) - \cos\left(k\phi + m\delta\right)\,. \end{aligned}$$

The FT of these two polarization states of the wave can be written

$$h_+(f) = h_{0_+}\tilde{h}(f) \simeq \frac{\nu\,h_{0_+}}{2w_{rot}} \sum_{k=-\infty}^{k=\infty} \sum_{m=-\infty}^{m=\infty} e^{i\mathcal{A}}\mathcal{B}\,[\tilde{\mathcal{C}} - i\tilde{\mathcal{D}}]\,, \tag{6.25}$$

$$\tilde{h}_\times(f) = -\,i\,h_{0_\times}\tilde{h}(f) \simeq \frac{\nu\,h_{0_\times}}{2w_{rot}} \sum_{k=-\infty}^{k=\infty} \sum_{m=-\infty}^{m=\infty} e^{i\mathcal{A}}\mathcal{B}\,[\tilde{\mathcal{D}} - i\tilde{\mathcal{C}}]\,. \tag{6.26}$$

Now it is simple to obtain the FT of complete response. One gets

$$\begin{aligned} \tilde{R}(f) &= e^{-i2\beta_0}\tilde{h}(f+2f_{rot})/2\,[h_{0_+}(F_{1_+}+iF_{2_+}) + h_{0_\times}(F_{2_\times} - iF_{1_\times})] \\ &+ e^{i2\beta_0}\tilde{h}(f-2f_{rot})/2\,[h_{0_+}(F_{1_+}-iF_{2_+}) - h_{0_\times}(F_{2_\times} + iF_{1_\times})] \\ &+ e^{-i\beta_0}\tilde{h}(f+f_{rot})/2\,[h_{0_+}(F_{3_+}+iF_{4_+}) + h_{0_\times}(F_{4_\times} - iF_{3_\times})] \\ &+ e^{i\beta_0}\tilde{h}(f-f_{rot})/2\,[h_{0_+}(F_{3_+}-iF_{4_+}) - h_{0_\times}(F_{4_\times} + iF_{3_\times})] \\ &+ \tilde{h}(f)\,[h_{0_+}F_{5_+} - i\,h_{0_\times}F_{5_\times}]\,. \end{aligned} \tag{6.27}$$

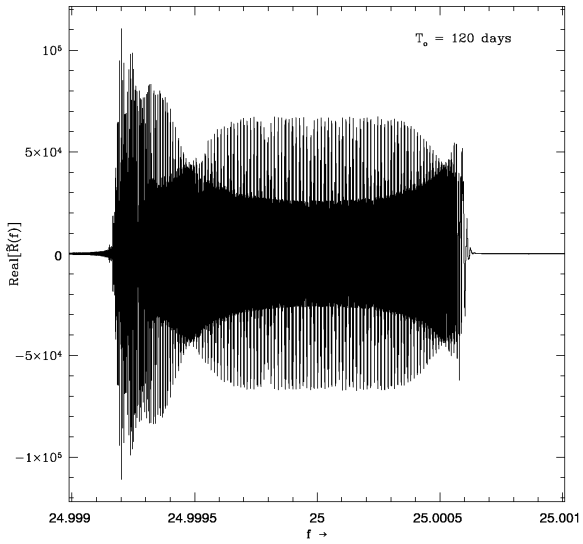

Figure 6.3: FT of a FM signal of a source located at $(\frac{\pi}{9}, \frac{\pi}{4})$ with a resolution of 9.67×10^{-8}.

The FT of FM signal for a data of 120 days and

$$\left.\begin{array}{lll} f_0 = 25 \text{ Hz}\,, & h_0 = h_\times = 1 & \\ \alpha = \frac{\pi}{6}\,, & \beta_0 = \frac{\pi}{3}\,, & \gamma = \frac{2\pi}{3} \\ \theta = \frac{\pi}{9}\,, & \phi = \frac{\pi}{4}\,, & \psi = \frac{\pi}{4} \end{array}\right\} \tag{6.28}$$

are plotted in Figure (6.3) with a resolution of $\frac{1}{2}T_0 \approx 9.67 \times 10^{-8}$ Hz. The corresponding power spectra are plotted in Figure (6.4).

§6.4 Spin down

Pulsars loose the rotational energy by the processes like electro-magnetic breaking, particles emission, and GW emission. Thus, the rotational frequency is not completely stable, but varies over a time scale which is of the order of the age of the pulsar. Typically, younger pulsars have largest spin down rates. Current observations suggest that spin down is primarily due to electro-magnetic breaking (Manchester, 1992; Kulkarni, 1992). Over the entire observing time T_0 the frequency drift would be small but it may be taken into account for better sensitivity. To account this aspect we consider the evaluation of FT in a sequence of

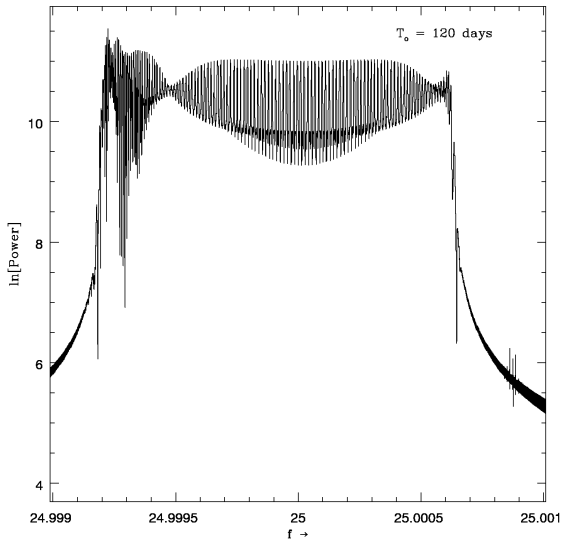

Figure 6.4: Power spectrum of the complete response of a Doppler modulated signal of a source located at $(\frac{\pi}{9}, \frac{\pi}{4})$ with a resolution of 9.67×10^{-8}.

time windows by splitting the interval $0 - T_0$ into M equal parts, each of $\triangle t$ ($T_0 = M \triangle t$) such that the signal over a window may be treated as monochromatic. The strategy is to evaluate the FT over the window and finally to add the result. This process has been suggested by Brady and Creighton (2000) and Schutz (1998) in numerical computing and called *stacking* and *tracking*. For any such window let the time interval of data under consideration be corresponding to $t = t_0 + n \triangle t$ and $t = t_0 + (n+1) \triangle t$, where t_0 is the instant representation of the start of the data set, and $0 \leqslant n \leqslant M - 1$. This is the n_{th} window. Now we have

$$I = \int_{t_0+n\triangle t}^{t_0+(n+1)\triangle t} h(\bar{t})\, e^{-i2\pi f \bar{t}}\, d\bar{t}$$

$$= \int_0^{\triangle t} h(t + t_0 \ + n \triangle t)\, e^{-i2\pi f(t+t_0+n\triangle t)}\, dt\,; \qquad (6.29)$$

$$\bar{t} = t + t_0 + n \triangle t\,. \qquad (6.30)$$

Hence, the FT to account spin down is given via

$$\big[\tilde{h}(f)\big]_s = \int_0^{\triangle t} \cos\big[\Phi\,(t + t_0 + n \triangle t)\big]\, e^{-i2\pi f(t+t_0+n\triangle t)}\, dt\,. \qquad (6.31)$$

Taking the initial time of the data set

$$t_0 = 0\,, \tag{6.32}$$

and following with the same way as in the previous §6.3, the FT is obtained as

$$\begin{aligned}\left[\tilde{h}(f)\right]_s \simeq\ & \frac{e^{i[2\pi n(f_0-f)\triangle t-\mathcal{R}-\mathcal{Q}]}}{2w_{rot}} \int_0^{\triangle t} e^{i\nu\xi} \\ & \times \left[J_0(\mathcal{Z}) + 2\sum_{k=1}^{k=\infty} J_k(\mathcal{Z})\, i^k \cos k\,(a\xi-\lambda)\right] \\ & \times \left[J_0(\mathcal{N}) + 2\sum_{m=1}^{m=\infty} J_m(\mathcal{N})\, i^m \cos m\,(\xi-\zeta)\right] d\xi\,. \end{aligned} \tag{6.33}$$

After integration we get

$$\left[\tilde{h}(f)\right]_s = \frac{\nu}{2\,w_{rot}} \sum_{k=-\infty}^{k=\infty} \sum_{m=-\infty}^{m=\infty} e^{i\mathcal{A}_s} \mathcal{B}\left[\mathcal{C}_s - i\mathcal{D}_s\right], \tag{6.34}$$

where

$$\left.\begin{aligned} \mathcal{A}_s &= \frac{(k+m)\,\pi}{2} + 2\,\pi\, n \triangle t(f_0-f) - \mathcal{R} - \mathcal{Q} \\ \mathcal{B} &= \frac{J_k(\mathcal{Z})\, J_m(\mathcal{N})}{\nu^2 - (ak+m)^2} \\ \mathcal{C}_s &= \sin(\nu\tau)\cos(ak\tau + m\tau - k\lambda - m\zeta) \\ &\quad - \frac{ak+m}{\nu}\left\{\cos(\nu\tau)\sin(ak\tau+m\tau-k\lambda-m\zeta)\right. \\ &\quad \left. + \sin(k\lambda+m\zeta)\right\} \\ \mathcal{D}_s &= \cos(\nu\tau)\cos(ak\tau+m\tau-k\lambda-m\zeta) \\ &\quad + \frac{ak+m}{\nu}\sin(\nu\tau)\sin(ak\tau+m\tau-k\lambda-m\zeta) \\ &\quad - \cos(k\lambda+m\zeta) \\ \lambda &= \phi - a\,n\,\tau_0\,, \qquad \zeta = \delta - n\tau_0 \\ \tau &= \xi_0 = w_{rot}\,T_0\,, \quad \tau_0 = w_{rot}\triangle t \\ n &= 0,1,2,3,\ldots,M-1 \end{aligned}\right\}. \tag{6.35}$$

The FT of the complete response would now be given via

$$\begin{aligned}
\big[\tilde{R}(f)\big]_s &= e^{-i2\beta_0}\big[\tilde{h}(f+2f_{rot})/2\big]_s\big[h_{0_+}(F_{1_+}+iF_{2_+})+h_{0_\times}(F_{2_\times}-iF_{1_\times})\big] \\
&+ e^{i2\beta_0}\big[\tilde{h}(f-2f_{rot})/2\big]_s\big[h_{0_+}(F_{1_+}-iF_{2_+})-h_{0_\times}(F_{2_\times}+iF_{1_\times})\big] \\
&+ e^{-i\beta_0}\big[\tilde{h}(f+f_{rot})/2\big]_s\big[h_{0_+}(F_{3_+}+iF_{4_+})+h_{0_\times}(F_{4_\times}-iF_{3_\times})\big] \\
&+ e^{i\beta_0}\big[\tilde{h}(f-f_{rot})/2\big]_s\big[h_{0_+}(F_{3_+}-iF_{4_+})-h_{0_\times}(F_{4_\times}+iF_{3_\times})\big] \\
&+ \big[\tilde{h}(f)\big]_s\big[h_{0_+}F_{5_+}-ih_{0_\times}F_{5_\times}\big]\,. \qquad (6.36)
\end{aligned}$$

§6.5 N-component signal

The FT in Eqs. (6.24) and (6.27) are for a pulsar which emits GW signal at a single frequency f_0. But there are known physical mechanisms which generate GW signals consisting of many components. An axially symmetric pulsar undergoing free precession, emits a quadrupole GW at two frequencies, one equal to the sum of the spin frequency and the precession frequency, and the other twice of it (Zimmermann, 1979, 1980). The quadrupole GW from a triaxial ellipsoid rotating about one of its axes consists of one component only (Thorne, 1987). In this case the signal has a frequency about twice the spin frequency of the star. In general, if a star is non-axisymmetric and precessing, the GW signal consists of more than two components. For the case of triaxial ellipsoid and small wobble angle there is a third component with a frequency twice of the spin frequency of the star (Zimmermann, 1979, 1980). Also, the mechanisms e.g. the r-mode instability of spinning neutron stars (Anderson, 1998; Lindblom et al., 1998; Owen et al., 1998) and the temperature asymmetry in the interior of a neutron star with the miss-aligned spin axis (Bildsten, 1998) have been discussed in the literature.

In view of the above discussion CGW signal may consists of frequencies which are multiple of some basic frequencies. An analysis of the GW data of N-component of signal has been made recently by Jaranowski and Królak (2000). In this §6.5 we present Fourier analysis of an N-component CGW signal. We model the N-component signal as

$$h(t) = \sum_{l=1}^{N} h_l(t)\,; \qquad (6.37)$$

$$h_{l+}(t) = h_{0_{l+}}\cos\big[\Phi_l(t)\big]\,, \qquad (6.38)$$

$$h_{l\times}(t) = h_{0_{l\times}}\sin\big[\Phi_l(t)\big]\,, \qquad l = 1, 2, \ldots, N\,; \qquad (6.39)$$

$$\Phi_l(t) = 2\pi f_l \left[t + \mathcal{Z}_l \cos\left(a\xi_{rot} - \phi\right) + \mathcal{N}_l \cos(\xi_{rot} - \delta_l) - \mathcal{R}_l - \mathcal{Q}_l \right], \quad (6.40)$$

where f_l represent the component frequency of the signal.

Now let us write

$$h_l(t) = \cos\left[\Phi_l(t)\right]. \quad (6.41)$$

It is trivial matter to obtain $\tilde{h}_l(f)$, $\tilde{R}_l(f)$, and to get

$$\tilde{h}_N(f) = \sum_l \tilde{h}_l(f), \quad (6.42)$$

$$\tilde{R}_N(f) = \sum_l \tilde{R}_l(f). \quad (6.43)$$

§6.6 Discussion and summary

The analysis and results obtained in the previous Chapter 5 regarding FT of the response of a laser interferometer have been generalized in the present Chapter. In this context following points must be noted:

1. For longer observation time, say, 120 days the resolution provided by FFT (equal to $1/T_0$) is sufficient to represent the structure of side bands;
2. Although in every case discussed, it turned out that the maximum power lies in the frequency $f + 2f_{rot}$. However, this is not established conclusively whether this result is generic. In any case, for any given detector location, we can know in advance if a similar type of behaviour is obtained;
3. The computer time required in computing analytical FT depends on the orientation of the source, and is independent from the time interval of the observation data set. In contrast to this factor, the computation cost increases for FFT with the increase of the data set;
4. Throughout our analysis in Chapters 5 and 6 we have employed following conditions:
   (i) The phase of the wave is zero at $t = 0$;
   (ii) The observation time of the data set is in the range from $t = 0$ to $t = T_0$;
5. As remarked in Chapter 5 the requirement 4(i) may be achieved by translation of time-origin. Now let us see how the condition 4(ii) can be relaxed. Let the data set is taken for

$$t = t_i \quad \text{to} \quad t = t_i + T_0. \quad (6.44)$$

Eqs. (6.29, 6.30, 6.31, 6.32) reveal that the results obtained there correspond to data set

$$t = n \triangle t \quad \text{to} \quad t = (n+1) \triangle t\,. \tag{6.45}$$

To obtain the sought generalization we set

$$t_i = n \triangle t \quad \text{and} \quad T_0 = \triangle t\,, \tag{6.46}$$

and may use the results of §6.3 by noting that for the present case we have

$$\lambda \;=\; \phi - n\, w_{orb} \triangle t \quad \Longrightarrow \quad \lambda = \phi - w_{orb}\, t_i\,, \tag{6.47}$$

$$\zeta \;=\; \delta - n\, w_{rot} \triangle t \quad \Longrightarrow \quad \zeta = \delta - w_{rot}\, t_i\,. \tag{6.48}$$

Chapter 7

TEMPLATES FOR AN ALL SKY SEARCH

§ 7.1 Introduction

Gravitational wave laser interferometer antennae are essentially omnidirectional with their response better than 50% of the average over 75% of the whole sky. Hence the data analysis systems will have to carry out all sky searches for the sources. We know that the amplitude of an intense GW believed bathing the Earth is very small, as compared to the sensitivity of GW detectors and is further masked by the dominant noise. In these circumstances, CGW sources are of prime importance because for such sources we can achieve enhanced SNR by investigating longer observation data set. However, a long observation time introduces modulation effects, arising due to the relative motion of the detector with respect to the source. As a consequence, there results a distribution of power in a forest of sidebands to such an extent that there is a reduction to the tune of 90% of the expected power due to AM. The problem of an all sky search gains another dimension in view of the fact that there are reasons to believe the presence of intense GW sources whose locations and even frequencies are unknown. Amongst such sources pulsars occupy an important position. Similar to all sky search one will also have to do all frequency search. All sky and all frequency search is the holy grail of gravitation pulsar astronomy.

Search of CGW without a priori knowledge appears to be computationally quite demanding even by the computers expected to be available in the near future. For example, in the case of a bandwidth 10^3 Hz, an observation time 10^7 sec, and a star's minimum decay time of 100 years one would require 10^{14} TFLOPS computer (Frasca, 2000). Very fast computer and large memories with an ample amount of the disk space seems inevitable. However, the choice of optimal data processing and clever programming is also an integral part of the solution to this problem. Amongst these the pre-correction of the time series due to Doppler modulation before the data are processed may be a method, which will reduce computational requirements. In reference to this, Schutz (1991) has introduced the concept of patches in the sky defined as the region of space for which similar Doppler corrections would be required. He has

also demonstrated that the number of the patches required for a 10^7 sec observation data set and one KHz signal would be about 1.3×10^{13}, if one takes into account the Earth's rotation. However, the size of such a patch would also depend on the data analysis technique being employed.

Matched Filtering is the most suitable technique for detection of signals from sources viz., pulsars whose wave form is known. The wave forms are used to construct a bank of templates, which represent the expected signal wave form with all possible ranges of its parameters. The time of arrival, the source location, the frequency of the signal, the ellipticity of the source and its spin down represent important parameters of a GW emitted by a pulsar. For detection of GW we set up a criterion to judge if the cross correlation of the templates with the corresponding data set exceeds the preassigned threshold. We would perform the data analysis employing the criterion of the *FF*.

§ 7.2 Matched filter analysis: templates

The bank of templates will be matched to only a discrete set of signals from amongst the continuum of possible signals. Consequently, it is natural that all the signals will not get detected with equal probability. However, it is possible to choose judiciously the set of templates so that all signals of a given amplitude are detected with a given minimum detection probability. The standard measure for deciding what class of wave form is good enough is the *FF* (Apostolatos, 1995). It quantitatively describes the closeness of the true signals to the template manifold in terms of the reduction of SNR due to a cross correlation between a signal outside the manifold and all the templates lying inside the manifold. If the *FF* of a template family is unity, the signal lies in the manifold. If the *FF* is less than unity, the signal lies outside manifold.

Even if the signal discrete templates lies within the template manifold it would be unlikely that any of the actual templates used would correspond to the signal. The parameters describing the search template (the source location, the ellipticity, etc.) can vary continuously throughout a finite range of values. The set of templates characterized by the continuously varying parameters is of course infinite. However, in practice the interferometer output must be cross correlated with a finite subset of the templates whose parameter values vary in discrete steps from one template to the next one. This subset ("the discrete template family") is zero on the manifold of the full set of possible templates ("the continuous template family"), so the template which most closely match a signal will generally lie between the signal and the nearest of

the discrete template family. The mismatch between the signal and the nearest of the discrete templates will cause some reduction in SNR. This would mean that the members of the discrete template family must be chosen so as to render acceptable loss of SNR.

The study of templates has been made by many researchers in time domain.* However, the analysis in frequency domain has the advantage of incorporating interferometer's spectral noise density. In order to determine the number of templates required to perform matched filtering analysis let us rewrite the formula expressing FF, see Eq. (4.12), as

$$FF(\theta,\phi) = \max_{\theta,\phi} \frac{\langle h(f)|h_T(f;\theta_T,\phi_T)\rangle}{\sqrt{\langle h_T(f;\theta_T,\phi_T)|h_T(f;\theta_T,\phi_T)\rangle\langle h(f)|h(f)\rangle}}\,, \quad (7.1)$$

where $h(f)$ and $h_T(f;\theta_T,\phi_T)$ are the FTs of the signal wave form and the templates, respectively. The template parameters θ_T, ϕ_T are chosen differing from the actual orientation of the source in discrete steps.

We have seen in the previous Chapters that the AM of CGW data output results into re-distribution of power at four additional frequencies $f \pm 2f_{rot}$, $f \pm f_{rot}$ according to the FM. Hence it is sufficient for the analysis of FF to consider only the frequency modulated FT. The results obtained in Chapter 6 regarding the FT of the frequency modulated data output, see Eq. (6.24), may be arranged using the symmetry property of the Bessel functions, and one may write

$$\begin{aligned}\tilde{h}(f) \;\simeq\; \frac{\nu}{w_{rot}} \Bigg[& \frac{J_0(\mathcal{Z})J_0(\mathcal{N})}{2\nu^2}\big[\{\sin(\mathcal{R}+\mathcal{Q}) - \sin(\mathcal{R}+\mathcal{Q}-\nu\xi_0)\} + \\ & + i\{\cos(\mathcal{R}+\mathcal{Q}) - \cos(\mathcal{R}+\mathcal{Q}-\nu\xi_0)\}\big] \\ & + J_0(\mathcal{Z}) \sum_{m=1}^{m=\infty} \frac{J_m(\mathcal{N})}{\nu^2-m^2}\big[(\mathcal{YU}-\mathcal{XV}) - i(\mathcal{XU}+\mathcal{YV})\big] \\ & + \sum_{k=1}^{k=\infty}\sum_{m=-\infty}^{m=\infty} e^{i\mathcal{A}}\mathcal{B}\big[\tilde{\mathcal{C}} - i\tilde{\mathcal{D}}\big]\Bigg], \end{aligned} \quad (7.2)$$

$$\left.\begin{aligned} \mathcal{X} &= \sin\left(\mathcal{R}+\mathcal{Q}-m\,\tfrac{\pi}{2}\right) \\ \mathcal{Y} &= \cos\left(\mathcal{R}+\mathcal{Q}-m\,\tfrac{\pi}{2}\right) \\ \mathcal{U} &= \sin\nu\xi_0\cos m(\xi_0-\delta) - \frac{m}{\nu}\cos\nu\xi_0\sin m(\xi_0-\delta) - \sin m\delta \\ \mathcal{V} &= \cos\nu\xi_0\cos m(\xi_0-\delta) + \frac{m}{\nu}\sin\nu\xi_0\sin m(\xi_0-\delta) - \cos m\delta \end{aligned}\right\}. \quad (7.3)$$

*Schutz (1991), Brady et al. (1998), Brady and Creighton (2000), Jaranowski et al. (1998), Jaranowski and Królak (2000).

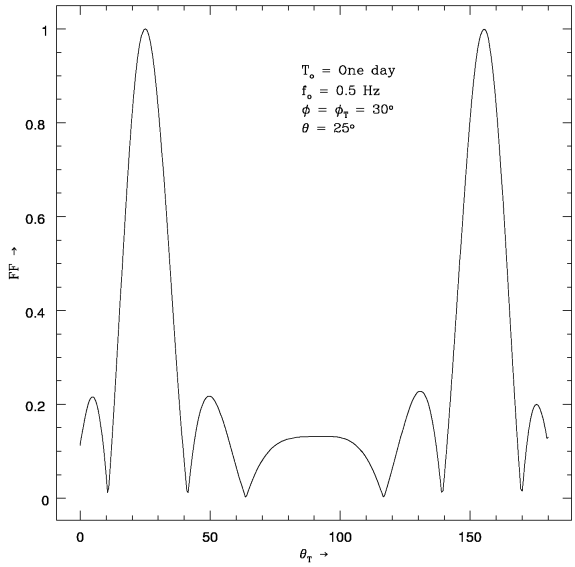

Figure 7.1: Variation of FF with θ_T.

Now it is straight forward to compute FF. To understand the procedure let us assume that there is a source at the location $(\theta, \phi) = (25^\circ, 30^\circ)$ emitting a frequency $f_0 = 0.5$ Hz. We wish to analyze the data set for T_0 = one sidereal day. We first fix the template parameter ϕ for the whole set given by $\phi_T = \phi = 30^\circ$ and vary θ_T in discrete steps over its entire range i.e. 0° to 180°. The results obtained are plotted graphically in Fig. (7.1). It is remarked that, in order to compute the inner product defined via Eq. (4.9), one would require to integrate the expression over the band width of the Doppler modulated signal. This may be determined either analytically by computing the maximum value of the Doppler shift in accordance with Eq. (5.25) or may be taken as the represented by the frequency spectrum of the FT. In the present case we have taken the band width equal to 0.002 Hz. In a similar manner one may fix the θ-parameter of the template set and obtain the variation of FF with the template parameter ϕ_T. Figures (7.2) and (7.3) represent respectively the behaviour for $f_0 = 25$ Hz, $\theta = \theta_T = 1^\circ$, T_0 = one sidereal day for source orientation $\phi = 35^\circ$ and 220°.

The following points in reference to these plots may be noted:

(i) The FF is unity for $\theta_T = 25^\circ$, 155°, see Fig (7.1, for $\phi_T = 35^\circ$, 145°, see Fig (7.2), and for $\phi_T = 220^\circ$, 320°, see Fig (7.3);

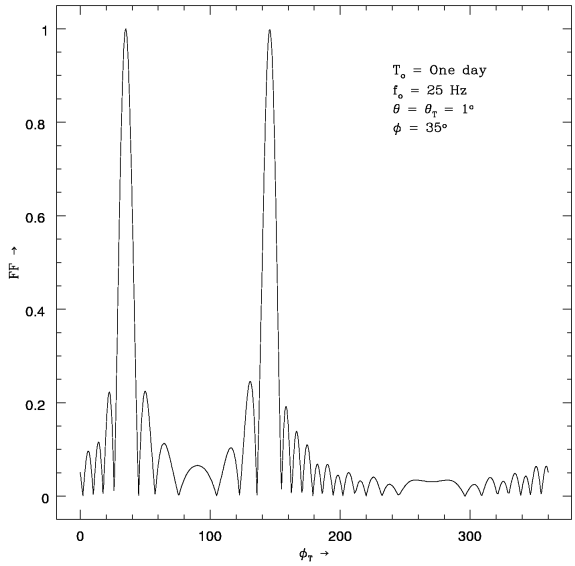

Figure 7.2: Variation of FF with ϕ_T.

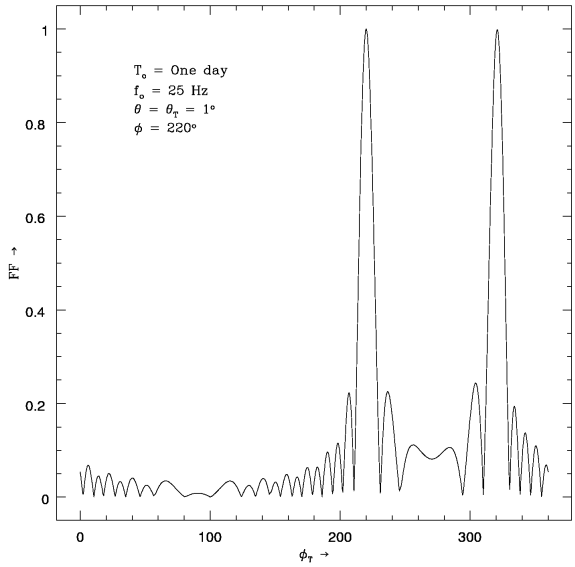

Figure 7.3: Variation of FF with ϕ_T.

(ii) It is observed that FF decreases exponentially with template variables θ_T and ϕ_T. The specific relations are found numerically

$$FF = e^{-0.00788(\theta_T - \theta)^2}, \tag{7.4}$$

$$FF = e^{-0.01778(\phi_T - \phi)^2}; \tag{7.5}$$

(iii) The oscillatory behaviours do not represent any real situation as it arises because of the improper choice of numerical integration technique. However, we are content with the technique we have employed as the region of such artificial facets falls into the region of $FF < 0.25$.

Finally, we end this §7.2 by noting but the symmetry property of the template parameters. A closer look of the graphs and the remark (i) that above reveal the following symmetry property. The FF is symmetrical under the following transformations

$$\theta_T \;\rightarrow\; \pi - \theta_T\,, \qquad 0 \leqslant \theta_T \leqslant \pi\,; \tag{7.6}$$

$$\phi_T \;\rightarrow\; \pi - \phi_T\,, \qquad 0 \leqslant \phi_T \leqslant \pi\,; \tag{7.7}$$

$$\phi_T \;\rightarrow\; 3\pi - \phi_T\,, \qquad \pi \leqslant \phi_T \leqslant 2\pi\,. \tag{7.8}$$

It should be noted that these symmetry properties are based on our results obtained for one sidereal day observation time. The generic nature of the symmetries may be established only after studying the variation of FF with T_0.

§7.3 The number of templates

It is important to study the problem of the number of templates for all sky search in the light of FF. The results of §7.2 reveal that the grid spacing $\triangle\theta$ in the θ-parameter of templates may be expressed symbolically as a function of FF, f_0, and T_0 i.e.

$$\triangle\theta = \mathcal{F}(FF,\, f_0,\, \theta,\, \phi,\, T_0)\,. \tag{7.9}$$

Similarly, we have

$$\triangle\phi = \mathcal{G}\,(FF,\, f_0,\, \theta,\, \phi,\, T_0)\,. \tag{7.10}$$

In view of this, Equations (9.13) and (9.20) may be equivalently expressed as

$$\mathcal{F}(FF,\, 0.5,\, 25^\circ,\, 30^\circ,\, T) = \left[-(0.00788)^{-1}\ln(FF)\right]^{1/2}, \tag{7.11}$$

$$\mathcal{G}\,(FF,\, 25,\, 1^\circ,\, 35^\circ,\, T) = \left[-(0.01788)^{-1}\ln(FF)\right]^{1/2}. \tag{7.12}$$

f_0 (Hz)	T_0 (d)	a $\times 10^{-2}$	b $\times 10^{-4}$	c $\times 10^{-5}$	d $\times 10^{-6}$	e $\times 10^{-7}$
50	30	2138.05	2071.43	7225.73	6239.43	2036.14
	180	2317.05	−71.3155	1746.61	2146.55	944.931
	365	2382.96	216.917	2464.42	2464.42	1031.54
20	120	2047.55	−794.473	3564.56	4650.68	1945.87
50		2266.59	4269.44	15655.0	17509.5	6484.51
100		2360.23	−206.906	1158.27	1491.01	733.520

Table 7.1: Coefficients of the best fit graphs obtained for the number of templates.

For any chosen value of FF one can determine $\triangle\theta$ and $\triangle\phi$. But there is no unique choice for it. Our interest would be in the assignment of $\triangle\theta$ and $\triangle\phi$ such that the spacing are maximum resulting into the least number of templates. As we have mentioned earlier, there is a stringent requirement on reducing computer time. Accordingly, there is a serious need of adopting some procedure/formalism to achieve it. For example, one may adopt the method of hierarchical search given by Mohanty and Dhurandhar (1996) and by Mohanty (1998). This search is carried out in two steps. At the first level one would start with the template bank with a coarse spacing in the parameter space but with a lower threshold. In the next level a more finely spaced set of templates and a higher threshold would be used but only around those templates of the previous level which crossed the previous threshold.

However, an important issue related to the problem of the number of templates is regarding the study of the behaviour of the template number with FF for different f_0 and T_0. We have investigated this aspect. Assume a source location $(\theta, \phi) = (1^\circ, 30^\circ)$. We choose some value of FF, say 0.995. Taking $\phi_T = 30^\circ$ we determine the spacing $\triangle\theta$ to yield the selected FF. In the case under investigation $\triangle\theta$ is found to be 4.5×10^{-5}. Thereafter, we introduce the spacing $\triangle\phi$ in the obtained bank of templates, and determine the resulting FF. The results obtained may be expressed in the form of a graph such as the shown in Figs. (7.4) and (7.5). Interestingly the nature of these curves are similar. We have obtained a best fit to the graphs, and the relation

$$N_{templ} = \exp\left[a - bx + cx^2 - dx^3 + ex^4\right]; \qquad (7.13)$$
$$x = FF\,, \quad 0.85 \leqslant x \leqslant 0.99\,,$$

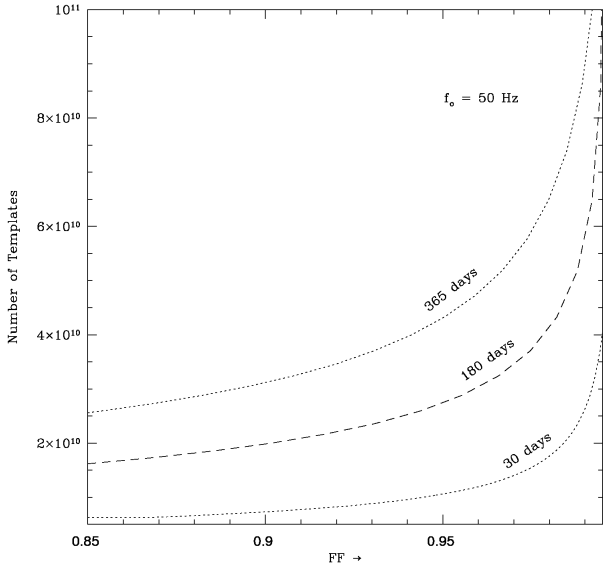

Figure 7.4: Variation of number of templates with FF for fixed f_0 at different T_0.

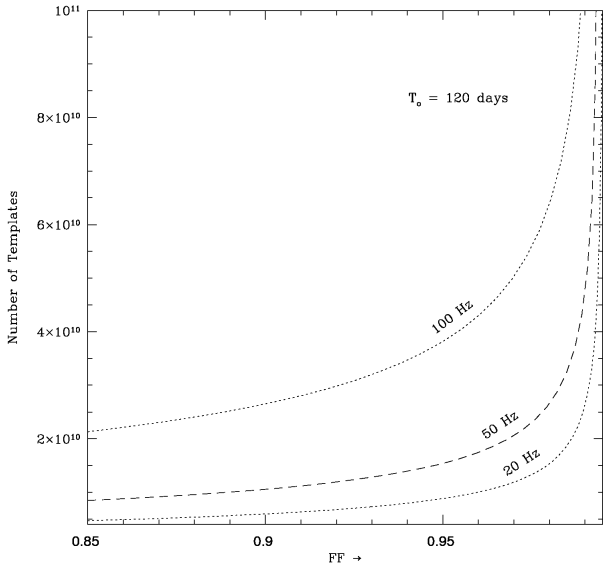

Figure 7.5: Variation of number of templates with FF for different frequencies at fixed T_0.

where a, b, c, d and e are constants. The numerical values of these constants are given in Table (7.1).

Note from the graphs, for sake of comparison, that the numbers of templates required for FF equal to 0.97 are respectively 1.44×10^{10}, 3.5×10^{10}, 5.5×10^{10} for the observation data set of 30, 120 365 days and $f_0 = 50$ Hz. Similarly the number of templates required to analyze the observation data set of 120 days of GW frequencies 20, 50 and 100 Hz are respectively 1.22×10^{10}, 2.16×10^{10}, and 5×10^{10}. It is observed that higher FF requires exponentially increasing the number of templates.

§ 7.4 Discussion

In view of the complexity of the FT which contains exponential as well as Bessel functions, one has to be careful in computing FF. We have found useful to employ the Romberg integration using Padé approximation. We have used (i) QROMO of numerical recipes instead of QROMB as the former takes care of singularities, and (ii) RATINT routine for Padé approximation. The Bessel functions are computed using the routine BESSJ0(X), BESSJ1(X) and BESSJ(N, X) of numerical recipes (Press et al., 1986). The BESSJ0(X) and BESSJ1(X) compute the Bessel function of the first kind of zeroth and first order respectively for any value of X, while BESSJ(N, X) computes the Bessel function of first kind of arbitrary integral order N for any value of X.

We have noticed marked symmetries in all sky search in both θ and ϕ space for one day observation time. It has been found that any FF corresponds to two values each in θ_T and ϕ_T. Accordingly, computation burden will be reduced by a factor of four. However, it is not clear whether the symmetry property can be established analytically as well. The source location, because of the symmetry, is uncertain. Some other analysis is to be adopted for getting the exact location.

We have computed the number of templates required for all sky search for matched filtering assuming the noise power spectral density $S_n(f)$ to be flat. However, for realistic situation, the effect of the noise have to be taken into consideration.

The optimum template parametrization and placement, and the related computational burden were discussed by Sathyaprakash and Dhurandhar (1991), Dhurandhar and Sathyaprakash (1994), Owen (1996), Apostolatos (1995, 1996), Mohanty and Dhurandhar (1996), Mohanty (1998), Owen and Sathayaprakash (1999). The possible efficient interpolated representation of the correlators is a problem of interest.

Chapter 8

MATCHING OF THE SIGNALS

§8.1 Introduction

The strength of CGW is largely dependent on the degree of the long-living asymmetry in the source. There are several mechanism for producing such an asymmetry (Pandharipande et al., 1976; Bonazzola and Gourgoulhon, 1996; Zimmermann and Szedenits, 1979; Zimmermann, 1980). The estimates of the asymmetry in neutron stars shows that the amplitude of CGW may be $\leqslant 10^{-25}$. Hence, long integration will be required to get the signature of the signal. But this in turn induces several other problems viz. Doppler modulation and non-stationarity of the noise in the detector.

Consequently data analysis becomes more, and more harder. However, Doppler modulation will provide an information about the position of the source in the sky.

The basic method to analyze the detector output to get the signature of GW signals relies on how efficiently one can process Fourier analyis of the data. In Chapter 5 and 6 we shown that amplitude modulation will only redistribute the power of the FM signal in five frequency bands $f \pm 2f_{rot}$, f, $f \pm f_{rot}$. Hence it is sufficient to consider only the FM signal for the analysis of the matching of the signals from different locations in the sky.

In the previous Chapter 7 the matching of the signals from locations in the sky that differ in their co-latitude and longitude by π radians has been made for 1-d data set and observed symmetries in the sky locations under the following transformations

$$\theta_T \;\rightarrow\; \pi - \theta_T\,, \qquad 0 \leqslant \theta_T \leqslant \pi\,; \tag{8.1}$$

$$\phi_T \;\rightarrow\; \pi - \phi_T\,, \qquad 0 \leqslant \phi_T \leqslant \pi\,; \tag{8.2}$$

$$\phi_T \;\rightarrow\; 3\pi - \phi_T\,, \qquad \pi \leqslant \phi_T \leqslant 2\pi\,. \tag{8.3}$$

However, it will be important to understand the generic nature of the matching of signals under the above transformations, and also check it in practice.

§8.2 Matching of the signal in celestial co-latitude

Let us consider that GEO600 detector (the position and orientation of the detectors can be found in Jaranowski et al., 1998) receives a CGW signal of a frequency $f_0 = 0.1$ Hz (such an unreasonably low frequency has been chosen for illustrative purposes limited by accessed computational power) from a source located at $(\theta, \phi) = (25°, 20°)$. In order to evaluate the matching of the signals in co-latitude, we first maximize FF over ϕ by choosing $\phi = \phi_T = 20°$. Now, we wish to check the symmetries in co-latitude represented by Equation (8.1) for the data set $T_{obs} = 120$ d. For the purpose we maximize the FF over θ by varying θ_T in discrete steps over entire range i.e. from 0° to 180°. For the present case it is sufficient to take the ranges of k and m as from 1 to 345 and from -3 to 3 respectively and the bandwidth equal to 20.1954×10^{-6} Hz. The results so obtained are shown in Fig. (8.1). To establish the observed symmetries, we similarly compute the FF for $T_{obs} = 1, 2, 3, \ldots, 365$ d and observe that the matching of signals remains almost the same. However, due to the obliquity of the ecliptic, the variation in the matching of signals will be dependent on the source frequency, the co-latitude, and the detector's position and orientation. We check the dependence of the FF on these parameters. The result so obtained for different Earth-based laser interferometric detectors are shown in Tables (8.1), (8.2), and Figs. (8.2), (8.3).

The analysis of the matching of signals in θ space shows that:

(i) For fixed f_0, the FF is
   (a) independent from T_{obs} and ϕ;
   (b) not varying significantly with the variation of the source location, the detector's position and orientation, see Tables (8.1) and (8.2) for detail;

(ii) The FF falls with the source frequency, see Figures (8.2) and (8.3) for detail. From the figure we find that it may not be relevant to take care of the symmetries in the sky locations for the search of CGW from the output of LIGO-I, GEO600 and TAMA detectors whose lower cut off frequency is 40/75 Hz (Owen and Sathyaprakash, 1999);

(iii) The approximate fall of FF based on the Figures (8.2)and (8.3) may be given as

$$\mathrm{FF} = A_0 + A_1 \left(\frac{f_0}{\mathrm{Hz}}\right) - A_2 \left(\frac{f_0}{\mathrm{Hz}}\right)^2 + A_3 \left(\frac{f_0}{\mathrm{Hz}}\right)^3, \tag{8.4}$$

where A_0, A_1, A_2, A_3 are constants given in Table (8.2).

θ°	θ_T°	FF ($\beta_0 = 0^\circ$)	FF ($\beta_0 = 90^\circ$)
0.5	179.5	0.9999	0.9970
1	179	0.9999	0.9970
5	175	0.9992	0.9970
10	170	0.9985	0.9968
15	165	0.9986	0.9966
20	160	0.9987	0.9963
25	155	0.9987	0.9959
30	150	0.9988	0.9954
35	145	0.9990	0.9949
40	140	0.9991	0.9944
45	135	0.9992	0.9939
50	130	0.9993	0.9933
55	125	0.9995	0.9985
60	120	0.9996	0.9988
65	115	0.9997	0.9992
70	110	0.9998	0.9994
75	105	0.9998	0.9997
80	100	0.9999	0.9998
85	95	0.9999	0.9999
89	91	0.9999	0.9999

Table 8.1: Matching of the signals of frequency 1 Hz under the transformation represented by Equation (8.1) for GEO600 detector.

Detector	A_0 $\times 10^{-3}$	A_1 $\times 10^{-5}$	A_2 $\times 10^{-5}$	A_3 $\times 10^{-7}$
GEO600 ($\beta_0 = 0^\circ$)	1000.02	124.524	129.030	137.774
GEO600 ($\beta_0 = 90^\circ$)	997.796	175.426	248.072	282.478
LIGO Hanford ($\beta_0 = 0^\circ$)	998.450	225.359	172.731	221.187
LIGO Hanford ($\beta_0 = 90^\circ$)	996.668	266.811	324.073	440.729
VIRGO ($\beta_0 = 0^\circ$)	998.548	243.480	191.503	259.026
VIRGO ($\beta_0 = 90^\circ$)	996.064	316.288	362.630	529.531
TAMMA300 ($\beta_0 = 0^\circ$)	997.914	342.746	249.527	390.874
TAMMA300 ($\beta_0 = 90^\circ$)	995.744	371.193	458.856	756.536
LIGO Livingston ($\beta_0 = 0^\circ$)	998.815	396.783	285.368	478.932
LIGO Livingston ($\beta_0 = 90^\circ$)	995.622	399.087	516.416	904.211

Table 8.2: Coefficients of the fall of FF with f_0 under the transformation represented by Equation (8.1) for $\beta_0 = 0^\circ$ and 90°.

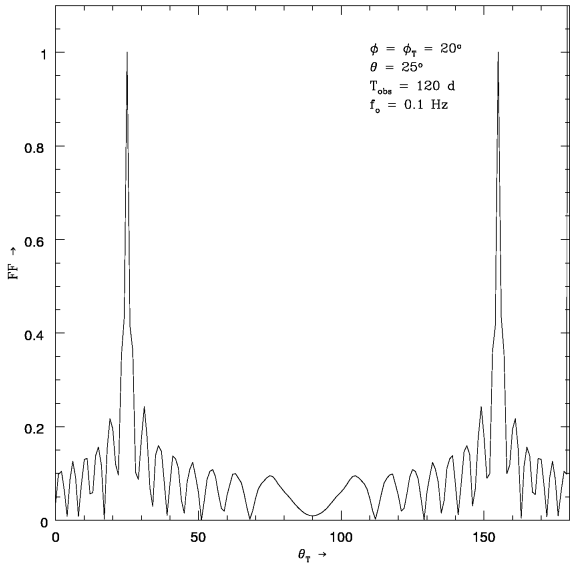

Figure 8.1: Variation of FF with θ_T.

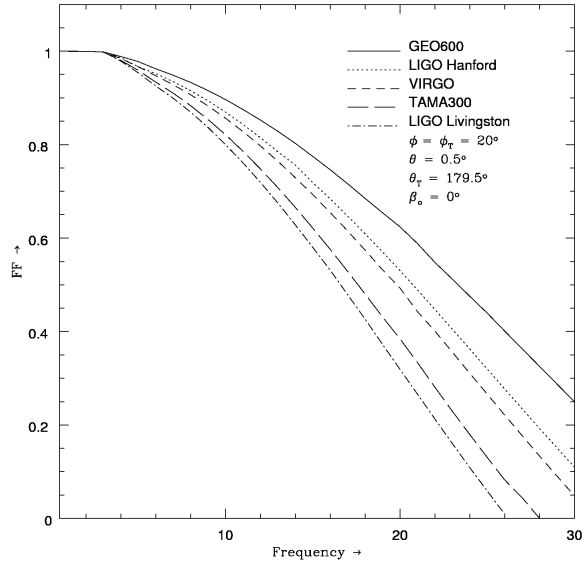

Figure 8.2: Fall of FF with f_0.

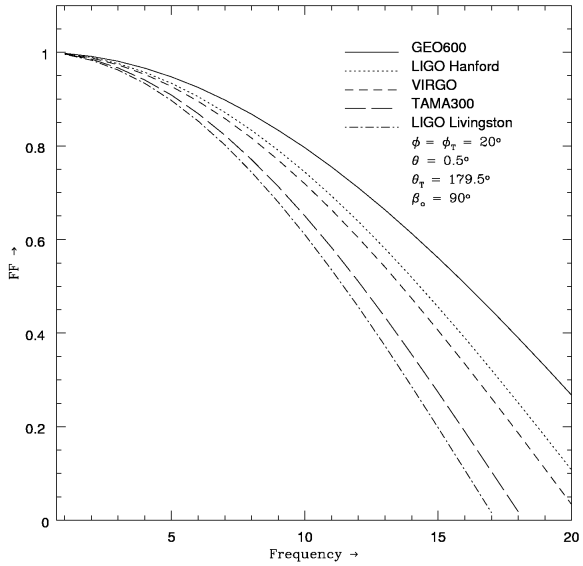

Figure 8.3: Fall of FF with f_0.

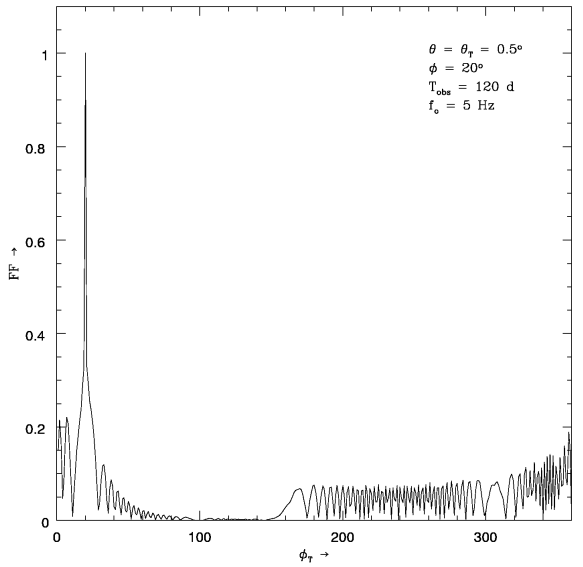

Figure 8.4: Variation of FF with ϕ_T.

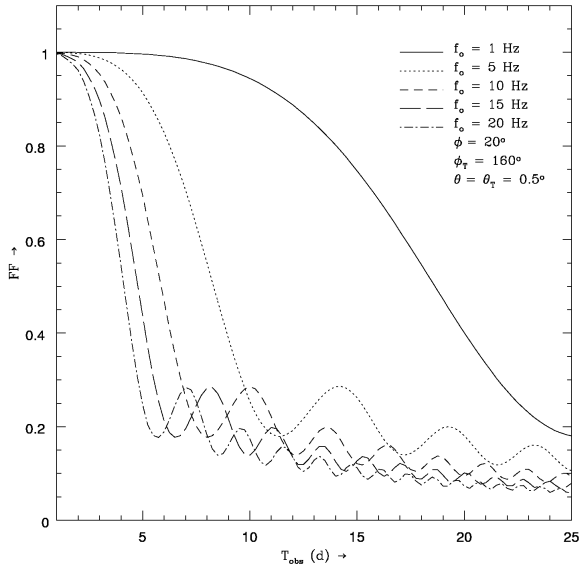

Figure 8.5: Fall of FF with T_{obs} for different f_0.

§8.3 Matching of the signal in celestial longitude

The Doppler shift due to the motion of the Earth is mainly dependent on the co-latitude and the source's frequency, and has much less dependence on the longitude. Consequently, the grid spacing of the templates for matched filtering in an all sky search will insignificantly be dependent on the longitude (Brady and Creighton 2000). Keeping this in view, we similarly check the matching of signals under the transformation given by Equation (8.2). We chosen the LIGO detector located at Livingston, selected a data set $T_{obs} = 120$ d, $(\theta, \phi) = (0.5°, 40°)$, $f_0 = 5$ Hz. In order to compute the FF, we first maximize Equation (7.1) over θ by selecting $\theta = \theta_T = 0.5°$, followed by the maximization over ϕ in discrete steps over its entire range, $0° \leqslant \phi \leqslant 360°$. The result so obtained is shown in Fig. (8.4). We also check the mismatch of the signals for different θ, ϕ, and f_0 by computing the FF for the data set of $T_{obs} = 1, 2, \ldots$ $\ldots, 25/100$ d. The results so obtained are shown in Figures (8.5), (8.6), and (8.7) respectively. Almost the same behaviour has been observed for the transformation represented by Equation (8.3).

From these Figures we note that the matching of the signals in the longitude decreases with T_{obs}, f_0, θ, and ϕ. However, the behaviours of

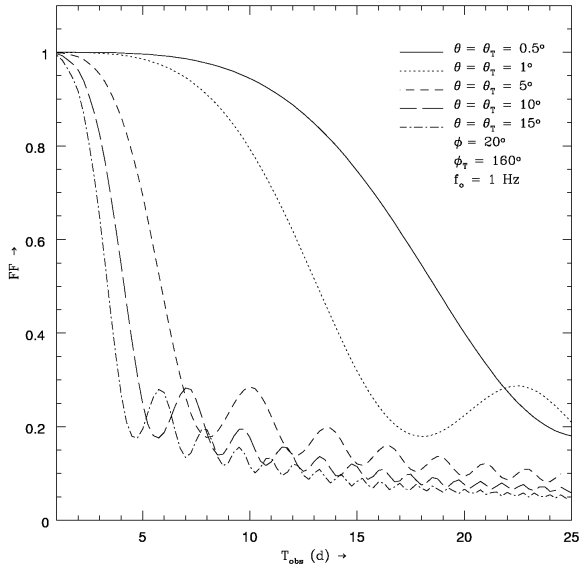

Figure 8.6: Fall of FF with T_{obs} for different θ.

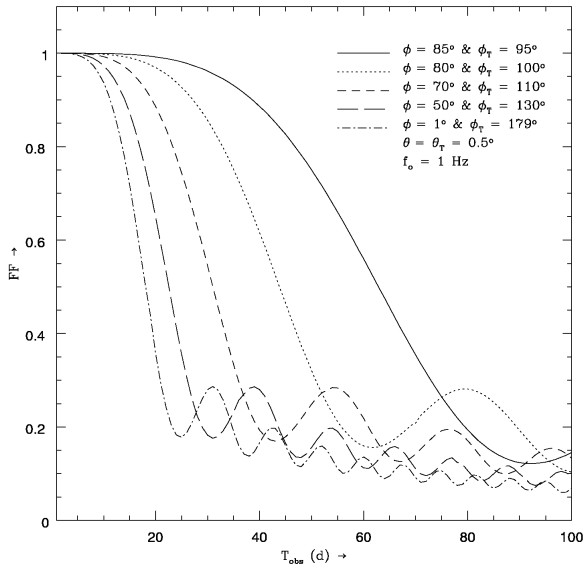

Figure 8.7: Fall of FF with T_{obs} for different ϕ and ϕ_T.

f_0 (Hz)	θ°	θ_T°	ϕ°	ϕ_T°	$B_0 \times 10^{-3}$	$B_1 \times 10^{-5}$	$B_2 \times 10^{-5}$	$B_3 \times 10^{-6}$	$B_4 \times 10^{-7}$
20					1032.39	13167.8	14036.2	56606.5	55088.4
15					1030.85	11101.8	10398.0	36450.9	30710.3
10	0.5	0.5			1028.79	8750.18	6813.74	19603.4	13481.1
5					1025.73	5842.30	3302.21	6795.19	3310.22
			20/200	160/340	1021.20	2348.47	616.661	579.752	126.575
	1	1			1023.31	3527.06	1287.73	1692.54	522.566
	5	5			1028.85	8758.50	6812.31	19567.0	13437.3
	10	10			1032.67	13220.3	14031.8	56298.5	54579.0
	15	15			1034.40	16673.7	21157.0	103289.0	122385.0
1			1/181	179/359	1031.20	2896.18	722.052	671.331	149.659
			50/230	130/310	1028.29	2216.41	452.688	341.054	61.1078
	0.5	0.5	70/250	110/290	1024.32	1473.47	225.270	125.891	16.4451
			80/260	100/280	1019.87	906.855	101.752	41.5159	3.84672
			85/265	95/275	1012.58	449.523	38.5174	11.9112	0.774374

Table 8.3: Coefficients of the fall of FF for LIGO Livingston detector under the transformation represented by Equations (8.2) and (8.3) for different θ and f_0.

the matching of signals are similar in nature, and they may be represented by

$$\mathrm{FF} = B_0 - B_1 T_{obs} + B_2 T_{obs}^2 - B_3 T_{obs}^3 + B_4 T_{obs}^4 \,, \qquad (8.5)$$

$$T_{obs} = 1, 2, \ldots, 25/100 \ \mathrm{d} \,,$$

where B_0, B_1, B_2, B_3, B_4 are the constants given in Table (8.3). Equations (8.4) and (8.5) does not represents the oscillatory part of these Figures.

§8.4 Summary

In view of blind all sky search for CGW, we have discussed the matching of the signals from different source locations assuming the noise to be stationary and Gaussian. For a fixed f_0, we observed that the matching of signals from the locations in the sky that differ in their co-latitude by π radians is independent from T_{obs} and ϕ. However, it falls with f_0. But in the longitude the matching of signals falls with T_{obs}, θ, ϕ, f_0. We believe that the matching of the signals will increase for the real data. This is due to the resolution provided by the Fast Fourier Transform (FFT). However, it may not be relevant to account this symmetries for the search of CGW from the output of LIGO-I, GEO600 and TAMA detectors. This analysis will be more relevant if one performs hierarchical search (Mohanty and Dhurandhar, 1996; Mohanty, 1998). This search is basically a two step search: in the first step the detection threshold is kept low, and in the second step a higher threshold is used. The higher threshold is used for those templates which exceed the first step threshold.

Chapter 9

THE EARTH AZIMUTH EFFECT

§ 9.1 Introduction

Search of CGW without a priori knowledge appears to computationally quite demanding even by the standard computers expected to be accessed in the near future. It appears that due to the limited computational resource it will be not feasible to perform all sky and all frequency search in the months/year data set. However, if advanced LIGO achieves its design sensitivity $\sim 10^{-23}$ or better (Weinstein, 2002), it may be feasible to perform all sky search for a day to week data set in a small frequency band for the sources emitting a signal of an amplitude of $\gtrsim 10^{-26}$. The search of the potential sources may be more significant, if done in the frequency band where most of the pulsars are detected by other means. Also, the choice of sophisticated, optimal data analysis methods and a clever programming is also an integral part to search the signal buried in the noise with the available computation power.

The current status of the search indicates that it is important to detect the GW rather finding the source location more accurately. Hence, one would like to do minimum Doppler correction or/and to make the search templates. In reference to an all sky search, the concept of patches (Schutz, 1991) in the sky may be interpreted as the number of templates required for the coherent all sky search. The size of the patch may be increased, hence reducing the number of points required for the Doppler correction, by manipulating the output of the detector, which in turn demands the detail understanding of the parameters affecting the phase of the modulated signal. In this, the initial azimuth of the Earth plays a vital role in the modulation of the signal, particularly for the analysis of day to week data set.

§ 9.2 Modified Fourier transform

In Chapters 5 and 6, the FT analysis of the FM signal has been done by taking into account the effects arising due to both rotational and orbital motion of the Earth. Here we incorporate the initial azimuth of the Earth, which affects significantly in the spacing of the parameters space for an all sky search.

§ 9.2.1 For one sidereal day

We proceed from Chapter 5, where a formula for the phase of the received CGW signal incorporating the initial azimuth of the Earth (β_{orb}) was given. Let us we rewrite the phase in such a way that it may be given as follows

$$\Phi(t) = 2\pi f_0 t + \mathcal{Z}\cos(a\xi_{rot} - \sigma) + \mathcal{N}\cos(\xi_{rot} - \delta) - \mathcal{M}\,, \qquad (9.1)$$

where it is denoted

$$\left.\begin{aligned}
\mathcal{M} &= \frac{2\pi f_0}{c}\left(R_{se}\sin\theta\cos\sigma + \sqrt{\mathcal{P}^2+\mathcal{Q}^2}\cos\delta\right)\\
\mathcal{Z} &= \frac{2\pi f_0}{c}R_{se}\sin\theta\,, \quad \mathcal{N} = \frac{2\pi f_0}{c}\sqrt{\mathcal{P}^2+\mathcal{Q}^2}\\
\mathcal{P} &= R_e\sin\alpha\,(\sin\theta\sin\phi\cos\epsilon + \cos\theta\sin\epsilon)\\
\mathcal{Q} &= R_e\sin\alpha\sin\theta\cos\phi\\
\sigma &= \phi - \beta_{orb}\,, \quad \delta = \tan^{-1}\frac{\mathcal{P}}{\mathcal{Q}} - \beta_{rot}\\
a &= w_{orb}/w_{rot} \approx 1/365.26\,, \quad w_{orb}t = a\xi_{rot}
\end{aligned}\right\}. \qquad (9.2)$$

Similarly as done in Chapter 5, it is straight forward to obtain FT for one sidereal day, and may be given as

$$\left[\tilde{h}(f)\right]_d \simeq \frac{\nu}{2\,w_{rot}}\sum_{k=-\infty}^{k=\infty}\sum_{m=-\infty}^{m=\infty} e^{i\mathcal{A}}\,\mathcal{B}\left[\mathcal{C} - i\mathcal{D}\right]; \qquad (9.3)$$

$$\begin{aligned}
\mathcal{A} &= \frac{(k+m)\,\pi}{2} - \mathcal{M}\,,\\
\mathcal{B} &= \frac{J_k(\mathcal{Z})\,J_m(\mathcal{N})}{\nu^2 - (a\,k+m)^2}\,,\\
\mathcal{C} &= \sin 2\nu\pi\cos(2\,a\,k\,\pi - k\sigma - m\delta)\\
&\quad - \frac{a\,k+m}{\nu}\left\{\cos 2\nu\pi\sin(2\,a\,k\,\pi - k\sigma - m\delta) + \sin(k\sigma + m\delta)\right\},\\
\mathcal{D} &= \cos 2\nu\pi\cos(2\,a\,k\,\pi - k\sigma - m\delta)\\
&\quad + \frac{k\,a+m}{\nu}\sin 2\nu\pi\sin(2\,a\,k\,\pi - k\sigma - m\delta) - \cos(k\sigma + m\delta)\,.
\end{aligned}$$

We use the symmetrical property of Bessel function. With the symmetrical property of Bessel function we reduce the computation time

appreciably by rewriting $\left[\tilde{h}(f)\right]_d$ as

$$\begin{aligned}\left[\tilde{h}(f)\right]_d \simeq \frac{\nu}{w_{rot}}\Bigg[&\frac{J_0(\mathcal{Z})\,J_0(\mathcal{N})}{2\nu^2}\left[\left\{\sin\mathcal{M}-\sin\left(\mathcal{M}-2\nu\pi\right)\right\}\right.\\&\left.+\,i\left\{\cos\mathcal{M}-\cos\left(\mathcal{M}-2\nu\pi\right)\right\}\right]\\&+J_0(\mathcal{Z})\sum_{m=1}^{m=\infty}\frac{J_m(\mathcal{N})}{\nu^2-m^2}\left[(\mathcal{YU}-\mathcal{XV})-i\,(\mathcal{XU}+\mathcal{YV})\right]\\&+\sum_{k=1}^{k=\infty}\sum_{m=-\infty}^{m=\infty}e^{i\mathcal{A}}\mathcal{B}\left(\tilde{\mathcal{C}}-i\tilde{\mathcal{D}}\right)\Bigg];\end{aligned}\tag{9.4}$$

$$\left.\begin{aligned}\mathcal{X}&=\sin\left(\mathcal{M}-m\,\tfrac{\pi}{2}\right)\\\mathcal{Y}&=\cos\left(\mathcal{M}-m\,\tfrac{\pi}{2}\right)\\\mathcal{U}&=\sin 2\nu\pi\cos m(2\pi-\delta)-\frac{m}{\nu}\left\{\cos 2\nu\pi\sin m(2\nu\pi-\delta)-\sin m\delta\right\}\\\mathcal{V}&=\cos 2\nu\pi\cos m(2\pi-\delta)+\frac{m}{\nu}\sin 2\nu\pi\sin m(2\pi-\delta)-\cos m\delta\end{aligned}\right\}.\tag{9.5}$$

§9.2.2 For an arbitrary observation time

Similarly, as done in Chapter 6 the FT for an arbitrary observation time of the received CGW signal with β_{orb}, may be given as

$$\tilde{h}(f)\simeq\frac{\nu}{2w_{rot}}\sum_{k=-\infty}^{k=\infty}\sum_{m=-\infty}^{m=\infty}e^{i\mathcal{A}}\mathcal{B}\left[\tilde{\mathcal{C}}-i\tilde{\mathcal{D}}\right];\tag{9.6}$$

where

$$\left.\begin{aligned}\nu&=\frac{f_0-f}{f_{rot}}\\\mathcal{A}&=\frac{(k+m)\,\pi}{2}-\mathcal{M}\\\mathcal{B}&=\frac{J_k(\mathcal{Z})\,J_m(\mathcal{N})}{\nu^2-(a\,k+m)^2}\\\tilde{\mathcal{C}}&=\sin\nu\xi_0\cos\left(a\,k\xi_0+m\xi_0-k\sigma-m\delta\right)\\&\quad-\frac{ak+m}{\nu}\left\{\cos\nu\xi_0\sin\left(ak\xi_0+m\xi_0-k\sigma-m\delta\right)+\sin\left(k\sigma+m\delta\right)\right\}\\\tilde{\mathcal{D}}&=\cos\nu\xi_0\cos\left(a\,k\xi_0+m\xi_0-k\sigma-m\delta\right)\\&\quad+\frac{ka+m}{\nu}\sin\nu\xi_0\sin\left(ak\xi_0+m\xi_0-k\sigma-m\delta\right)-\cos\left(k\sigma+m\delta\right)\\\xi_0&=w_{rot}T_{obs}\end{aligned}\right\}.\tag{9.7}$$

Similarly for efficient computation we rewrite $\tilde{h}(f)$ as

$$\begin{aligned}\tilde{h}(f) \simeq \frac{\nu}{w_{rot}}\Bigg[& \frac{J_0(\mathcal{Z})\,J_0(\mathcal{N})}{2\nu^2}\left[\left\{\sin\mathcal{M}-\sin\left(\mathcal{M}-\nu\xi_0\right)\right\}\right. \\ & \left.+\,i\left\{\cos\mathcal{M}-\cos\left(\mathcal{M}-\nu\xi_0\right)\right\}\right] \\ & +\,J_0(\mathcal{Z})\sum_{m=1}^{m=\infty}\frac{J_m(\mathcal{N})}{\nu^2-m^2}\left[\left(\mathcal{Y}\mathcal{U}-\mathcal{X}\mathcal{V}\right)-i\left(\mathcal{X}\mathcal{U}+\mathcal{Y}\mathcal{V}\right)\right] \\ & +\sum_{k=1}^{k=\infty}\sum_{m=-\infty}^{m=\infty}e^{i\mathcal{A}}\mathcal{B}\left(\tilde{\mathcal{C}}-i\tilde{\mathcal{D}}\right)\Bigg]; \end{aligned} \tag{9.8}$$

$$\left.\begin{aligned}\mathcal{X} &= \sin\left(\mathcal{M}-m\,\tfrac{\pi}{2}\right) \\ \mathcal{Y} &= \cos\left(\mathcal{M}-m\,\tfrac{\pi}{2}\right) \\ \mathcal{U} &= \sin\nu\xi_0\cos m(\xi_0-\delta)-\frac{m}{\nu}\left\{\cos\nu\xi_0\sin m(\xi_0-\delta)-\sin m\delta\right\} \\ \mathcal{V} &= \cos\nu\xi_0\cos m(\xi_0-\delta)+\frac{m}{\nu}\sin\nu\xi_0\sin m(\xi_0-\delta)-\cos m\delta\end{aligned}\right\}. \tag{9.9}$$

§9.3 Bank of search templates

The study of the independent points for an all sky search has been made by many researchers* for the coherent and/or incoherent search. The coherent search means cross correlating the data with the bank of search templates. While incoherent search implies adding up the power spectra by dividing the data into N subsets, performing a full search for each subset, and adds up the power spectra of the resulting searches. In this case, there is loss in S/N ratio by a factor of $\sqrt{N}$ in relation to coherent search as power spectra are added incoherently. However, irrespective of the method of search, the optimal spacing in the (θ, ϕ) parameters for an all sky search is a problem of interest.

To estimate optimal spacing in the parameters space one have to careful investigate the parameters contain in the phase of the modulated signal. Hence, for the coherent search, we investigate the β_{orb} effect in the bank of search templates of an all sky search.

§9.3.1 For one sidereal day

To estimate the number of search templates for one sidereal day data, we consider the LIGO detector at Hanford. Let it receives a CGW signal

*See Schutz (1991), Brady et al. (1998), Brady and Creighton (2000), Jaranowski and Królak (1999, 2001), Astone et al. (2002).

of a frequency of $f_0 = 50$ Hz from a source located at $(\theta, \phi) = (0.1^\circ, 30^\circ)$. We chosen the data set such that $\beta_{orb} = 0$ at $t = 0$. In this case we take the ranges of k and m as from 1 to 310 and from -10 to 10 respectively and the bandwidth equal to 2.0×10^{-3} Hz for the integration. Now, we select the spacing $\triangle\theta = 4.5 \times 10^{-5}$, thereafter we maximize over ϕ by introducing a spacing $\triangle\phi$ in the so obtained bank of search templates and determine the resulting FF. In similar manner we obtain the FF at $\beta_{orb} = \frac{\pi}{4}$ and $\frac{\pi}{2}$. The results obtained are shown in Figure (9.1) and the best fit of the graphs may be given as

$$N_{templ} = 10^{15}\left[c_0 + c_1 x - c_2 x^2 + c_3 x^3 - c_4 x^4 + c_5 x^5 - c_6 x^6 + c_7 x^7\right]; \quad (9.10)$$

$$0.80 \leqslant x \leqslant 0.995\,,$$

where c_0, c_1, c_2, c_3, c_4, c_5, c_6, c_7 are the constants which are given in Table (9.1).

In view of the above investigation, the grid spacing $(\triangle\theta, \triangle\phi)$ in the (θ, ϕ)-parameter of templates may be expressed as

$$\triangle\theta = \mathcal{F}(FF, f_0, \theta, \phi, T_{obs}, \beta_{orb})\,. \quad (9.11)$$

Similarly,

$$\triangle\phi = \mathcal{G}\,(FF, f_0, \theta, \phi, T_{obs}, \beta_{orb})\,. \quad (9.12)$$

In Chapter 7, for one sidereal data set, the dependence of FF on the template variables θ_T and ϕ_T is given as

$$FF = e^{-0.00788(\theta - \theta_T)^2}\,. \quad (9.13)$$

$$FF = e^{-0.01778(\phi - \phi_T)^2}\,. \quad (9.14)$$

From Eqs. (9.11), (9.19), (9.13), and (9.20), we may write

$$\mathcal{F}(FF, 50, 0.1^\circ, 30^\circ, 1\mathrm{d}, \beta_{orb}) = \left[-(0.00788)^{-1}\ln(FF)\right]^{1/2}, \quad (9.15)$$

$$\mathcal{G}\,(FF, 50, 0.1^\circ, 30^\circ, 1\mathrm{d}, \beta_{orb}) = \left[-(0.01778)^{-1}\ln(FF)\right]^{1/2}. \quad (9.16)$$

Hence, for the selected FF one can determine $\triangle\theta$ and $\triangle\phi$. However, there is no unique choice for it.

§ 9.3.2 For one week

In this case, we consider the LIGO detector at Livingston which is getting a CGW signal of a frequency $f_0 = 50$ Hz from a source located at $(\theta, \phi) = (1^\circ, 45^\circ)$. First, we chosen the data set such that $\beta_{orb} = 0$ at

β_{orb}	c_0	c_1	c_2	c_3	c_4	c_5	c_6	c_7
0°	-4.36537	34.4523	116.44	218.462	245.734	165.719	62.0404	9.94642
45°	-403.012	3187.44	10795.5	20296.6	22877.7	15459.9	5799.45	931.641
90°	-263.622	2086.48	7071.80	13305.6	15008.9	10150.3	3810.65	612.645

Table 9.1: Coefficients of the best fit graphs obtained for the bank of search templates.

β_{orb}	a_0	a_1	a_2	a_3	a_4	a_5	a_6	a_7
0	-1.71829	13.1670	43.2234	78.7956	86.1505	56.4921	20.5716	3.20919
$\pi/6$	-35.7699	273.770	897.636	1634.42	1784.84	1168.99	425.178	66.2488
$\pi/2$	-40.7053	311.849	1023.49	1865.42	2039.12	1336.86	486.720	75.9142

Table 9.2: Coefficients of the best fit graphs obtained for the number of templates with FF.

β_{orb}	b_0	b_1	b_2	b_3
0	0.994123	0.149451	3.94494	2.64819
$\pi/6$	0.993544	2.00186	366.375	1651.88
$\pi/2$	0.996774	2.11099	2914.21	37817.3

Table 9.3: Coefficients of the best fit graphs obtained for the FF with $\triangle\phi$.

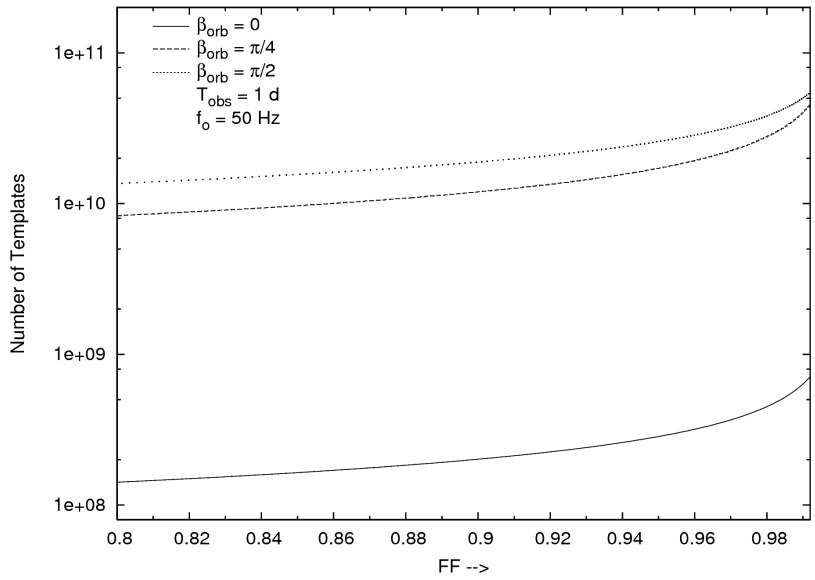

Figure 9.1: Variation in the number of search templates with FF at at different values of β_{orb}.

$t = 0$. In this case we take the ranges of k and m as from 1 to 2800 and from -15 to 15 respectively and the bandwidth equal to $50 \pm 3.28 \times 10^{-4}$ Hz for the integration. Now, we select the spacing $\triangle\theta = 0.45 \times 10^{-4}$, thereafter we maximize over ϕ by introducing a spacing $\triangle\phi$ in the so obtained number of templates and determine the resulting FF. In similar manner we obtain the number of templates for $\beta_{orb} = \frac{\pi}{6}$ and $\frac{\pi}{2}$. The results obtained are shown in Fig. (9.2). We also plot the templates spacing $\triangle\phi$ in the ϕ-parameter with FF shown in Fig. (9.3) and the best fit of curves may be given as

$$N_{templ} = 10^{18}\left[a_0 + a_1 x - a_2 x^2 + a_3 x^3 - a_4 x^4 + a_5 x^5 - a_6 x^6 + a_7 x^7\right]; \quad (9.17)$$

$$0.85 \leqslant x \leqslant 0.995;$$

$$FF = b_0 + b_1 y - b_2 y^2 + b_3 y^3; \quad 0.037 \leqslant y \leqslant 0.69; \quad (9.18)$$

where $a_0 \ldots a_7$ and $b_0 \ldots b_3$ are constants as given in Table (9.2) and (9.3) respectively.

In view of the above investigation, the spacing $\triangle\phi$ in the ϕ-parameter may be expressed as

$$\triangle\phi = \mathcal{G}\left(FF,\ f_0,\ \theta,\ \phi,\ T_{obs},\ \beta_{orb}\right). \quad (9.19)$$

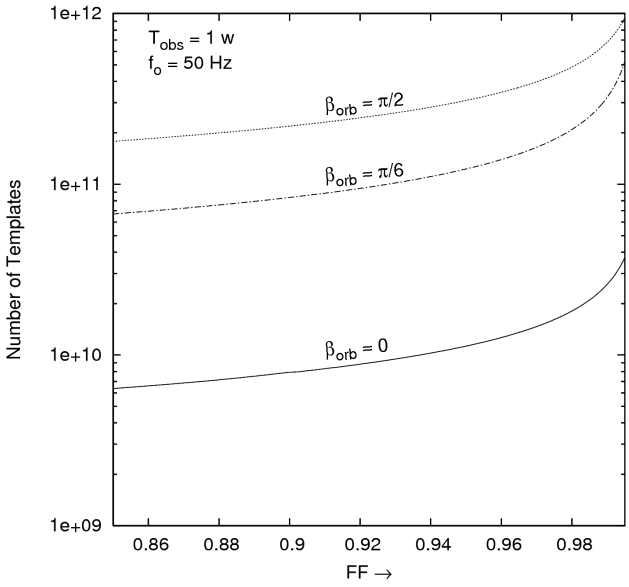

Figure 9.2: Number of templates with FF at different β_{orb}.

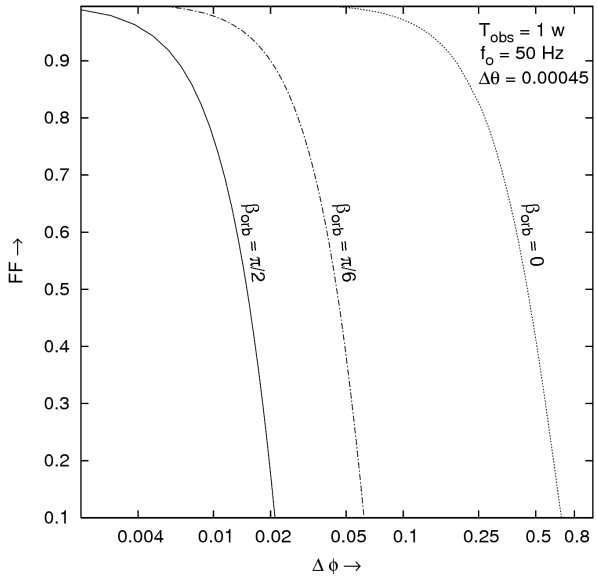

Figure 9.3: FF with $\triangle\phi$ at different β_{orb}.

Equation (9.18) is a third order polynomial, hence complicates the solution. However, one would like to get data analysis for $FF > 0.90$. Therefore from Figure (9.3) we obtain a very good dependence of FF for a minimum number of templates that may be given as

$$FF = -\,2.85657 \triangle \phi^2 + 0.00230059 \triangle \phi + 1.00018\,. \tag{9.20}$$

From Eqs. (9.19) and (9.20), we may write

$$\mathcal{F}(FF,\, 50,\, 1^\circ,\, 45^\circ,\, 1w,\, \beta_{orb}) \approx 4.02684 \times 10^{-4} \pm 0.591667\,\sqrt{1.00018 - FF}\,. \tag{9.21}$$

The above equation can be relevant to make trade-off between computational costs and sensitivities i.e. for the selected FF one can estimate the number of templates.

§9.4 Computational costs

In view of the above analysis it will be interesting to know the feasibility of the all sky search with the target sensitivity of the advanced LIGO. The computational costs of the data analysis basically depends on the floating point operations (flops) requires to perform the Fast Fourier Transform (FFT). Hence in terms of FFT, the flops for the data reduction upto the frequency f for T_{obs} of the interferometer output may be given as (Press et al., 1986)

$$N_{flops} = 2 f T_{obs} \log_2\big(2 f_{max} T_{obs}\big)\,. \tag{9.22}$$

Now for the given mismatch (FF), if N_p is the number of independent points to perform an all sky search, the flops will be

$$N_{flops}(FF, N_p) = 2 f T_{obs} N_p \log_2\big(2 f_{max} T_{obs}\big)\,. \tag{9.23}$$

Hence, for the mismatch of 3% and without manipulating the data in reference to β_{orb}, the flops for the search of a CGW signal upto 50 HZ in the week data set will be 2.38×10^{19}, 2.58×10^{20}, and 6.23×10^{20} for $\beta_{orb} = 0$, $\frac{\pi}{6}$ and $\frac{\pi}{2}$ respectively, assuming other operation need negligible flops compared to FFT. However, the lower cut off frequency of the LIGO I/II is 10/40 Hz. Hence the analysis shall be done above the lower cut off. Also, the search will be more significant if one performs the most sensitive band of the detector. In this, if one would like to perform an all sky search in a small band, say 5 Hz, the minimum flops for the on-line analysis (a week data gets analyzed in a $\sim$ week time) will be 3.44×10^{12}. The flops require may be further reduction, if one

performs a hierarchical search. Hence, it may be feasible to perform a limited frequency all sky search of a signal amplitude $\gtrsim 10^{-26}$ in the output of such a sensitive detector with a TFLOPS computer.

§9.5 Summary

The initial azimuth of the Earth has been incorporated in the FT of the frequency modulated signal, and its effect in the bank of templates required for the search of CGW in an all sky search is discussed. In the investigation for one sidereal day data set of a signal of 50 Hz, we observe that the number of search templates varies significantly with β_{orb}. From the analysis we found that for $FF = 0.97$ approximately 24.8267×10^{10}, 22.7840×10^{12}, and 32.3097×10^{12} search templates may be required, if $\beta_{orb} = 0, \frac{\pi}{4}$ and $\frac{\pi}{2}$ respectively.

Similarly, the number of search templates for the search in the output of one week data set. We observe that for $FF = 0.97$ there approximately 1.53×10^{10}, 1.66×10^{11}, and 4.0×10^{11} templates will be required when $\beta_{orb} = 0, \frac{\pi}{6}$ and $\frac{\pi}{2}$ respectively. Hence, the analysis may be useful to reduce the computational cost for a coherent all sky search. However, also the inspection of the phase of the modulated signal reveals that the reduction in the bank of search templates depends on the time scale of integration, shorter than T_{obs}, resulting more difference in the number of templates.

The reduction in the number of templates is large, so we studied the feasibility of all sky search in reference to the advanced LIGO and found that in the band of 5 Hz one may perform an on-line all sky search of a CGW signal of an amplitude of $\gtrsim 10^{-26}$ with a TFLOPS computer. The relation given by Equation (9.22) may be useful to make trade-off between computational costs and sensitivities for the search of CGW. The issue to reduce the flops for all sky search is a problem of interests and hence needs more studies.

Bibliography

1. Abramovici A., Althouse W.E., Drever R.W.P., Gürsel Y., Kanwamura S., Raab F.J. Shoemaker D., Sievers L., Spero R.E., Thorne K.S., Vogt R.E., Weiss R., Whitcomb S.E., and Zucker Z.E. *Science*, 1992, v. 256, 325.
2. Abrmowitz M. and Stegun I.A. In: *Handbook of Mathematical Functions*, Dover Publication, New York, 10th printing with corrections of first edition, 1972.
3. Allen B. In: *Relativistic Gravitation and Gravitational Radiation*, ed. by Marck J.A. and Lasota J.P, Cambridge University Press, Cambridge, 1997.
4. Andersson N. *Astrophys. J.*, 1998, v. 502, 708.
5. Apostolatos T.A. *Phys. Rev. D*, 1995, v. 52, 605.
6. Apostolatos T.A. *Phys. Rev. D*, 1996, v. 54, 2421.
7. Astone P., Borkowski K.M., Jaranowski P. and Królak A. *Phys. Rev. D*, 2002, v. 65, 042003.
8. Bildsten L. *Astrophys. J. Lett.*, 1998, v. 501, L89.
9. Blair D. and Ju L. *Monthly Not. RAS*, 1996, v. 283, 648.
10. Blair D.G. In: *Gravitational Wave Data Analysis*, ed. by Schutz B.F., Kluwer Press, Dordrecht, 1989.
11. Blair D.G. In: *The Detection of Gravitational Waves*, ed. by Blair D.G. Cambridge University Press, Cambridge, England, 1991.
12. Bonazzola S. and Gourgoulhon E. *Astron. and Astrophys.*, 1996, v. 312, 675.
13. Bradaschia C., Calloni E., Cobal M., Fabbro R.D., Virgilio A.D., Giazotto A., Holloway L.E., Kautzky H., Michelozzi B., Montelatici V., Passuello D., and Velloso W. In: *Gravitation 1990, Proceedings of the Banff Summer Institute*, edited by Mann R. and Wesson P. World Scientific, Singapore, 1991.
14. Brady P.R., Creighton T., Cutler C., and Schutz B.F. *Phys. Rev. D*, 1998, v. 57, 2101.
15. Brady P.R. and Creighton T. *Phys. Rev. D*, 2000, v. 61, 082001.
16. Bracewell Ron. The Fourier Transform and Its Application. 2nd revised edition, McGraw-Hill, New York, 1984.
17. Brigham E.O. The Fast Fourier Transform and its Application. Prentice-Hall International, 1988.
18. Cutler C., Apostolatos T.A., Bildsten L., Finn L.S., Flanagan E.E., Kennefick D., Markovic D.M., Ori A., Poisson E., Sussman G.J. and Thorne K.S. *Phys. Rev. Lett.*, 1993, v. 70, 2984.

19. Damour T. Three Hundred Years of Gravitation. Ed. by Hawking S.W. and Israel W., Cambridge University Press, Cambridge, England, 1987.
20. Damour T. In: *Gravitation in Astrophysics*, ed. by Carter B. and Hartle J.B., Plenum Press, New York, 1987.
21. Danzmann K. In: *Gravitational Wave Experiment*, ed. by Coccia E., Pizzela G., and Ronga F., World Scientific, Singapore, 1995, 100–111.
22. Dhurandhar S.V. and Sathyaprakash B.S. *Phys. Rev. D*, 1994, v. 49, 1707.
23. Frasca S. *Int. J. Mod. Phys. D.*, 2000, v. 9, 369.
24. Giazotto A., Bonazzola S., and Gourgoulhon E. *Phys. Rev. D*, 1997, v. 55, 2014.
25. Goldstein H. Classical Mechanics. Addison-Wesley, New York, 1980.
26. Green R.M. Spherical Astronomy. Cambridge University Press, Cambridge, England, 1985.
27. Grishchuk L.P. *Class. Quant. Gravity*, 1997, v. 14, 1445.
28. Helstrom C.W. Statistical Theory of Signal Detection. 2nd ed., Pergamon Press, London, 1968.
29. Hough J. In: *Gravitational Wave Experiment*, ed. by Coccia E., Pizzela G., and Ronga F., World Scientific, Singapore, 1995, 50–63.
30. Hulse R.A. and Taylor J.H. *Astrophys. J. Lett.*, 1975, v. 195, L51–L53.
31. Jaranowski P., Królak A., and Schutz B.F. *Phys. Rev. D*, 1998, v. 58, 063001.
32. Jaranowski P. and Królak A. *Phys. Rev. D*, 1999, v. 59, 063003.
33. Jaranowski P. and Królak A. *Phys. Rev. D*, 2000, v. 61, 062001.
34. Jotania K. and Dhurandhar S.V. *Bull. Astron. Soc. India*, 1994, v. 22, 303.
35. Jotania et al. *Astron. and Astrophys.*, 1996, v. 306, 317–325.
36. Kulkarni S.R. *Philos. Trans. R. Soc. London*, 1992, v. 341, 77.
37. Królak A. In *Gravitational Wave Data Analysis*, ed. by Schutz B.F., Kluwer Press, Dordrecht, 1989.
38. Landau L.D. and Lifshitz E.M. Mechanics. Pergamon Press, Oxford, England, 1969.
39. Landau L.D. and Lifshitz E.M. The Classical Theory of Fields. Pergamon Press, Oxford, England, 1975.
40. Lindblom L., Owen B.J., and Morsink S.M. *Phys. Rev. Lett.*, 1998, v. 80, 4843.
41. Manchester R.N. *Philos. Trans. R. Soc. London*, 1992, v. 341, 3.
42. McCleland et al. In: *Proceedings of the 3rd Edoardo Amaldi Conference*, ed. by S. Meshkov, AIP Conference Proceedings, v. 523, 140, Melville, New York, 2000.
43. Misner C.W., Thorne K.S., and Wheeler J.A. Gravitation. W.H. Freeman and Company, San Francisco, 1973.
44. Mohanty S.D. and Dhurandhar S.V. *Phys. Rev. D*, 1996, v. 54, 7108.
45. Mohanty S.D. *Phys. Rev. D*, 1998, v. 57, 630.

46. Narayan R., Piran T., and Shemi A. *Astrophys. J. Lett.*, 1991, v. 379, L17.
47. Owen B.J. *Phys. Rev. D*, 1996, v. 53, 6749.
48. Owen B.J. and Sathyaprakash B.S. *Phys. Rev. D*, 1999, v. 60, 022002.
49. Owen B.J., Lindblom L., Cutler C., Schutz B.F., Vecchio A., and Andersson N. *Phys. Rev. D*, 1998, v. 58, 084020.
50. Pandharipande V.R., Pines D., and Smith R.A. *Astrophys. J.*, 1976, v. 208, 550.
51. Papoulis A. Signal Analysis. McGraw-Hill Inc., Singapore, 1977.
52. Phinney E.S. *Astrophys. J. Lett.*, 1991, v. 330, L17.
53. Press W.H., Flannery B.P., Teukoslsky S.A., and Vetterling W.T. Numerical Recipes: The Art of Scientific Computing. Cambridge Univ. Press, Cambridge, 1986.
54. Sahay S.K. *Int. J. Mod. Phys. D.*, 2003, v. 12, no. 7, 1227.
55. Sahay S.K. *Int. J. Mod. Phys. D.*, 2006, v. 15, no. 2, 225.
56. Saulson P.R. Fundamentals of Interfeometric Gravitational Wave Detectors. World Scientific Publishing, Singapore, 1994.
57. Sathyaprakash B.S. and Dhurandhar S.V. *Phys. Rev. D*, 1991, v. 44, 3819.
58. Sathyaprakash B.S. In: *Black Holes, Gravitational Radiation and the Universe*, ed. by Iyer B.R. and Bhawal B., Kluwer Press, Dordrecht, 1999.
59. Schutz B.F., Davier M., and Hello P., eds. *Proceedings of Gravitational Wave Data Analysis Workshop*, Orsay, France 1997, Editions Frontieres, Paris, 113–143.
60. Schutz B.F. *Class. Quant. Gravity*, 1993, v. 10, 135.
61. Schutz B.F. *Class. Quant. Gravity*, 1999, v. 16, A131.
62. Schutz B.F. and Tinto M. *Monthly Not. RAS*, 1987, v. 224, 131.
63. Schutz B.F. The Detection of Gravitational Waves. Ed. by Blair, D.G., Cambridge University Press, Cambridge, England, 1991.
64. Schutz B.F. A First Course in General Relativity. Cambridge University Press, Cambridge, England, 1989.
65. Shanmugam K.S. and Breiphol A.M. Random Signals: Detection, Estimation and Data Analysis. Willey, New York, 1989.
66. Smart W.M. In: *Textbook on Spherical Astronomy*, Cambridge University Press, Cambridge, 1977.
67. Srivastava D.C. and Sahay S.K. *Monthly Not. RAS*, 2002, v. 337, 305.
68. Srivastava D.C. and Sahay S.K. *Monthly Not. RAS*, 2002, v. 337, 315.
69. Srivastava D.C. and Sahay S.K. *Monthly Not. RAS*, 2002, v. 337, 322.
70. Tagoshi H., Kanda N., Tanaka T., Tatsumi D., Telada S., Ando M., Arai K., Araya A., Asada H., et al. *Phys. Rev. D*, 2001, v. 63, 062001.
71. Tsubona K. In: *Gravitational Wave Experiment*, ed. by Coccia E., Pizzela G., and Ronga F., World Scientific, Singapore, 1995, 112–114.
72. Thorne K.S. In: *Three Hundred Years of Gravitation*, ed. by Hawking S.W., Israel W., Cambridge University Press, Cambridge, 1987.

73. Weber J. *Phys. Rev.*, 1960, v. 117, 306.
74. Weinstein A. *Class. Quant. Gravity*, 2002, v. 19, 1575–1584.
75. Weiss R. *Reviews of Modern Physics*, 1999, v. 71, 187.
76. Zimmermann M. and Szedenits E. *Phys. Rev. D*, 1979, v. 20, 351.
77. Zimmermann M. *Phys. Rev. D*, 1980, v. 21, 891.

About the author

Sanjay Kumar Sahay (b. 1970 in East Singhbhum, India) was educated from Ranchi University, India. He obtained PhD in data analysis of gravitational waves from D.D.U. Gorakhpur University, India, in 2003. After submission of PhD, during 2002–2003, he continued his work on gravitational waves at Inter University Centre for Astronomy and Astrophysics, Pune, India. In 2003–2005 he worked on the multi-wavelength astronomy project, ASTROSAT at Raman Research Institute, Bangalore, India. On 2005 he worked as post doctoral fellow at Tel Aviv University, Israel, with the ultra violet detector TAUVEX (Tel Aviv University Ultra-violet Explorer), under training of Prof. Noah Brosch. Commencing in December, 2005, he is joined as a lecturer in Birla Institute of Technology and Science, Pilani — Goa Campus, India, and is still working independently on gravitational waves.

Svenska fysikarkivet books

A Revised Electromagnetic Theory with Fundamental Applications *by Bo Lehnert*

Svenska fysikarkivet, 2008, 158 pages. ISBN 978-91-85917-00-6

Summary: There are important areas within which the conventional electromagnetic theory of Maxwell's equations and its combination with quantum mechanics does not provide fully adequate descriptions of physical reality. As earlier pointed out by Feynman, these difficulties are not removed by and are not directly associated with quantum mechanics. Instead the analysis has to become modified in the form of revised quantum electrodynamics, for instance as described in this book by a Lorentz and gauge invariant theory. The latter is based on a nonzero electric charge density and electric field divergence in the vacuum state, as supported by the quantum mechanical vacuum fluctuations of the zero-point energy. This theory leads to new solutions of a number of fundamental problems, with their applications to leptons and photon physics. They include a model of the electron with its point-charge-like nature, the associated self-energy, the radial force balance in presence of its self-charge, and the quantized minimum value of the free elementary charge. Further there are applications on the individual photon and on light beams, in respect to the angular momentum, the spatially limited geometry with an associated needle-like radiation, and the wave-particle nature in the photoelectric effect and in two-slit experiments.

Spin-Curvature and the Unification of Fields in a Twisted Space *by Indranu Suhendro*

Svenska fysikarkivet, 2008, 78 pages. ISBN 978-91-85917-01-3

Summary: The book draws theoretical findings for spin-curvature and the unification of fields in a twisted space. A space twist, represented through the appropriate formalism, is related to the anti-symmetric metric tensor. Kaluza's theory is extended and given an appropriate integrability condition. Both matter and the isotropic electromagnetic field are geometrized through common field equations: trace-free field equations giving the energy-momentum tensor for such an electromagnetic field solely via the (generalized) Ricci curvature tensor and scalar are obtained. In the absence of electromagnetic fields the theory goes to Einstein's 1928 theory of distant parallelism where only matter field is geometrized (through the twist of space-time). The above results in common with respective wave equations are joined into a "unified field theory of semi-classical gravoelectrodynamics".

Particles Here and Beyond the Mirror *by D. Rabounski and L. Borissova*

Svenska fysikarkivet, 2008, 118 pages. ISBN 978-91-85917-03-7

Summary: This is a research on all kinds of particles, which could be conceivable in the space-time of General Relativity. In addition to mass-bearing particles and light-like particles, zero-particles are predicted: such particles can exist in a fully degenerate space-time region (zero-space). Zero-particles seems as standing light

waves, which travel in instant (non-quantum teleportation of photons); they might be observed in a further development of the "stopped light experiment" which was first conducted in 2001, at Harvard, USA. The theoretical existence of two separate regions in the space-time is also shown, where the observable time flows into the future and into the past (our world and the mirror world). These regions are separated by a space-time membrane wherein the observable time stops. A few other certain problems are considered. It is shown, through Killing's equations, that geodesic motion of particles is a result of stationary geodesic rotation of the space which hosts them. Concerning the theory of gravitational wave detectors, it is shown that both free-mass detector and solid-body detector may register a gravitational wave only if such a detector bears an oscillation of the butt-ends.

Data Analysis of Gravitational Waves *by S. K. Sahay*

Svenska fysikarkivet, 2008, 118 pages. ISBN 978-91-85917-05-1

Summary: The detection of GW in the noisy output of the detectors has its own problem, not the least of which is the sheer volume of data analysis. The data analysis of the signals is computationally demanding even for the standard computer expected to be available in the near future. Hence, the book discusses the data analysis problem of the signal by developing the analytical Fourier Transform with taking into account the Earth's rotational motion around its axis, and its revolution around the Sun for efficient data analysis, efficient not only in a picking weak signal from the noisy data but also in terms of the computing-cost. Taking the advanatage of the analytical Fourier Transform over the Fast Fourier Transform in terms of resolution and computational cost, we applied the technique of "Matched Filtering" and esitmated the number of templates required for matched filtering in an all sky search of the signal, and also an analysis has been done for the possible symmetries in the sky location as the parameters of the signal manifold and templates corresponding to the different source locations. The trade-off between computational cost and sensitivies arises due the Earth azimuth in the bank of search templates for an all-sky search of the singal has been also discussed.

Data Analysis of Gravitational Waves *by S. K. Sahay*

The detection of GW in the noisy output of the detectors has its own problem, not the least of which is the sheer volume of data analysis. The data analysis of the signals is computationally demanding even for the standard computer expected to be available in the near future. Hence, the book discusses the data analysis problem of the signal by developing the analytical Fourier Transform with taking into account the Earth's rotational motion around its axis, and its revolution around the Sun for efficient data analysis, efficient not only in a picking weak signal from the noisy data but also in terms of the computing-cost. Taking the advantage of the analytical Fourier Transform over the Fast Fourier Transform in terms of resolution and computational cost, we applied the technique of "Matched Filtering" and estimated the number of templates required for matched filtering in an all sky search of the signal, and also an analysis has been done for the possible symmetries in the sky location as the parameters of the signal manifold and templates corresponding to the different source locations. The trade-off between computational cost and sensitivities arises due the Earth azimuth in the bank of search templates for an all-sky search of the singal has been also discussed.

Databehandling av gravitationsvågor *av S. K. Sahay*

Att kunna isolera gravitationsvågor vid hög brusnivå hos detektorn är förknippad med en del problem, inte minst med tanke på de stora beräkningsvolymerna som behövs för dataanalysen. Analysen av alla data och själva signalen är mycket krävande, även för en standarddator, som förväntas vara tillgänglig inom närmaste framtiden. I boken behandlas dataanalysproblemet genom utveckling av en analytisk Fourier transform som tar hänsyn till Jordens rotation runt egen axel och runt solen. Genom detta förbättras möjligheten att isolera den svaga signalen med en mycket lägre datorkapacitet, än det som annars hade behövts. Genom att använda sig av de fördelar som den analytiska Fourier trasformen, jämfört med FFT, ger i fråga av upplösning och beräkningskostnader, vi tillämpade en teknik som vi kallar "anpassad filtrering" för att få en uppskattning på antalet mallar som behövs för anpassad filtrering i en omfattande avsökning av himlen. En kompromiss mellan beräkningskostnaderna och känslighet som uppkommer inom sökmallbanken beroende av Jordens azimut vid en omfattande avsökning efter signalen har också diskuterats i boken.

Svenska fysikarkivet, Stockholm, 2008, 118 pages

ISBN 978-91-85917-05-1